Transmit Antenna Selection for Multiple-Input Multiple-Output Spatial Modulation Systems

Ping Yang, *Senior Member, IEEE*, Yue Xiao, *Member, IEEE*, Yong Liang Guan, *Member, IEEE*, Shaoqian Li, *Fellow, IEEE*, and Lajos Hanzo, *Fellow, IEEE*

***Abstract*—The benefits of transmit antenna selection (TAS) invoked for spatial modulation (SM) aided multiple-input multiple-output (MIMO) systems are investigated. Specifically, we commence with a brief review of the existing TAS algorithms and focus on the recently proposed Euclidean distance-based TAS (ED-TAS) schemes due to their high diversity gain. Then, a pair of novel ED-TAS algorithms, termed as the improved QR decomposition (QRD)-based TAS (QRD-TAS) and the error-vector magnitude-based TAS (EVM-TAS) are proposed, which exhibit an attractive system performance at low complexity. Moreover, the proposed ED-TAS algorithms are amalgamated with the low-complexity yet efficient power allocation (PA) technique, termed as TAS-PA, for the sake of further improving the system's performance. Our simulation results show that the proposed TAS-PA algorithms achieve signal-to-noise ratio (SNR) gains of up to 9 dB over the conventional TAS algorithms and up to 6 dB over the TAS-PA algorithm designed for spatial multiplexing systems.**

***Index Terms*—Antenna selection, MIMO, power allocation, spatial modulation, link adaptation.**

I. Introduction

SPATIAL modulation (SM) and its variants constitute a class of promising low-complexity and low-cost multiple-input multiple-output (MIMO) transmission techniques [1]–[5]. However, the conventional SM schemes only achieve receiver-diversity, but no transmit diversity [6]. To circumvent this impediment, recently some SM solutions have been proposed [7]–[11] on how to glean a beneficial transmit-diversity gain both with the aid of open-loop as well as closed-loop transmit-symbol design techniques.

As an attractive closed-loop regime, transmit antenna selection (TAS) constitutes a promising technique of providing a high diversity potential as offered by the classic MIMO architectures. TAS has been lavishly researched in the context of spatial multiplexing systems [12]. As a new MIMO technique, SM can also be beneficially combined with TAS. Recently, several TAS algorithms have been conceived for the class of SM-MIMO systems with the goal of enhancing either its bit error rate (BER) or its capacity [13]–[20]. In [13], a norm-based TAS algorithm was proposed for providing diversity gain. In [14], a closed-form expression of the SM scheme's outage probability was derived for norm-based TAS. In [16], a two-stage TAS-based SM scheme was proposed for overcoming the specific constraint of SM, namely that the number of transmit antennas has to be a power of two. In [17], a novel TAS criterion was proposed for circumventing the detrimental effects of antenna correlation. In [18], the joint design of TAS and constellation breakdown was investigated and a graph-based search algorithm was proposed for reducing the search complexity imposed. In [19], a low-complexity TAS algorithm based on circle packing was proposed for a transmitter-optimized spatial modulation (TOSM) system, which trades off the spatial constellation size against the amplitude and phase modulation (APM) constellation size for improving the system's average bit error probability (ABEP). The adaptive TAS algorithm conceived for TOSM was further developed in [20], where a low-complexity two-stage optimization was proposed for selecting the best transmission mode.

More recently, the research of TAS-aided SM has been focused on the optimization of the Euclidean Distance (ED) of the received constellation points, since they achieve a high diversity gain at a moderate complexity compared to other TAS criteria [21]–[24]. Specifically, in [21] and [22] the ED-based TAS algorithm (ED-TAS) was compared to the signal-to-noise ratio (SNR)-optimized and capacity-optimized algorithms, and a low-complexity realization of ED-TAS, termed as the QR decomposition-based TAS (QRD-TAS) was proposed. The QRD-TAS algorithm constructs an ED-element matrix and exploits the QRD of the resultant matrix for reducing the imposed complexity. Moreover, in [24], the authors exploited the rotational symmetry of the APM adopted for the sake of reducing the complexity of QRD-TAS. Compared to directly optimizing the ED, in [23], Ntontin *et al*. proposed a low-complexity singular value decomposition-based TAS (SVD-TAS) algorithm for maximizing the lower bound of the ED. In [25], the complexity of SVD-TAS was reduced through an alternative computation of the singular value. In [26], the transmit diversity order of ED-TAS was quantified. In [27], the authors proposed several low-complexity TAS schemes relying

Manuscript received October 10, 2015; revised February 22, 2016; accepted March 24, 2016. This work was supported of the National Science Foundation of China under Grant 61501095, in part by the National High-Tech R&D Program of China ("863" Project under Grant 2014AA01A707), and in part by the European Research Council's Advanced Fellow Grant. The associate editor coordinating the review of this paper and approving it for publication was V. Raghavan.

P. Yang, Y. Xiao, and S. Li are with the National Key Laboratory of Science and Technology on Communications, University of Electronic Science and Technology of China, Sichuan 611731, China (e-mail: yplxw@163.com; xiaoyue@uestc.edu.cn; lsq@uestc.edu.cn).

Y. L. Guan is with the School of Electrical and Electronic Engineering, Nanyang Technological University, Singapore (e-mail: eylguan@ntu.edu.sg).

L. Hanzo is with the School of Electronics and Computer Science, University of Southampton, Southampton SO17 1BJ, U.K. (e-mail: lh@ecs.soton.ac.uk).

Color versions of one or more of the figures in this paper are available online at http://ieeexplore.ieee.org.

Digital Object Identifier 10.1109/TCOMM.2016.2547900

on exploiting the channel's amplitude, the antenna correlation, the ED between transmit vectors and their combinations for selecting the optimal TA subset for the sake of improving the system's reliability. However, as shown in [21]–[27], the QRD-TAS achieves an attractive BER performance at the cost of adopting high-complexity QRD operations, while the low-complexity SVD-TAS may suffer some performance loss.

On the other hand, power allocation (PA) is another promising link adaptation technique for MIMO systems. Recently, PA has been extended to SM systems [28]–[31]. For example, in [28], an adaptive PA algorithm based on maximizing the minimum ED was proposed, which is capable of improving the system's BER performance, while retaining all the single-RF benefits of SM. Subsequently, this attractive PA algorithm was further simplified in [29]. However, to the best of our knowledge, the potential benefits of TAS intrinsically amalgamated with PA have not been investigated in SM-MIMO systems.

Against this background, the contributions of this paper are:

1) We investigate the benefits of ED-TAS and propose a pair of novel ED-TAS schemes for SM-MIMO systems. In these schemes, we first classify the legitimate EDs into three specific subsets and then invoke a carefully designed upper bound as well as a set-reduction method for the most dominant set imposing a high complexity.
2) Specifically, we propose an improved QRD-TAS, where a tighter QRD-based lower bound of the ED is derived to replace the SVD-based bound of [23]. A low-complexity method is proposed for directly calculating the bound parameters, in order to avoid the high-complexity QRD or SVD operations of [21]–[24]. More importantly, compared to the conventional SVD-TAS of [25], the achieved QRD-based tighter bound can achieve a better BER performance.
3) Moreover, for striking a flexible tradeoff in terms of the BER attained and the complexity imposed, we propose an error-vector magnitude based TAS (EVM-TAS), which exploits the error vector selection probability to shrink the search space. The relevant optimization metrics of EVM-TAS are also derived for different PSK and QAM schemes.
4) Finally, we intrinsically amalgamate the proposed ED-TAS with the recently conceived PA technique of [29] for fully exploiting the MIMO channel's resources. A pair of different joint TAS-PA algorithms are conceived, which provide beneficial gains over both the conventional TAS algorithms and over the TAS-PA techniques designed for spatial multiplexing systems [32].

The organization of the paper is as follows. Section II introduces the system model of TAS-based SM, while Section III reviews the family of existing TAS algorithms designed for SM. In Section IV, we introduce the proposed QRD-TAS and EVM-TAS algorithms. In Section V, the joint design of the ED-TAS and PA algorithms is proposed. Then, we carry out their complexity analysis. Our simulation results and performance comparisons are presented in Section VI. Finally, Section VII concludes the paper.

Notation: $(\cdot)^*$, $(\cdot)^T$ and $(\cdot)^H$ denote conjugate, transpose, and Hermitian transpose, respectively. Furthermore, $\|\cdot\|_F$ stands for the Frobenius norm. $\mathbf{I}_b$ denotes a $(b \times b)$-element identity matrix and the operator diag$\{\cdot\}$ is the diagonal operator. $\Re\{\mathbf{x}\}$ and $\Im\{\mathbf{x}\}$ represent the real and imaginary parts of $\mathbf{x}$, respectively.

II. SYSTEM MODEL

Consider a SM system having N_t transmit and N_r receive antennas, as depicted in Fig. 1. The frequency-flat quasi-static fading MIMO channel is represented by $\mathbf{H} = [\mathbf{h}(1), \mathbf{h}(2), \cdots, \mathbf{h}(N_t)] \sim \mathcal{CN}(0, \mathbf{I}_{N_r \times N_t})$, where $\mathbf{h}(1), \mathbf{h}(2), \cdots, \mathbf{h}(N_t)$ are the column vectors corresponding to each transmit antenna (TA) in $\mathbf{H}$. The receiver first selects L TAs according to a specific selection criterion. Then, the receiver sends this information to the transmitter via a feedback link. As shown in [23], let U_u denote the uth legitimate TA subset, where we have

$$\begin{aligned} U_1 &= \{1, 2, \cdots, L\}, \\ U_2 &= \{1, 2, \cdots, L-1, L+1\}, \\ &\vdots \\ U_{N_U} &= \{N_t - L + 1, \cdots, N_t\}. \end{aligned} \tag{1}$$

In Eq. (1), there are $N_U = \binom{N_t}{L}$ possible TA subsets, each of which corresponds to an $(N_r \times L)$-element MIMO channel. As shown in Fig. 1, $\mathbf{b} = [b_1, \ldots, b_L]$ is the transmit bit vector in each time slot, which contains $m = \log_2(LM)$ bits, where M is the size of the APM constellation. In SM, the input vector $\mathbf{b}$ is partitioned into two sub-vectors of $\log_2(L)$ and $\log_2(M)$ bits, denoted as $\mathbf{b}_1$ and $\mathbf{b}_2$, respectively. The bits in $\mathbf{b}_1$ are used for selecting a unique TA index q for activation, while the bits of $\mathbf{b}_2$ are mapped to a Gray-coded APM symbol $s_l^q \in \mathbb{S}$. Then, the SM symbol $\mathbf{x} \in \mathbb{C}^{L \times 1}$ is formulated as

$$\mathbf{x} = s_l^q \mathbf{e}_q = [0, \cdots, \overset{\downarrow qth}{s_l^q}, \cdots, 0]^T, \tag{2}$$

where $\mathbf{e}_q (1 \le q \le L)$ is selected from the L-dimensional basis vectors (as exemplified by $\mathbf{e}_1 = [1, 0, \cdots, 0]^T$). In the scenario that U_u is selected, the signal observed at the N_r receive antennas is given by

$$\mathbf{y} = \mathbf{H}_u \mathbf{x} + \mathbf{n}, \tag{3}$$

where $\mathbf{H}_u$ is the $(N_r \times L)$-element TAS matrix corresponding to the selected TA set U_u, and $\mathbf{n}$ is the $(N_r \times 1)$-element noise vector. The elements of the noise vector $\mathbf{n}$ are complex Gaussian random variables obeying $\mathcal{CN}(0, N_0)$.

The receiver performs maximum-likelihood (ML) detection over all legitimate SM symbols $\mathbf{x} \in \mathbb{C}^{L \times 1}$ to obtain

$$\hat{\mathbf{x}} = \arg\min_{\mathbf{x} \in \mathbb{X}} \|\mathbf{y} - \mathbf{H}_u \mathbf{x}\|_F^2 = \arg\min_{\mathbf{x} \in \mathbb{X}} \left\|\mathbf{y} - \mathbf{h}_u(q) s_l^q\right\|_F^2, \tag{4}$$

where $\mathbb{X}$ is the set of all legitimate transmit symbols and $\mathbf{h}_u(q)$ is the qth column of the equivalent channel matrix $\mathbf{H}_u$. The complexity of the single-stream ML detection of Eq. (4) is low, since a single TA is activated during any time slot [34], [35].

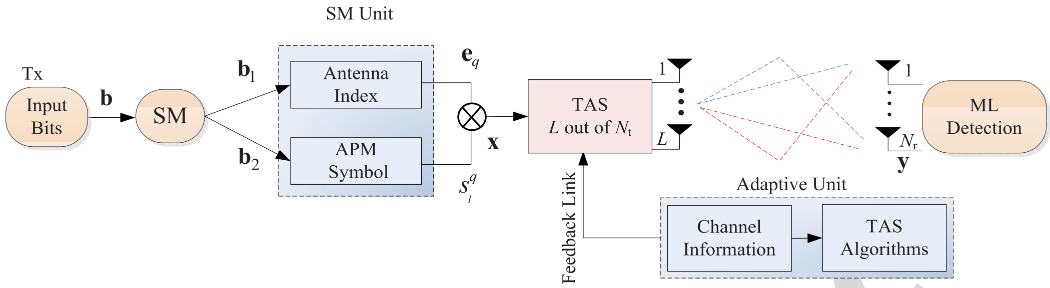

Fig. 1. The system model of the TAS-based SM system.

III. Conventional TAS Algorithms

This section offers a brief state-of-the-art review of the existing TAS algorithms proposed for SM systems.

A. The Maximum-Capacity and The Maximum-Norm Based TAS Algorithms

The capacity C_u of the SM-aided MIMO system depends on the classic transmitted signal s_l^q and the TA index signal $\mathbf{e}_q$. As shown in [21], [33], the capacity C_s relying on the signal s_l^q and the channel $\mathbf{H}_u$ is lower bounded by

$$\alpha = \frac{1}{L}\sum_{i=1}^{L} \log_2(1+\rho\,\|\mathbf{h}_u(i)\|_F^2) \leq C_s, \tag{5}$$

where $\mathbf{h}_u(i)$ is the ith column of $\mathbf{H}_u$ and ρ is the average SNR at the receiver. Moreover, the capacity C_{TA} relying on the signal $\mathbf{e}_q$ is bounded by $C_{\text{TA}} \leq \log_2(L)$ [33]. It is proved in [33] that the total capacity $C_u = C_{\text{TA}} + C_s$ is bounded by

$$\alpha \leq C_u \leq \alpha + \log_2(L), \tag{6}$$

Based on the bound of Eq. (6), a maximum-capacity based TAS algorithm was formulated in [21] as

$$\mathbf{H}_{\hat{u}} = \arg \max_{u\in\{1,\cdots,N_U\}} \alpha. \tag{7}$$

Based on Eq. (5), the optimization objective α of Eq. (7) is maximized by selecting the L TAs associated with the largest channel norms out of the N_t TAs, which is equivalent to the maximum-norm based TAS [13] given by

$$\mathbf{H}_{\hat{u}} = \arg \max_{u\in\{1,\cdots,N_U\}} \|\mathbf{H}_u\|_F^2 . \tag{8}$$

B. The Exhaustive Max-$d_{\min}$ Based ED-TAS

In order to improve the BER performance of SM, the free distance (FD) $d_{\min}$ was optimized in [21]. For a given channel $\mathbf{H}_u$, its FD can be formulated as

$$\begin{aligned} d_{\min}(\mathbf{H}_u) &= \min_{\substack{\mathbf{x}_i,\mathbf{x}_j\in\mathbb{X}\\ \mathbf{x}_i\neq\mathbf{x}_j}} \left\|\mathbf{H}_u(\mathbf{x}_i-\mathbf{x}_j)\right\|_F^2 \\ &= \min_{\mathbf{e}_{ij}\in\mathbb{E}} \left\|\mathbf{H}_u\mathbf{e}_{ij}\right\|_F^2 = \min_{\mathbf{e}_{ij}\in\mathbb{E}} \mathbf{e}_{ij}^H\mathbf{H}_u^H\mathbf{H}_u\mathbf{e}_{ij}, \end{aligned} \tag{9}$$

where we have the error vector $\mathbf{e}_{ij} = \mathbf{x}_i - \mathbf{x}_j$, $\mathbf{x}_i, \mathbf{x}_j \in \mathbb{X}$. In [21], the max-$d_{\min}$ aided ED-TAS algorithm is defined as

$$\mathbf{H}_{\hat{u}} = \arg \max_{u\in\{1,\cdots,N_U\}} d_{\min}(\mathbf{H}_u). \tag{10}$$

The optimum solution obeying the objective function of Eq. (10) can be found by an exhaustive search over all possible $\binom{N_t}{L}$ candidate channel matrices and all the different error vectors, which imposes a complexity order of $\mathcal{O}(N_t^2M^2)$. This results in an excessive complexity, when high data rates are required.

C. The Conventional QRD-Based ED-TAS

In order to reduce the complexity of the exhaustive ED-TAS of Eq. (10), in [21] an ED-TAS based on an equivalent decision metric $\mathbf{D}(u)$ was formulated as:

$$\mathbf{H}_{\hat{u}} = \arg \max_{u\in\{1,\cdots,N_U\}} \{\min[\mathbf{D}(u)]\}\,, \tag{11}$$

where $\mathbf{D}(u)$ is an $(L\times L)$-element sub-matrix of an upper triangular $(N_t\times N_t)$-element matrix $\mathbf{D}$ obtained by deleting the specific rows and columns that are absent in u, while $\min[\mathbf{D}(u)]$ is the minimum non-zero value of $\mathbf{D}(u)$. Here, the $(i,j)-th$ element of $\mathbf{D}$ can be expressed as

$$\begin{aligned} \mathbf{D}_{ij} &= \min_{s_1,s_2\in\mathbb{S}} \left\|\mathbf{H}(s_1\mathbf{e}_i - s_2\mathbf{e}_j)\right\|_F^2 \\ &= \min_{s_1,s_2\in\mathbb{S}} \|\mathbf{h}(i)s_1 - \mathbf{h}(j)s_2\|_F^2\,, \end{aligned} \tag{12}$$

where s_1 and s_2 are M-ary APM constellation points, while $\mathbf{h}(i)$ and $\mathbf{h}(j)$ are the ith and jth columns of $\mathbf{H}$. Provided that we have $i=j$ in Eq. (12), the corresponding element becomes $\mathbf{D}_{ii} = \min_{s_1,s_2\in\mathbb{S}}(\|\mathbf{h}(i)\|_F^2\,|s_1-s_2|^2) = d_{\min}^{\text{APM}}\,\|\mathbf{h}(i)\|_F^2$, where $d_{\min}^{\text{APM}}$ is the minimum distance of the APM constellation. For the case of $i\neq j$, $\mathbf{D}_{ij}$ is re-formulated in the real-valued representation of the QRD as

$$\mathbf{D}_{ij} = \min_{\substack{s_{1I},s_{2I}\in\mathfrak{R}\{\mathbb{S}\},\\ s_{1Q},s_{2Q}\in\mathfrak{I}\{\mathbb{S}\}}} \left\|\mathbf{R}[s_{1I}, s_{1Q}, -s_{2I}, -s_{2Q}]^T\right\|_F^2, \tag{13}$$

where we have $s_{nI} = \mathfrak{R}\{s_n\}$ and $s_{nQ} = \mathfrak{I}\{s_n\}$ for $n = 1, 2$, while $\mathbf{R}$ is a (4×4)-element upper triangular matrix created by the QRD of the resultant channel matrix [21]. As shown in [21], the complexity order of this QRD-TAS is $\mathcal{O}(N_t^2M)$, which increases only linearly with the modulation order M. In [22] and [24], both the modulus and the symbol set symmetry of the APM constellations were exploited for further reducing the complexity of this algorithm.

D. The Conventional SVD-Based ED-TAS

Although the QRD-based ED-TAS of Eq. (13) is capable of finding the optimal solution, its complexity imposed is a function of the modulation order M. Moreover, the high-complexity QRD has to be applied to the $(2N_r \times 4)$-element channel matrices [21], [22], [24]. Hence, the complexity of this TAS remains high. This problem was circumvented in [23], where the ED was classified into three categories as follows

$$d_{\min}(\mathbf{H}_u) = \min\left\{d_{\min}^{\text{signal}}, d_{\min}^{\text{spatial}}, d_{\min}^{\text{joint}}\right\}, \tag{14}$$

where we have

$$\begin{aligned} d_{\min}^{\text{signal}} &= \min_{i=1,\cdots,L} \|\mathbf{h}_u(i)\|_F^2 \min_{s_a \neq s_b \in \mathbb{S}} |s_a - s_b|^2 \\ &= d_{\min}^{\text{APM}} \min_{i=1,\cdots,L} \|\mathbf{h}_u(i)\|_F^2 , \end{aligned} \tag{15}$$

$$\begin{aligned} d_{\min}^{\text{spatial}} &= \min_{\substack{i,j=1,\cdots,L \\ i\neq j}} \|\mathbf{h}_u(i) - \mathbf{h}_u(j)\|_F^2 \min_{s_l \in \mathbb{S}} |s_l|^2 \\ &= d_{\min}^{\text{Modulus}} \min_{\substack{i,j=1,\cdots,L \\ i\neq j}} \|\mathbf{h}_u(i) - \mathbf{h}_u(j)\|_F^2 , \end{aligned} \tag{16}$$

$$d_{\min}^{\text{joint}} = \min_{\substack{i,j=1,\cdots,L,i\neq j \\ s_a,s_b,\in\mathbb{S},a\neq b}} \|\mathbf{h}_u(i)s_a - \mathbf{h}_u(j)s_b\|_F^2 . \tag{17}$$

In Eq. (16), the term $d_{\min}^{\text{Modulus}} = \min_{s_l\in\mathbb{S}} |s_l|^2$ is the minimum squared modulus value of the APM constellation. Since the calculations of $d_{\min}^{\text{signal}}$ and $d_{\min}^{\text{spatial}}$ in Eqs. (15) and (16) do not depend on the size of APM constellation and the corresponding complexity is low, the complexity of computing the FD of Eq. (14) is dominated by the computation of $d_{\min}^{\text{joint}}$ in Eq. (17). To reduce this complexity, in [23] the Rayleigh-Ritz theorem was utilized for driving a lower bound of $d_{\min}^{\text{joint}}$ as

$$\begin{aligned} d_{\min}^{\text{joint}} &= \min_{\substack{i,j=1,\cdots,L,i\neq j \\ s_a,s_b\in\mathbb{S},a\neq b}} \left\|[\mathbf{h}_u(i), -\mathbf{h}_u(j)][s_a, s_b]^T\right\|_F^2 \\ &\geq d_{\min}^{\text{SVD-bound}} \\ &= \min_{i,j=1,\cdots,L,i\neq j} \lambda_{\min}^2(\mathbf{H}_{u,ij}) \min_{s_a,s_b\in\mathbb{S}} \left\|[s_a, s_b]^T\right\|_F^2 \\ &= \min_{i,j=1,\cdots,L,i\neq j} \lambda_{\min}^2(\mathbf{H}_{u,ij}) d_{\min}^{\text{all}} \end{aligned} , \tag{18}$$

where we have $d_{\min}^{\text{all}} = \min_{s_a,s_b\in\mathbb{S}} \left\|[s_a, s_b]^T\right\|_F^2$ and $\mathbf{H}_{u,ij} = [\mathbf{h}_u(i), -\mathbf{h}_u(j)]$ is an $(N_r \times 2)$-element matrix. Here, $\lambda_{\min}^2(\mathbf{H}_{u,ij})$ is the minimum squared singular value of the submatrix $\mathbf{H}_{u,ij}$. Upon exploiting Eq. (18), the distance $d_{\min}(\mathbf{H}_u)$ of Eq. (14) is bounded by

$$d_{\min}^{\text{SVD}}(\mathbf{H}_u) = \min\{d_{\min}^{\text{signal}}, d_{\min}^{\text{spatial}}, d_{\min}^{\text{SVD-bound}}\}. \tag{19}$$

Based on Eq. (19), the SVD-TAS algorithm is given by

$$\mathbf{H}_{\hat{u}} = \arg \max_{u\in\{1,\cdots,N_U\}} d_{\min}^{\text{SVD}}(\mathbf{H}_u). \tag{20}$$

Compared to the conventional QRD-based TAS, this bound-aided algorithm has the following advantages:

- Using the SVD-based bound of Eq. (18), the calculation of the distance $d_{\min}^{\text{joint}}$ is independent of the APM modulation order;
- Moreover, the SVD operation of Eq. (18) is performed on the smaller channel matrices of size $(N_r \times 2)$ compared to the QRD-based ED-TAS, which is performed on $(2N_r \times 4)$-element matrices. In [25], the complexity of SVD-TAS [23] was further reduced through an alternative computation of the singular value.

IV. The Proposed Low-Complexity ED-TAS

As shown in subsection III, the conventional QRD-based ED-TAS is capable of achieving the optimal BER, but it imposes high complexity. In contrast, the SVD-based ED-TAS imposes a lower complexity at the cost of a BER performance degradation, because the derived bound may be loose and the corresponding TAS results may be suboptimal.

To circumvent this problem, in this section, a pair of ED-TAS algorithms are proposed. Specifically, an improved QRD-TAS is proposed, where a tighter QRD-based lower bound of the ED is found for replacing the SVD-based bound of [23], while the sparse nature[1] of the error vectors of SM is exploited to avoid the full-dimensional QRD operation. Then, for striking a further flexible BER vs complexity tradeoff, we propose an EVM-based ED-TAS algorithm, which exploits the error vector selection probability to shrink the search space.

A. The Proposed QRD-Based ED-TAS

1) The QRD-Based Bounds: To evaluate the value of $d_{\min}^{\text{joint}}$ more accurately, in this paper, we apply the QRD-based bound to replace the SVD-bound of Eq. (18). Specifically, the submatrix $\mathbf{H}_{u,ij}$ of Eq. (18) is first subjected to the QRD [38], yielding $\mathbf{H}_{u,ij} = \tilde{\mathbf{Q}}\tilde{\mathbf{R}}$, where $\tilde{\mathbf{Q}}$ is an $(N_r \times 2)$ column-wise orthonormal matrix and $\tilde{\mathbf{R}}$ is a (2×2) upper triangular matrix with positive real-valued diagonal entries formulated as

$$\tilde{\mathbf{R}} = \begin{bmatrix} \tilde{R}_{1,1} & \tilde{R}_{1,2} \\ 0 & \tilde{R}_{2,2} \end{bmatrix}. \tag{21}$$

Let $[\tilde{\mathbf{R}}]_k = \tilde{R}_{k,k}$ denote the kth diagonal entry of $\tilde{\mathbf{R}}$. Based on this decomposition, another lower bound of the distance $d_{\min}^{\text{joint}}$ in Eq. (18) can be formulated as

$$\begin{aligned} d_{\min}^{\text{joint}} &\geq d_{\min}^{\text{QRD-bound}} \\ &= \min_{i,j=1,\cdots,L,i\neq j} \{[\tilde{\mathbf{R}}]_{\min}^2\} \min_{s_a\neq s_b\in\mathbb{S}} \|[s_a, s_b]\|_F^2 , \\ &= \min_{i,j=1,\cdots,L,i\neq j} \{[\tilde{\mathbf{R}}]_{\min}^2\} d_{\min}^{\text{all}} \end{aligned} \tag{22}$$

[1] In SM, the transmit vector $\mathbf{x}$ only has a single non-zero element, hence the number of non-zero elements of the error vectors $\mathbf{e}_{ij}$ of SM is no more than 2.

where $[\tilde{\mathbf{R}}]^2_{\min}$ is the minimum squared nonzero diagonal entry of the upper matrix $\tilde{\mathbf{R}}$, given by

$$\left[\tilde{\mathbf{R}}\right]_{\min} = \min\{\tilde{R}_{1,1}, \tilde{R}_{2,2}\}. \tag{23}$$

Lemma 1: For an $(N_r \times 2)$-element full column-rank matrix $\mathbf{H}_{u,ij}$ associated with its minimum squared singular non-zero value $\lambda^2_{\min}(\mathbf{H}_{u,ij})$ for SVD and its minimum squared diagonal non-zero entry $[\tilde{\mathbf{R}}]^2_{\min}$ of $\tilde{\mathbf{R}}$ for QRD, respectively, the inequality $[\tilde{\mathbf{R}}]^2_{\min} \geq \lambda^2_{\min}(\mathbf{H}_{u,ij})$ is satisfied.

According to the analysis process in Section III of [38], the formulation of Lemma 1 is straightforward. As a result, the lower bound of Eq. (22) achieved by the QRD is tighter than that of the SVD algorithm in Eq. (18).

To derive an even tighter upper QRD bound than that of Eq. (22), the permutation matrix $\mathbf{\Pi}_m$ can be invoked for calculating $d^{\text{joint}}_{\min}$ of Eq. (22) as

$$d^{\text{joint}}_{\min} = \min_{\substack{i,j=1,\cdots,L,\\ i\neq j, s_a,s_b\in\mathbb{S}}} \left\| [\mathbf{h}_u(i), -\mathbf{h}_u(j)]\mathbf{\Pi}_m\mathbf{\Pi}_m^{-1}[s_a, s_b]^T \right\|^2_F, \tag{24}$$

where $\mathbf{\Pi}_m$ is an orthogonal matrix satisfying $\mathbf{\Pi}_m^{-1} = \mathbf{\Pi}_m^T$. Since the size of the channel matrix $\mathbf{H}_{u,ij} = [\mathbf{h}_u(i), -\mathbf{h}_u(j)]$ is $N_r \times 2$, we only have two legitimate permutation matrices $\mathbf{\Pi}_m \in \mathbb{C}^{2\times 2}$, $m = 1, 2$, namely

$$\mathbf{\Pi}_1 = \begin{bmatrix} 1 & 0 \\ 0 & 1 \end{bmatrix} \text{ and } \mathbf{\Pi}_2 = \begin{bmatrix} 0 & 1 \\ 1 & 0 \end{bmatrix}. \tag{25}$$

For each matrix $\mathbf{\Pi}_m$, similar to Eq. (22), the corresponding QRD-based bound is

$$\begin{aligned} d^{\text{joint}}_{\min} &\geq \min_{i,j=1,\cdots,L,i\neq j} \left\{\left[\tilde{\mathbf{R}}_m\right]^2_{\min}\right\} \min_{s_a,s_b\in\mathbb{S}} \left\| \mathbf{\Pi}_m^T[s_a, s_b]^T \right\|^2_F \\ &= \left[\tilde{\mathbf{R}}_m\right]^2_{\min} d^{\text{all}}_{\min}, \end{aligned} \tag{26}$$

where $\tilde{\mathbf{R}}_m$ is the upper triangular part of the QRD of the equivalent matrix $\mathbf{H}_{u,ij}\mathbf{\Pi}_m$. Note in Eq. (26) that the permutation matrix does not change the distance of $\left\|\mathbf{\Pi}_m^T[s_a, s_b]\right\|^2_F$ and we have $\min_{s_a,s_b\in\mathbb{S}} \left\|\mathbf{\Pi}_m^T[s_a, s_b]^T\right\|^2_F = \min_{s_a,s_b\in\mathbb{S}} \left\|[s_a, s_b]^T\right\|^2_F = d^{\text{all}}_{\min}$. For the permutation matrices given in Eq. (25), we can obtain two different values $[\tilde{\mathbf{R}}_m]_{\min}$, $(m = 1, 2)$, which are given by $[\tilde{\mathbf{R}}_1]_{\min} = \min\{\tilde{R}_{1,1}(\mathbf{\Pi}_1), \tilde{R}_{2,2}(\mathbf{\Pi}_1)\}$ and $[\tilde{\mathbf{R}}_2]_{\min} = \min\{\tilde{R}_{1,1}(\mathbf{\Pi}_2), \tilde{R}_{2,2}(\mathbf{\Pi}_2)\}$. Here, $\tilde{R}_{1,1}(\mathbf{\Pi}_m)$ and $\tilde{R}_{2,2}(\mathbf{\Pi}_m)$, $m = 1, 2$ are the diagonal elements of $\tilde{\mathbf{R}}_m$.

Remark: The bound of Eq. (22) constitutes a special case of the bound of Eq. (26), which can be obtained by setting $m = 1$.

Based on Eq. (26), an improved QRD-based upper bound of the distance $d^{\text{joint}}_{\min}$ is given by

$$\begin{aligned} d^{\text{joint}}_{\min} &\geq d^{\text{QRD-bound\_P}}_{\min} \\ &= \min_{i,j=1,\cdots,L,i\neq j} \{[\tilde{\mathbf{R}}_{QRQ\_P}]^2_{\min}\} d^{\text{all}}_{\min}. \end{aligned} \tag{27}$$

where we have $[\tilde{\mathbf{R}}_{QRQ\_P}]^2_{\min} = \max\{[\tilde{\mathbf{R}}_1]^2_{\min}, [\tilde{\mathbf{R}}_2]^2_{\min}\}$.

Lemma 2: For an $(N_r \times 2)$-element full column-rank matrix $\mathbf{H}_{u,ij}$ having a minimum squared diagonal non-zero entry $[\tilde{\mathbf{R}}]^2_{\min}$ for its QRD and a value of $[\tilde{\mathbf{R}}_{QRQ\_P}]^2_{\min} = \max\{[\tilde{\mathbf{R}}_1]^2_{\min}, [\tilde{\mathbf{R}}_2]^2_{\min}\}$ based on the pair of legitimate permutation matrices $\mathbf{\Pi}_m \in \mathbb{C}^{2\times 2}$, $m = 1, 2$, respectively, the inequality $[\tilde{\mathbf{R}}_{QRQ\_P}]^2_{\min} \geq [\tilde{\mathbf{R}}]^2_{\min}$ is satisfied.

Since we have $[\tilde{\mathbf{R}}]^2_{\min} = [\tilde{\mathbf{R}}_1]^2_{\min}$, Lemma 2 can be obtained.

2) The Proposed QRD-Based ED-TAS: According to Lemma 2, the QRD bound of Eq. (27) is tighter than that of Eq. (22). Hence, we use this tighter bound to derive the proposed QRD-based ED-TAS as

$$\mathbf{H}_{\hat{u}} = \arg \max_{u\in\{1,\cdots,N_U\}} \left\{d^{\text{signal}}_{\min}, d^{\text{spatial}}_{\min}, d^{\text{QRD-bound\_P}}_{\min}\right\}. \tag{28}$$

Note that the complexity of the QRD-based TAS is dominated by the computation of $[\tilde{\mathbf{R}}_m]_{\min}$. In general, the full QRD can be adopted in Eq. (26) for solving Eq. (27). However, this may impose a high complexity. In order to reduce this complexity, for a fixed channel $\mathbf{H}_{u,ij}$, we found that the value of $[\tilde{\mathbf{R}}_m]_{\min}$ only depends on the diagonal entries of $\tilde{\mathbf{R}}_m$, namely $\tilde{R}_{k,k}(\mathbf{\Pi}_m)(k = 1, 2)$, which can be directly calculated as [38]

$$[\tilde{\mathbf{R}}_m]_k = \tilde{R}_{k,k}(\mathbf{\Pi}_m) = \sqrt{\frac{\det[(\mathbf{G}(1:k))^H\mathbf{G}(1:k)]}{\det[(\mathbf{G}(1:k-1))^H\mathbf{G}(1:k-1)]}}, \tag{29}$$

where $\mathbf{G}(1:k)$ denotes a matrix consisting of the first k columns of $\mathbf{H}_{u,ij}\mathbf{\Pi}_m$. In the classic V-BLAST systems, the calculation of Eq. (29) suffers from the problem of having a high complexity [38]. In SM, the number of non-zero elements of the error vectors of SM is up to 2. This sparse character leads to the simple sub-matrix $\mathbf{H}_{u,ij} = [\mathbf{h}_u(i), -\mathbf{h}_u(j)] \in \mathbb{C}^{N_r\times 2}$ and hence the values of $\tilde{R}_{k,k}(\mathbf{\Pi}_m)(m = 1, 2, k = 1, 2)$ are given by

$$\tilde{R}_{1,1}(\mathbf{\Pi}_1) = \sqrt{\|\mathbf{h}_u(i)\|^2_F}, \tag{30}$$

$$\tilde{R}_{2,2}(\mathbf{\Pi}_1) = \sqrt{\frac{\|\mathbf{h}_u(i)\|^2_F + \|\mathbf{h}_u(j)\|^2_F - 2\mathcal{R}\{\mathbf{h}_u(i)^H\mathbf{h}_u(j)\}}{\|\mathbf{h}_u(i)\|^2_F}} \tag{31}$$

$$\tilde{R}_{1,1}(\mathbf{\Pi}_2) = \sqrt{\|\mathbf{h}_u(j)\|^2_F} \tag{32}$$

and

$$\tilde{R}_{2,2}(\mathbf{\Pi}_2) = \sqrt{\frac{\|\mathbf{h}_u(i)\|^2_F + \|\mathbf{h}_u(j)\|^2_F - 2\mathcal{R}\{\mathbf{h}_u(i)^H\mathbf{h}_u(j)\}}{\|\mathbf{h}_u(j)\|^2_F}} \tag{33}$$

The complexity of our proposed QRD-TAS of Eq. (28) is dominated by the computation of $\tilde{R}_{k,k}(\mathbf{\Pi}_m)$, $m = 1, 2$. In SM, these values only depend on the values of $\|\mathbf{h}_u(i)\|^2_F$, $\|\mathbf{h}_u(j)\|^2_F$ and $\mathbf{h}_u(i)^H\mathbf{h}_u(j)$, which are elements of the matrix $\mathbf{H}^H\mathbf{H}$, as shown in Eqs. (30)-(33). Based on this observation, we can calculate the values of $\tilde{R}_{k,k}(\mathbf{\Pi}_m)$, $m = 1, 2$ by reusing these elements for the different TAS candidates $\mathbf{H}_u$,

TABLE I
COMPLEXITY COMPARISON OF DIFFERENT TAS ALGORITHMS FOR SM SYSTEMS

TAS algorithm	ED Optimality	Computational complexity
Exhaustive ED-TAS [13]	optimal	$\frac{N_t(N_t-1)}{2}(5N_r-1)M^2$
Maximum-norm based TAS of [21]	sub-optimal	$2N_tN_r - N_t$
Minimum-correlation based TAS of [15]	sub-optimal	$2N_t^2N_r - N_t^2 + \frac{3}{2}N_t(N_t-1)$
Conventional QRD-based ED-TAS of [24]	optimal	$2N_tN_r - N_t + 32N_t(N_t-1)(N_r-\frac{2}{3})\frac{M}{N_{APM}}$ ($N_{APM}=M$ for PSK, $N_{APM}=4$ for QAM)
Conventional SVD-based ED-TAS of [23]	sub-optimal	$2N_tN_r - N_t + \frac{19}{2}N_t(N_t-1)(N_r-\frac{1}{3})$
Simplified SVD-TAS [25]	sub-optimal	$\frac{N_t(N_t-1)}{2}(2N_r+11) + N_t(2N_r-1)$
Proposed QRD-based ED-TAS	sub-optimal	$2N_t^2N_r + \frac{3}{2}N_t(N_t-1)$
Proposed EVM-based ED-TAS	M-PSK: optimal	$2N_t^2N_r - N_t^2 + \frac{1}{2}N_t(N_t-1)(M+7)$
	$M-\text{QAM}\begin{cases}\text{sub-optimal}, & K<\upsilon\\ \text{optimal}, & K=\upsilon\end{cases}$	$2N_t^2N_r - N_t^2 + \frac{15}{2}GN_t(N_t-1)$
Exhaustive TAS&PA	——	$\binom{N_t}{L}C_{\text{PA}}$
Low-complexity TAS&PA	——	$C_{\text{TAS}} + C_{\text{PA}} = \begin{cases} C_{\text{PQRD}} + C_{\text{PA}} \\ C_{\text{EVM}} + C_{\text{PA}} \end{cases}$

hence the resultant complexity is considerably reduced compared to the conventional QRD-based ED-TAS, as will show in Table I.

To confirm the benefits of the QRD-based bound derived in Eq. (27), Fig. 2 shows the BER performance of the proposed QRD-based ED-TAS algorithm in contrast to the existing SVD-based ED-TAS of [23]. Moreover, we add the performance of the norm-based TAS of [13] and of the exhaustive-search based optimal ED-TAS of [21] as benchmarks. In Fig. 2, the number of TAs is set to $N_t = 4$, where $L = 2$ out of $N_t = 4$ TAs were selected in these TAS algorithms. As expected, since the proposed QRD-based ED-TAS has a tighter bound, in Fig. 2 it performs better than the SVD-based ED-TAS. Quantitatively, observe in Fig. 2 that this scheme provides an SNR gain of about 1.2 dB over the SVD-based ED-TAS at the BER of 10^{-5}. In Fig. 2, we also observe that the QRD-based ED-TAS achieves a near-optimum performance, where the performance gap between the proposed QRD-based ED-TAS and the exhaustive-search-based optimal ED-TAS is only about 0.2 dB. We will provide more detailed comparisons about the BER and the complexity issues in Section VI.

B. The Proposed EVM-Based ED-TAS

In this section, for striking a further flexible tradeoff in terms of the BER attained and the complexity imposed, we propose an EVM-based ED-TAS algorithm. The proposed EVM-TAS directly calculates the value of $d_{\min}(\mathbf{H}_u)$ for the specific TAS candidate $\mathbf{H}_u$, rather than exploiting the equivalent decision metric of Eq. (13) or the estimated bound of (18). Specifically, we will derive simple optimization metrics for both PSK and QAM constellations, where the error-vector selection probability is exploited for reducing the search space.

1) The Calculation of $d_{\min}(\mathbf{H}_u)$ in EVM-Based ED-TAS: Specifically, the M-PSK constellation can be expressed as $\mathbb{S}_{PSK} = \{e^{j\frac{2m\pi}{M}}, m = 0, \cdots, M-1\}$, and the symbols of the rectangular $M = 4^k$ QAM constellation belong to the set of [36]

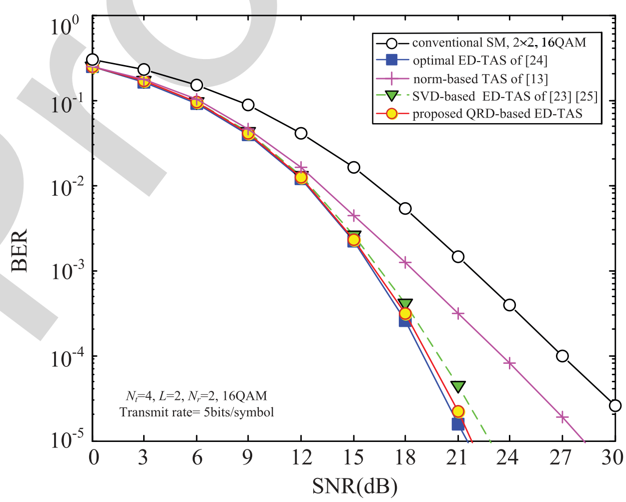

Fig. 2. BER performance comparison of the existing TAS algorithms and the proposed QRD-based ED-TAS algorithm. The setup of the simulation is based on $N_t = 4$, $N_r = 2$, $L = 2$ and 16-QAM. The transmit rate is 5 bits/symbol.

$$\mathbb{S}_{QAM} = \frac{1}{\sqrt{\beta_k}}\{a+bj, a-bj, -a+bj, -a-bj\}, \quad (34)$$

where we have $\beta_k = \frac{2}{3}(4^k - 1)$ and $a, b \in \{1, 3, \cdots, 2^k - 1\}$. Similar to Eq. (14), the calculation of $d_{\min}(\mathbf{H}_u)$ is partitioned into three cases: $d_{\min}^{\text{signal}}$, $d_{\min}^{\text{spatial}}$ and $d_{\min}^{\text{joint}}$. As shown in Eqs. (15)-(16), $d_{\min}^{\text{signal}}$ depends the minimum distance of the APM $d_{\min}^{\text{APM}}$ as [39]

$$d_{\min}^{\text{APM}} = \begin{cases} 4\sin^2(\pi/M) & \text{for} \quad M-\text{PSK} \\ \frac{4}{\beta_k} & \text{for} \quad M-\text{QAM} \end{cases}, \quad (35)$$

while $d_{\min}^{\text{spatial}}$ relies on the minimum squared modulus value $d_{\min}^{\text{Modulus}}$ of the APM constellation as

$$d_{\min}^{\text{Modulus}} = \begin{cases} 1 & \text{for} \quad M-\text{PSK} \\ \frac{2}{\beta_k} & \text{for} \quad M-\text{QAM} \end{cases}. \quad (36)$$

Based on Eqs. (35) and (36), the complexity of computing the values of $d_{\min}^{\text{signal}}$ and $d_{\min}^{\text{spatial}}$ in Eqs. (15)-(16) may be deemed negligible. Hence, we only have to reduce the complexity of computing $d_{\min}^{\text{joint}}$, which can be achieved as follows:

$$\begin{aligned} d_{\min}^{\text{joint}-EVM} &= \min_{\substack{i,j=1,\cdots,L,i\neq j\\ s_a,s_b\in\mathbb{S}}} \|\mathbf{h}_u(i)s_a - \mathbf{h}_u(j)s_b\|_F^2 \\ &= \min_{\substack{i,j=1,\cdots,L,\\ i\neq j,s_a,s_b\in\mathbb{S}}} |s_a|^2\,\|\mathbf{h}_u(i)\|_F^2 + |s_b|^2\,\|\mathbf{h}_u(j)\|_F^2 - 2m_{\text{APM}}, \end{aligned} \tag{37}$$

where we have $m_{\text{APM}} = \mathcal{R}\{s_a^H s_b \mathbf{h}_u(i)^H \mathbf{h}_u(j)\}$, which relies on the specific APM scheme adopted. Next, we will derive the simplified metrics $d_{\min}^{\text{joint}-EVM}$ for the general family of M-PSK and M-QAM modulated SM systems.

2) Simplification for M-PSK Schemes: For a pair of M-PSK symbols $s_a = e^{j\frac{2a\pi}{M}}$ and $s_b = e^{j\frac{2b\pi}{M}}$, the possible values of $s_a^H s_b$ obey $e^{j\frac{2(b-a)\pi}{M}}$, $(b-a) \in \{-(M-1), \cdots, (M-1)\}$. As a result, m_{APM} of the general M-PSK scheme obeys:

$$m_{\text{APM}} \in \{\mathcal{R}\{\mathbf{h}_u(i)^H\mathbf{h}_u(j)\}\cos\theta_n - \mathcal{J}\{\mathbf{h}_u(i)^H\mathbf{h}_u(j)\}\sin\theta_n\}, \tag{38}$$

where $\theta_n = \frac{2n\pi}{M}$, $n = -(M-1), \cdots, (M-1)$. Since the minimum ED is considered in Eq (37), only the maximum value of m_{APM} needs to be considered, which is given by Eq. (39), shown at the bottom of the page. As shown in Eq. (39), the number of possible θ_n values is reduced from $2M-1$ to $\frac{M}{4}+1$. According to Eq. (39), $|s_a|^2 = 1$ and $|s_b|^2 = 1$, the distance $d_{\min}^{\text{joint}-EVM}$ of Eq. (37) is simplified for M-PSK as follows:

$$d_{\min}^{\text{joint}-EVM} = \min_{\substack{i,j=1,\cdots,L,\\ i\neq j}} \|\mathbf{h}_u(i)\|_F^2 + \|\mathbf{h}_u(j)\|_F^2 - 2m_{M-\text{PSK}}(\mathbf{H}_u). \tag{40}$$

Example: The constellation points s_a and s_b of BPSK and QPSK modulation schemes belong to the set $\mathbb{S}_{\text{BPSK}} = \{\pm 1\}$ and $\mathbb{S}_{\text{QPSK}} = \{\pm 1, \pm j\}$, respectively. Based on Eq. (39), the corresponding optimized metrics $m_{M-\text{PSK}}(\mathbf{H}_u) = \max m_{\text{APM}}$ are simplified to $m_{2-\text{PSK}}(\mathbf{H}_u) = \left|\mathcal{R}\{\mathbf{h}_u(i)^H\mathbf{h}_u(j)\}\right|$ and $m_{4-\text{PSK}}(\mathbf{H}_u) = \max\{\left|\mathcal{R}\{\mathbf{h}_u(i)^H\mathbf{h}_u(j)\}\right|, \left|\mathcal{J}\{\mathbf{h}_u(i)^H\mathbf{h}_u(j)\}\right|\}$, respectively.

As shown in Eqs. (37)-(40), since we have $|s_a|^2 = 1$, $|s_b|^2 = 1$ and a reduced set $s_a^H s_b$ for M-PSK constellation, the complexity of calculating $d_{\min}^{\text{joint}-EVM}$ is low, as it will be shown in Table I.

3) Simplification for M-QAM Schemes: When M-QAM constellations are considered, the calculation of $d_{\min}^{\text{joint}-EVM}$ in Eq. (37) becomes substantially complicated, because there are many combinations of the values of $|s_a|^2$, $|s_b|^2$ and $s_a^H s_b$ in Eq. (37), which lead to different received SM-symbol distances. To derive a simplified optimized metrics for M-QAM, we first introduce the following Lemma.

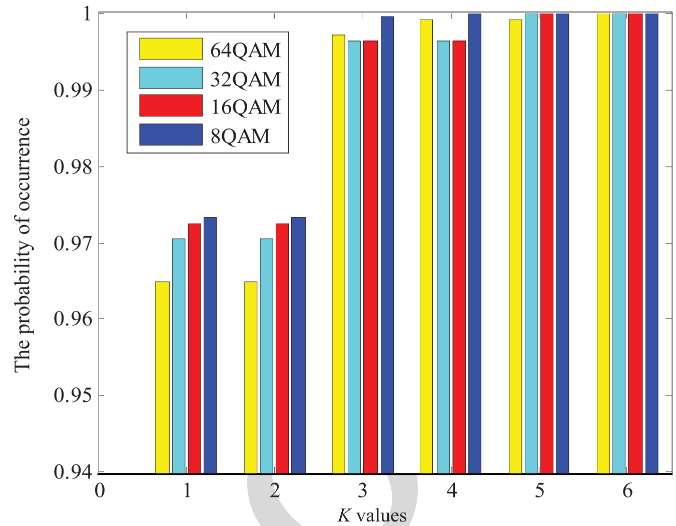

Fig. 3. The statistical probability of the norm error vectors relying on K minimum moduli, yielding the optimal ED-TAS solution, where the system setup is $N_t = 4$, $N_r = 2$ and $L = 2$.

Lemma 3: It is highly likely that an error vector associated with a small norm value yields the FD value of Eq. (9). Thus, the search space to be evaluated for finding the FD can be reduced to a few dominant error vectors having small norm values.

Proof: Based on the Rayleigh-Ritz theorem of [37], for a fixed channel matrix $\mathbf{H}_{u,ij}$ and a given error vector $\mathbf{e}_{ij}$, the distance amongst the received symbols is bounded by $\lambda_{\max}^2(\mathbf{H}_{u,ij})\left\|\mathbf{e}_{ij}\right\|^2 \geq \left\|\mathbf{H}_u\mathbf{e}_{ij}\right\|^2 \geq \lambda_{\min}^2(\mathbf{H}_{u,ij})\left\|\mathbf{e}_{ij}\right\|^2$, where $\lambda_{\max}^2(\mathbf{H}_{u,ij})$ is the maximum squared singular value of the submatrix $\mathbf{H}_{u,ij} = [\mathbf{h}_u(i), -\mathbf{h}_u(j)]$. It may be readily shown that the values of $\lambda_{\max}^2(\mathbf{H}_{u,ij})$ and $\lambda_{\min}^2(\mathbf{H}_{u,ij})$ are constants for a fixed channel realization $\mathbf{H}_{u,ij}$, while the value of $\left\|\mathbf{e}_{ij}\right\|^2$ depends on the specific APM constellation points. Based on the bound above, it is highly likely that an $\mathbf{e}_{ij}$ with a small norm yields low upper bound and lower bound. Hence it has a high probability of generating the FD value, as it will be exemplified in Fig. 3. ■

Based on Lemma 3, for the sake of striking a beneficial trade-off between the BER performance and complexity for M-QAM, the search space is limited to the error vectors having small modulus values and only these vectors are utilized to compute the FD metric. Specifically, we first evaluate all possible modulus values $T_1, T_2, T_3, \cdots, T_v$ of all the legitimate error vectors $\mathbf{e}_{ij}$, then we find the K smallest T_K from the full set of $\{T_1, T_2, T_3, \cdots, T_v\}$ and only consider the set of $\mathbf{e}_{ij}$ having moduli lower than T_K to compute $d_{\min}(\mathbf{H}_u)$. In this process, the error vectors can be divided into the pair of sub-sets $\mathbb{D}_1$ and $\mathbb{D}_2$ based on their sparsity, where $\mathbb{D}_1$ contains the error vectors, which have only a single non-zero element, while $\mathbb{D}_2$ contains

$$\begin{aligned} m_{M-\text{PSK}}(\mathbf{H}_u) = \max_n m_{\text{APM}} &= \max_{n\in\{-(M-1),\cdots,M-1\}} \{\mathcal{R}\{\mathbf{h}_u(i)^H\mathbf{h}_u(j)\}\cos\theta_n - \mathcal{J}\{\mathbf{h}_u(i)^H\mathbf{h}_u(j)\}\sin\theta_n\} \\ &= \max_{n\in\{0,\cdots,M/4\}} \{\left|\mathcal{R}\{\mathbf{h}_u(i)^H\mathbf{h}_u(j)\}\cos\theta_n - \mathcal{J}\{\mathbf{h}_u(i)^H\mathbf{h}_u(j)\}\sin\theta_n\right|\}. \end{aligned} \tag{39}$$

the error vectors, which have two non-zero elements. As will be shown in our simulation results, $K=3$ is a good choice for diverse configurations, hence we only provide the simplified expressions of $d_{\min}^{\text{joint}-EVM}$ for $K \le 3$ as follows.

For $K=1$, according to the M-QAM constellation of Eq. (34), only error vectors having $T_1 = \sqrt{\frac{4}{\beta_k}}$ are considered and the associated sets $\mathbb{D}_1$ and $\mathbb{D}_2$ are given by $\mathbb{D}_1 = \frac{1}{\sqrt{\beta_k}}\{\pm 2\mathbf{e}_i, \pm 2\mathrm{j}\mathbf{e}_i\}, i = 1, \cdots, L$ and $\mathbb{D}_2 = \frac{1}{\sqrt{\beta_k}}\{(\pm 1 \pm 1\mathrm{j})\mathbf{e}_i - (\pm 1 \pm 1\mathrm{j})\mathbf{e}_j\}, i, j = 1, \cdots, L, i \neq j$, respectively, where $\mathbf{e}_i$ and $\mathbf{e}_j$ are the active TA selection vectors in Eq. (2). Since only the minimum ED is considered, the set $\mathbb{D}_1$ can be reduced to $\mathbb{D}_1 = \frac{1}{\sqrt{\beta_k}}\{2\mathbf{e}_i\}, i = 1, \cdots, L$. Moreover, based on the set $\mathbb{D}_2$, it is find that the elements s_a and s_b belong to the reduced set $\frac{1}{\sqrt{\beta_k}}\{\pm 1 \pm 1\mathrm{j}\}$ and we have $|s_a|^2 = \frac{2}{\beta_k}$, $|s_b|^2 = \frac{2}{\beta_k}$ and $s_a^H s_b \in \frac{2}{\beta_k}\{\pm 1, \pm 1\mathrm{j}\}$. Substituting these values into Eq. (37), we get the simplified optimized metric for $K=1$ as

$$d_{\min,K=1}^{\text{joint}-EVM} = \min_{\substack{i,j=1,\cdots,L,\\ i\neq j,}} \frac{2}{\beta_k}\|\mathbf{h}_u(i)\|_F^2 + \frac{2}{\beta_k}\|\mathbf{h}_u(j)\|_F^2 - 2m_{M-QAM}^{K=1}, \tag{41}$$

where we have

$$\begin{aligned} m_{M-QAM}^{K=1} &= \max m_{\text{APM}} \\ &= \max\left\{\frac{2}{\beta_k}\left|\mathcal{R}\{\mathbf{h}_u(i)^H\mathbf{h}_u(j)\}\right|, \frac{2}{\beta_k}\left|\mathcal{I}\{\mathbf{h}_u(i)^H\mathbf{h}_u(j)\}\right|\right\}. \end{aligned} \tag{42}$$

For the case of $K=2$, all the error vectors $\mathbf{e}_{ij}$ having moduli lower than T_2 are used for FD calculation. Compared to $K=1$, we have to consider the added error vectors $\frac{1}{\sqrt{\beta_k}}\{\pm 2 \pm 2\mathrm{j}\mathbf{e}_i\} (i = 1, \cdots, L)$ having $T_2 = \sqrt{\frac{8}{\beta_k}}$, which belong to $\mathbb{D}_1$ and do not change the set $\mathbb{D}_2$. After eliminating all collinear elements, the set $\mathbb{D}_1$ of $K=2$ is reduced to $\frac{1}{\sqrt{\beta_k}}\{2\mathbf{e}_i, \pm 2 \pm 2\mathrm{j}\mathbf{e}_i\}, i = 1, \cdots, L$. Moreover, since only the minimum distance is investigated, the set is further reduced to $\mathbb{D}_1 = \frac{1}{\sqrt{\beta_k}}\{2\mathbf{e}_i\}, i = 1, \cdots, L$, which is the same as that of $K=1$. Therefore, the setups of $K=1$ and $K=2$ will provide the same FD $d_{\min}(\mathbf{H}_u)$.

Moreover, for the case of $K=3$, besides the error vectors $\mathbf{e}_{ij}$ for $K=2$, the error vectors having $T_3 = \sqrt{\frac{10}{\beta_k}}$ should be considered, which are given by $\frac{1}{\sqrt{\beta_k}}\{(\pm 3 \pm 1\mathrm{j})\mathbf{e}_i - (\pm 1 \pm 1\mathrm{j})\mathbf{e}_j, (\pm 1 \pm 3\mathrm{j})\mathbf{e}_i - (\pm 1 \pm 1\mathrm{j})\mathbf{e}_j\}$, $i, j = 1, \cdots, L, i \neq j$. For these added error vectors, we have $s_a^H s_b \in \frac{1}{\beta_k}\{\pm 2 \pm 4\mathrm{j}, \pm 4 \pm 2\mathrm{j}\}$ and two legitimate combinations of the values of $|s_a|^2$ and $|s_b|^2$ as: (1) $|s_a|^2 = \frac{2}{\beta_k}$, $|s_b|^2 = \frac{10}{\beta_k}$ and (2) $|s_a|^2 = \frac{10}{\beta_k}$, $|s_b|^2 = \frac{2}{\beta_k}$. For each combination, similar to the process of Eqs. (41)-(42), we can substitute the values of $|s_a|^2$, $|s_b|^2$ and $s_a^H s_b$ into Eq. (37) and get the simplified optimized metric for $K=3$ as

$$d_{\min,K=3}^{\text{joint}-EVM} = \min\{d_{\min,K=1}^{\text{joint}-EVM}, d_{\min,(1)}^{\text{joint}-EVM}, d_{\min,(2)}^{\text{joint}-EVM}\} \tag{43}$$

where $d_{\min,(1)}^{\text{joint}-EVM}$ and $d_{\min,(2)}^{\text{joint}-EVM}$ are the simplified ED for the above-mentioned two combinations, given by Eq. (44), shown at the bottom of the page.

4) The Proposed EVM-Based ED-TAS: Based on the simplified versions of $d_{\min}^{\text{joint}-EVM}$ for M-PSK and M-QAM schemes derived in Eqs. (41) and (43), the solution of our EVM-based ED-TAS algorithm is given by

$$\mathbf{H}_{\hat{u}} = \arg \max_{u\in\{1,\cdots,N_U\}} \left\{d_{\min}^{\text{signal}}, d_{\min}^{\text{spatial}}, d_{\min}^{\text{joint}-EVM}\right\}. \tag{45}$$

Note that similar to the proposed QRD-TAS, the terms $\|\mathbf{h}_u(i)\|_F^2$, $\|\mathbf{h}_u(j)\|_F^2$ and $\mathbf{h}_u(i)^H\mathbf{h}_u(j)$ in Eqs. (40)-(44) are elements of the matrix $\mathbf{H}^H\mathbf{H}$. Then, we can find the solution of Eq. (45) by reusing these elements for different TAS candidates $\mathbf{H}_u$.

Fig. 3 shows the probability that the error vectors having the minimum norm do result in finding the optimal ED-TAS solution as a function of K. For example, we have a probability of 97% for 16-QAM modulated SM for $K=1$ using $N_t=4$, $L=2$ and $N_r=2$. Moreover, it is observed from Fig. 3 that this probability is also high for other QAM schemes; hence the EVM-based ED-TAS can be readily used in diverse scenarios. In general, for striking a flexible BER vs complexity tradeoff, we can adjust the parameter K to reduce the search space to a subset of the error vectors that may yield the optimal ED-TAS solution with a high probability.

Note that in [17] a PEP-based TAS (PEP-TAS) algorithm was proposed, which was based on a different search set reduction. The main differences of the proposed EVM-TAS and the PEP-TAS of [17] are:

- The PEP-TAS is based on the assumption that a smaller APM symbol amplitude leads to a smaller distance $d_{\min}^{\text{joint}}$, whereas based on our analysis it is highly likely that an error vector with a small norm yields the distance $d_{\min}^{\text{joint}}$.
- Moreover, in EVM-TAS, we propose to use the parameter K for striking a flexible tradeoff between the conflicting factors of the computational complexity imposed and the attainable BER.

Remark: Compared to the EVM-TAS, the PEP-TAS considers only the error vectors generated by M-QAM symbols having the minimum amplitude. It can be shown that the nonlinear error vectors of the PEP-TAS are the same as those of the

$$\begin{cases} d_{\min,(1)}^{\text{joint}-EVM} = \min\limits_{\substack{i,j=1,\cdots,L\\ i\neq j}} \frac{2}{\beta_k}\|\mathbf{h}_u(i)\|_F^2 + \frac{10}{\beta_k}\|\mathbf{h}_u(j)\|_F^2 - 2m_{M-QAM}^{K=3} \\ d_{\min,(2)}^{\text{joint}-EVM} = \min\limits_{\substack{i,j=1,\cdots,L\\ i\neq j}} \frac{10}{\beta_k}\|\mathbf{h}_u(i)\|_F^2 + \frac{2}{\beta_k}\|\mathbf{h}_u(j)\|_F^2 - 2m_{M-QAM}^{K=3} \end{cases} \tag{44}$$

$$m_{M-QAM}^{K=3} = \max \frac{1}{\beta_k}\left\{\left|2\mathcal{R}\{\mathbf{h}_u(i)^H\mathbf{h}_u(j)\}\right| + \left|4\mathcal{I}\{\mathbf{h}_u(i)^H\mathbf{h}_u(j)\}\right|, \left|4\mathcal{R}\{\mathbf{h}_u(i)^H\mathbf{h}_u(j)\}\right| + \left|2\mathcal{I}\{\mathbf{h}_u(i)^H\mathbf{h}_u(j)\}\right|\right\}$$

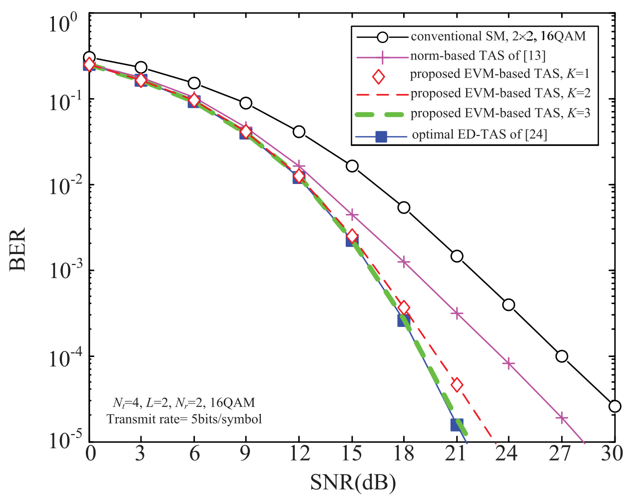

Fig. 4. BER performance comparison of the existing TAS algorithms and the proposed EVM-based TAS algorithm for $N_t = 4$, $N_r = 2$, 16QAM and $L = 2$. The transmit rate is 5 bits/symbol.

EVM-TAS associated with $K = 1$. Therefore, it can be viewed as a special case of EVM-TAS by setting $K = 1$.

Fig. 4 shows our BER comparison for the existing TAS algorithms and the proposed EVM-TAS algorithm. The simulation parameters are the same as those of Fig. 2. Firstly, as proved in Section IV-B and observed in Fig. 3, the probability that the error vectors do indeed result in the optimal ED-TAS solution is the same for the cases of $K = 1$ and $K = 2$. Hence, they provide the same BER performance, as shown in Fig. 4. Furthermore, we observe in Fig. 3 that this probability is increased from 0.975 to 0.998 upon increasing K from 1 to 3. As a result, in Fig. 4 the performance of the EVM-based ED-TAS associated with $K = 3$ is improved compared to that scheme with $K = 1$. Moreover, compared the results in Figs. 2 and 4, the EVM-based ED-TAS outperforms the SVD-based ED-TAS for $K = 3$.

V. Joint TAS and PA Algorithms for SM

Similar to the TAS technique, PA is another attractive link adaptation technique conceived for SM, which has been advocated in [7], [11], [28], [29]. The process of PA can be modeled by the PA matrix $\mathbf{P}$, which is given by

$$\mathbf{P} = \text{diag}\{p_1, \cdots, p_q, \cdots, p_L\}, \tag{46}$$

where p_q controls the channel gain of the qth TA. Here, we let $\sum_{q=1}^{L} p_q^2 = 1$ for normalizing the transmit power. Based on our TAS algorithms, we propose a pair of combined algorithms for jointly considering the PA and TAS as follows:

1) **TAS&PA**
   - *Step 1*: Each $(N_r \times N_t)$ channel matrix $\mathbf{H}$ has $N_U = \binom{N_t}{L}$ possible subchannel matrices $\mathbf{H}_u$, each of which corresponds to a specifically selected $(N_r \times L)$ MIMO channel. For each $\mathbf{H}_u$, we calculate the corresponding PA matrix $\mathbf{P}_u$ and its FD with the aid of the algorithm of [29].
   - *Step 2*: The particular combinations of $\mathbf{H}_u\mathbf{P}_u (u = 1, \cdots, N_U)$ constitute the legitimate TAS&PA candidates. Let us interpret the matrices $\mathbf{H}_u\mathbf{P}_u$ $(u = 1, \cdots, N_U)$ as being the equivalent channel matrices of Section IV and select the specific candidate with the maximum free distance as the final solution.

   Since for each channel realization $\mathbf{H}$, there are N_U possible PA matrices $\mathbf{P}_u (u = 1, \cdots, N_U)$, we have a high computational complexity if N_U is high. Next, we introduce a lower-complexity solution for this joint TAS and PA algorithm.

2) **Low-complexity TAS&PA**
   - *Step 1*: Assume $\mathbf{P}_u = \mathbf{I}_L (u = 1, \cdots, N_U)$ and use the proposed low-complexity QRD-based ED-TAS or the EVM-based ED-TAS algorithm to select a particular subset of TAs from the set of options, which corresponds to $\mathbf{H}_{\hat{u}}$.
   - *Step 2*: Calculate the power weights for the selected TAs, which can be represented by the PA matrix $\mathbf{P}_{\hat{u}}$. During this step, the low-complexity PA algorithm of [29] can be invoked. In the simple TAS&PA, the PA matrix only has to be calculated once, hence the associated complexity is low.

VI. Simulation Results

In this section, we provide simulation results for further characterizing the proposed QRD-based ED-TAS, EVM-based ED-TAS and TAS&PA schemes for transmission over frequency-flat fading MIMO channels. For comparison, these performance results are compared to various existing TAS-SM schemes of [13], [21], [23], [25], to the classic TAS/maximal-ratio combining (TAS/MRC) schemes of [40], as well as to the TAS&PA aided V-BLAST of [32]. In our simulations, the single-stream ML detector of [34], [35] is utilized.

A. BER Comparisons of Different TAS Algorithms for SM

In Fig. 5, we compare the BER performance of various TAS-SM schemes for 4 bits/symbol associated with $N_t = 8$, $L = 4$, $N_r = 4$ and QPSK. We also considered the conventional single-RF based TAS/MRC arrangement of [40] as benchmarker. As seen from Fig. 5, the proposed QRD-based ED-TAS outperforms the conventional SVD-based ED-TAS of [23], as also formally shown in Fig. 2. Moreover, as expected, in Fig. 5 the EVM-based TAS is capable of achieving the same performance as the optimal ED-TAS of [21]. We also confirm that our proposed EVM-based ED-TAS schemes outperform the norm-based TAS of [13] and the QRD-based ED-TAS proposed for PSK modulation. These results are consistent with the analysis results in Section IV, where the EVM-based TAS has considered all legitimate error vectors for simplifying $d_{\min}^{\text{joint}}$ in Eq. (40), while the QRD-based ED-TAS may achieve uncorrect estimation of $d_{\min}^{\text{joint}}$ due to the employment of lower bound of Eq. (27).

Fig. 5 also shows that our new TAS-SM schemes outperform the TAS/MRC scheme of [40]. The main reason behind the poorer performance of TAS/MRC is the employment of a higher modulation order required for achieving the same

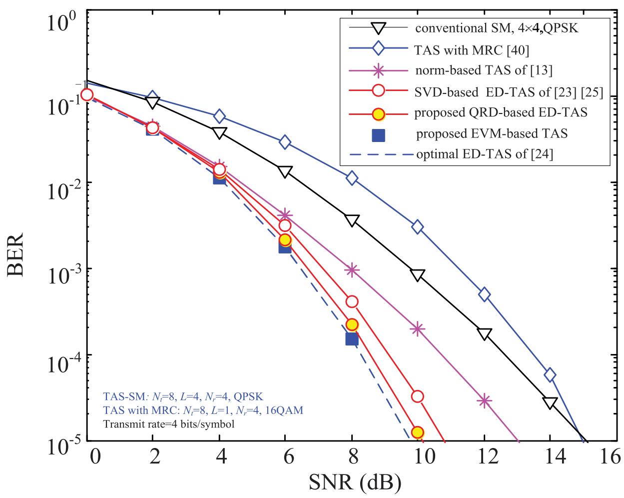

Fig. 5. BER comparison at $m = 4$ bits/symbol for the proposed TAS-SM schemes, the existing TAS-SM schemes and the classic TAS/MRC scheme having $N_t = 8$ and $L = 4$.

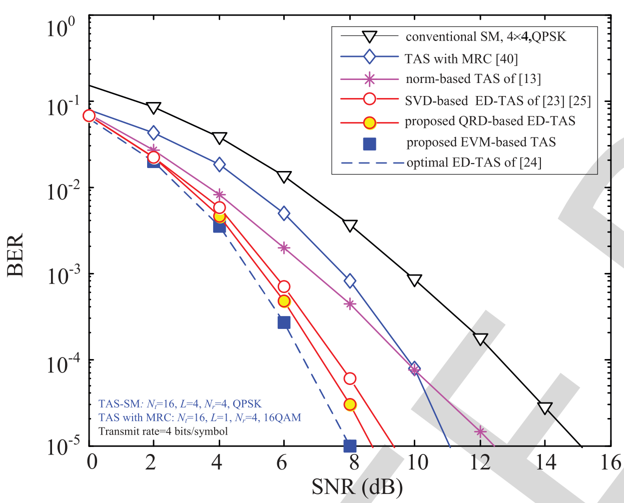

Fig. 6. BER comparison at $m = 4$ bits/symbol for the proposed TAS-SM schemes, the existing TAS-SM schemes and the classic TAS/MRC scheme having $N_t = 16$ and $L = 4$.

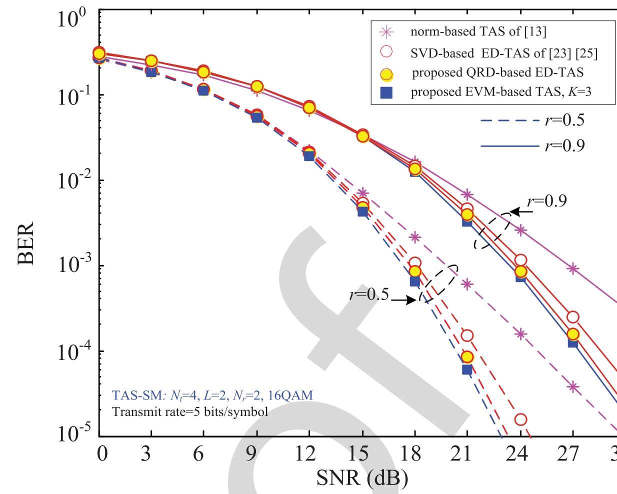

Fig. 7. BER comparison of different TAS algorithms for SM systems in correlated Rayleigh fading channels.

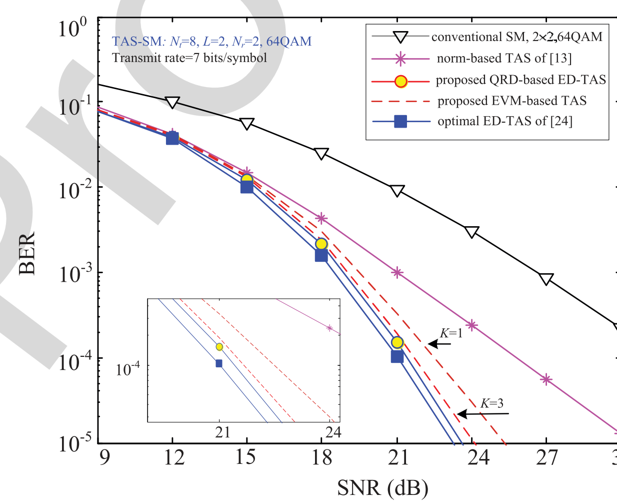

Fig. 8. BER comparison at $m = 7$ bits/symbol for the proposed QRD-based ED-TAS and EVM-based ED-TAS with 64-QAM.

throughput as our SM-based schemes. Note that this benefit depends on the particular MIMO setups. To be specific, as noted in [23], the TAS-SM and the TAS/MRC schemes exhibit different BER advantages for different system setups. However, similar to the results achieved in [23], our new TAS-SM schemes strike an attractive tradeoff between the complexity and the BER attained. The above-mentioned trends of these proposed TAS-SM schemes are also confirmed in Fig. 6, where the number N_t of TAs increases from 8 to 16.

In Fig. 7, a spatially correlated MIMO channel model characterized by $\mathbf{H}^{corr} = \mathbf{R}_r^{1/2}\mathbf{H}\mathbf{R}_t^{1/2}$ [24], [41] is considered for the proposed QRD-based ED-TAS and EVM-based TAS ($K = 3$) schemes, where $\mathbf{R}_t = [r_{ij}]_{N_t \times N_t}$ and $\mathbf{R}_r = [r_{ij}]_{N_r \times N_r}$ are the positive definite Hermitian matrices that specify the transmit and receive correlations, respectively. In Fig. 7, the components of $\mathbf{R}_t$ and $\mathbf{R}_r$ are calculated as $r_{ij} = r_{ji}^* = r^{j-i}$ for $i \le j$, where r is the correlation coefficient ($0 \le r \le 1$). Here, the simulation parameters are the same as those of Figs. 2 and 4 for 5 bits/symbol transmissions. We found that the BER curves of the EVM-based TAS schemes and of the optimal ED-TAS are almost overlapped (similar to the results seen in Fig. 4), hence for clarity in Fig. 7 we simply provide the BER curves for the EVM-based TAS schemes only. Compared to the BER curves in Figs. 2 and 4 for the correlation coefficient $r = 0$, we observe in Fig. 7 that the BER performance of all schemes is substantially degraded by these correlations. However, the proposed schemes remain capable of operating efficiently for the correlated channels.

In Fig. 8, we further compare the proposed QRD-based ED-TAS scheme and the proposed EVM-based TAS schemes for a higher modulation order, where the 64-QAM scheme is employed. Observe in Fig. 8 that the proposed QRD-based ED-TAS scheme outperforms the EVM-based TAS scheme in conjunction with $K = 1$ and the corresponding performance gain is seen to be about 1 dB. Similar to the results in Figs. 2 and 4, the EVM-based TAS associated with $K = 3$ provide an improved BER compared to that scheme with $K = 1$. At

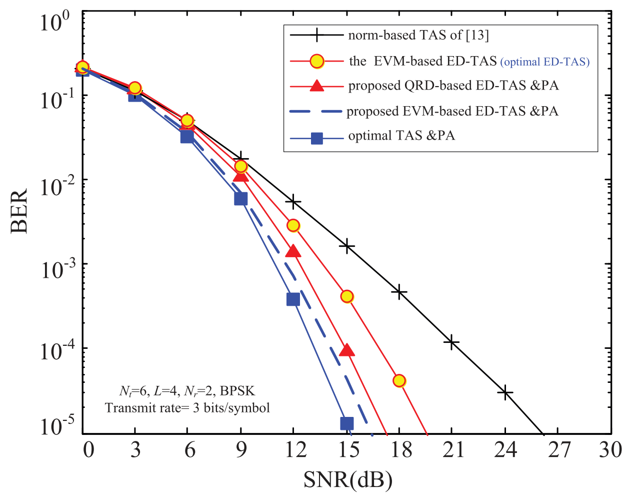

Fig. 9. BER performance comparison of the TAS algorithms and of the proposed TAS &PA algorithms in SM systems, having the transmit rate of 3 bits/symbol.

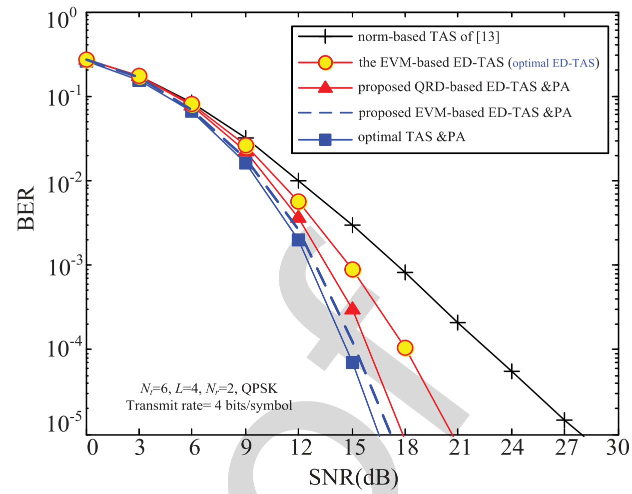

Fig. 10. BER performance comparison of the TAS algorithms and of the proposed TAS &PA algorithms in SM systems, having the transmit rate of 4 bits/symbol.

BER=10^{-5}, the performance gap between the proposed EVM-based TAS with $K = 3$ and the proposed QRD-based ED-TAS becomes negligible.

The main conclusions observed from Figs. 2, 4 and 5–8 are: (1) the proposed EVM-based TAS and QRD-based ED-TAS schemes exhibit different BER advantages for different system setups; (2) the proposed QRD-based ED-TAS is preferred to the QAM-modulated SM schemes, since its complexity is independent of the modulation order; (3) The proposed EVM-based TAS is preferred to the PSK-modulated SM schemes, since it can achieve the performance of optimal ED-TAS at the reduced error vector set. (4) For the QAM-modulated SM schemes, the parameter K of the proposed EVM-based TAS can be flexibly selected for striking a beneficial trade-off between the complexity imposed and the BER attained.

B. BER Comparisons of TAS Algorithms and TAS &PA Algorithms for SM

In this subsection, we focus our attention on studying the BER performance of our TAS&PA algorithms. Here, for the low-complexity TAS&PA, the proposed QRD-based ED-TAS as well as the EVM-based ED-TAS algorithms are utilized and the corresponding algorithms are termed as the QRD-based ED-TAS &PA and the EVM-based ED-TAS &PA, respectively. Note that the EVM-based ED-TAS achieves the same performance as the optimal ED-TAS for the PSK-modulated SM schemes. The BER performances of other TAS algorithms are similar to the results seen in Figs. 2, 4 and 5–8. Hence, for clarity, when only pure TAS is considered, we simply provide the corresponding BER curves of the proposed EVM-based ED-TAS and of the conventional norm-based TAS as benchmarkers.

Fig. 9 compares the BER performance of the proposed TAS&PA arrangement to that of other SM-based schemes. In Fig. 9, the parameter setup is $N_t = 6$, $L = 4$, $N_r = 2$ and $M = 2$. It becomes clear from Fig. 9 that the TAS&PA algorithms advocated outperform both the EVM-based ED-TAS and the norm-based ED-TAS. At a BER of 10^{-5}, the exhaustive-search based optimal TAS&PA provides 9.5 dB and 4 dB SNR gains over the norm-based ED-TAS and over the EVM-based ED-TAS, respectively. Moreover, the low-complexity QRD-based ED-TAS &PA provides about 4 dB SNR gain over the EVM-based TAS operating without PA.

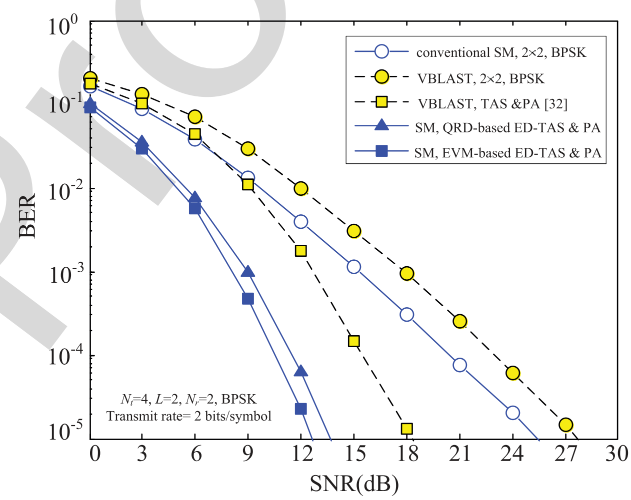

Fig. 11. BER performance comparison of the proposed TAS &PA algorithms in SM systems and the conventional identical-throughput TAS&TA algorithm in V-BLAST systems, where the throughput is 2 bits/symbol ($N_t = 4$, $N_r = 2$, $L = 2$).

Fig. 9 also shows that the EVM-based ED-TAS &PA outperforms the QRD-based ED-TAS&PA and is capable of achieving almost the same BER performance as the optimal TAS&PA. The performance advantages of our schemes are attained as a result of exploiting all the benefits of MIMO channels. The above-mentioned trends of these TAS&PA algorithms recorded for SM are also visible in Fig. 10, where a SM system using $N_t = 6$, $L = 4$, $N_r = 2$ and QPSK modulation is considered.

In Fig. 11, the BPSK-modulated V-BLAST scheme and its TAS&PA-aided counterpart [32] associated with zero-forcing successive interference cancellation (ZF-SIC) are compared to

TABLE II

COMPLEXITY COMPARISON OF DIFFERENT TAS-SM ALGORITHMS IN DIVERSE CONFIGURATIONS

TAS algorithm	Configuration 1 ($N_t = 4$, $N_r = 2$ $L = 2$, 16QAM)	Configuration 2 ($N_t = 8$, $N_r = 4$ $L = 4$, QPSK)	Configuration 3 ($N_t = 8$, $N_r = 2$ $L = 2$, 64-QAM)
Exhaustive ED-TAS [13]	13824	8512	1032192
Maximum-norm based TAS [21]	12	56	24
Conventional QRD-based ED-TAS [24]	2060	6029	38253
SVD-based ED-TAS [25]	102	588	444
Proposed QRD-based ED-TAS	82	596	340
Proposed EVM-based ED-TAS	84, $K = 1$; 180, $K = 3$	756	360, $K = 1$; 808, $K = 3$
Exhaustive TAS&PA	4626	46340	256788
Proposed QRD-based ED-TAS&PA	853	1004	9511
Proposed EVM-based ED-TAS&PA	855, $K = 1$; 951, $K = 3$	1164	9531, $K = 1$; 9979, $K = 3$

our TAS&PA based schemes. For maintaining an identical-throughput, in Fig. 11 we let $N_t = 4$, $N_r = 2$, $L = 2$ and use BPSK for all schemes. Observe in Fig. 11 that our TAS&PA based SM schemes outperform the TAS&PA aided V-BLAST schemes by about 5-6 dB SNR at the BER of 10^{-5}.

C. Complexity Comparison

Table I shows the complexity comparison of various TAS algorithms conceived for SM, where the total number of floating point operations is considered. The Appendix provides the details of our computational complexity evaluations for the proposed TAS algorithms list in Table I. The complexity estimation of the existing TAS algorithms can be found in [15], [23] and [24]. Moreover, our complexity analysis is similar to that of [23] and [24].

Explicitly, in Table II, the quantified complexity of different TAS algorithms for some specific configurations are provided. As shown in Table I, the proposed QRD-based ED-TAS has a similar complexity order to that of the low-complexity SVD-based ED-TAS of [23], while exhibiting a lower complexity compared to the conventional QRD-based ED-TAS of [24]. For example, the proposed QRD-based ED-TAS imposes an approximately 168 times and 25 times lower complexity than the exhaustive ED-TAS and the conventional QRD-based ED-TAS for configuration 1. This is due to the fact that it is capable of avoiding the high-complexity QRD operation by directly computing the bound parameters of Eq. (27). Moreover, as shown in Tables I-II and Figs. 4-8, the EVM-based ED-TAS advocated is capable of striking a flexible BER vs complexity trade-off by employing the parameter K for diverse M-QAM schemes. Furthermore, the proposed low-complexity TAS&PA schemes impose a lower complexity than the exhaustive-search based TAS&PA and only impose a slightly increased complexity compared to the proposed EVM-based TAS and QRD-based TAS schemes. By considering the BER vs complexity results of Tables I-II and Figs. 9-11, the proposed low-complexity TAS&PA is seen to provide an improved BER performance at a modest complexity cost.

VII. CONCLUSIONS

In this paper, we have investigated TAS algorithms conceived for SM systems. Firstly, a pair of low-complexity ED-TAS algorithms, namely the QRD-based ED-TAS and the EVM-based ED-TAS, were proposed. The theoretical analysis and simulation results indicated that the QRD-based ED-TAS exhibits a better BER performance compared with the conventional SVD-based ED-TAS, while the EVM-based ED-TAS is capable of striking a flexible BER vs complexity trade-off. To further improve the attainable performance, the proposed TAS algorithms were amalgamated with PA. A pair of beneficial joint TAS-PA algorithms were proposed and our simulation results demonstrated that they outperform both the pure TAS algorithms and the TAS&PA algorithm designed for spatial multiplexing systems.

APPENDIX

Computational complexity of the proposed TAS algorithms designed for SM systems.

A. The Proposed QRD-Based ED-TAS

As detailed in Section IV-A, the calculation of the QRD-based bound of Eq. (27) only depends on the elements of the matrix $\mathbf{H}^H\mathbf{H}$, which incurs a complexity in the order of $comp(\mathbf{H}^H\mathbf{H}) = 2N_t^2N_r - N_t^2$. Then, we can calculate the values of $\tilde{R}_{k,k}(\mathbf{\Pi}_m), (m = 1, 2,\ \ k = 1, 2)$ in Eqs. (30)-(33) by reusing these elements for the different TAS candidates $\mathbf{H}_u$. Specifically, the calculation of $\sqrt{\|\mathbf{h}_u(j)\|_F^2}$, $j = 1, \cdots, N_t$ for estimating $\tilde{R}_{1,1}(\mathbf{\Pi}_m)$, $m = 1, 2$ in Eqs. (30) and (32) requires N_t flops. Moreover, to calculate the values of $\tilde{R}_{2,2}(\mathbf{\Pi}_m)$, $m = 1, 2$ in Eqs. (31) and (33), we have to consider $\binom{N_t}{2}$ possible combinations (i, j) for computing the value of $\sqrt{\frac{\|\mathbf{h}_u(i)\|_F^2+\|\mathbf{h}_u(j)\|_F^2-2\mathcal{R}\{\mathbf{h}_u(i)^H\mathbf{h}_u(j)\}}{\|\mathbf{h}_u(j)\|_F^2}}$. For each combination, the complexity imposed is 5 flops. Hence, the complexity of computing $\tilde{R}_{2,2}(\mathbf{\Pi}_m)$, $m = 1, 2$ is $5\binom{N_t}{2}$ flops. The overall complexity of the proposed QRD-based ED-TAS is

$$C_{\text{PQRD}} = 2N_t^2N_r - N_t^2 + N_t + 5\binom{N_t}{2} = 2N_t^2N_r + \tfrac{3}{2}N_t(N_t - 1). \tag{47}$$

Note that based on Eq. (28), $d_{\min}^{\text{Modulus}}$, $d_{\min}^{\text{APM}}$ and $d_{\min}^{\text{all}}$ are constants for a specific APM scheme and the calculation of $d_{\min}^{\text{signal}}$ and $d_{\min}^{\text{spatial}}$ can also exploit the common elements, such as $\|\mathbf{h}_u(i)\|_F^2 + \|\mathbf{h}_u(j)\|_F^2 - 2\mathcal{R}\{\mathbf{h}_u(i)^H\mathbf{h}_u(j)\}$, $\|\mathbf{h}_u(i)\|_F^2$, in the calculation of the bound of $d_{\min}^{\text{joint}}$, as shown in Eqs. (15) and (16). Hence, the complexity imposed can be deemed negligible.

B. The Proposed EVM-Based ED-TAS

Similar to the proposed QRD-based ED-TAS, the computational complexity of EVM-based ED-TAS is also dominated by computing $d_{\min}^{\text{joint}}$. Specifically, we also first have to evaluate the elements $\|\mathbf{h}_u(i)\|_F^2$, $\|\mathbf{h}_u(j)\|_F^2$ and $\mathbf{h}_u(i)^H\mathbf{h}_u(j)$, which incurs a complexity of $2N_t^2N_r - N_t^2$ flops. Then, for M-PSK, the simplified version of $d_{\min}^{\text{joint}}$ is given in Eq. (40), which has to consider $\binom{N_t}{2}$ legitimate TA combination (i, j). For each combination (i, j), the computation of the term $m_{M\text{–PSK}}(\mathbf{H}_u)$ of Eq. (39) has to consider $(\frac{M}{4}+1)$ possible θ_n values. For each θ_n, the complexity of evaluating $\left|\Re\{\mathbf{h}_u(i)^H\mathbf{h}_u(j)\}\cos\theta_n - \Im\{\mathbf{h}_u(i)^H\mathbf{h}_u(j)\}\sin\theta_n\right|$ is 4 flops. Moreover, for a specific $m_{M\text{–PSK}}(\mathbf{H}_u)$ and a fixed combination (i, j), the computation of $\|\mathbf{h}_u(i)\|_F^2 + \|\mathbf{h}_u(j)\|_F^2 - 2m_{M\text{–PSK}}(\mathbf{H}_u)$ in Eq. (40) requires 3 flops. Hence, the overall complexity of the M-PSK modulated EVM-based ED-TAS is

$$\begin{aligned} C_{\text{EVM}} &= 2N_t^2N_r - N_t^2 + \binom{N_t}{2}\left\{4\left(\frac{M}{4}+1\right)+3\right\} \\ &= 2N_t^2N_r - N_t^2 + \frac{1}{2}N_t(N_t-1)(M+7). \end{aligned} \tag{48}$$

For the M-QAM scheme, this complexity depends on the parameter K. Specifically, the simplified versions of $d_{\min}^{\text{joint}}$ are different for different values of K. In general, for a given K, we first characterize all possible combinations of $|s_a|^2$ and $|s_b|^2$ by using the method of Section IV-B. Let us assume that the number of these combinations is G. For each combination, we can simplify Eq. (37) similar to the process of Eqs. (43)-(44), which corresponds to G simplified equations and each requires 15 flops, as shown in Eq. (37). Since $\binom{N_t}{2}$ legitimate TA combinations (i, j) should be considered in Eq. (37), we arrive at a complexity of $15G\binom{N_t}{2}$ for all possible combinations. Overall, the complexity of the EVM-based TAS for M-QAM modulated SM is

$$C_{\text{EVM}} = 2N_t^2N_r - N_t^2 + 15G\binom{N_t}{2}. \tag{49}$$

Note that the complexity of Eq. (49) is an approximate result, which can be further refined based on the specific simplified version of $d_{\min}^{\text{joint}}$. For example, based on Eqs. (41) and (43) derived for $K = 1$ and $K = 3$, similar to the complexity analysis of M-PSK, the computational complexity orders of the EVM-based TAS for $K = 1$ and $K = 3$ are

$$C_{\text{EVM-TAS}} = 2N_t^2N_r - N_t^2 + 6\binom{N_t}{2}, \tag{50}$$

and

$$C_{\text{EVM-TAS}} = 2N_t^2N_r - N_t^2 + 22\binom{N_t}{2}. \tag{51}$$

C. The Proposed PA & TAS

The exhaustive-search based TAS&PA algorithm has to calculate all legitimate PA matrix candidates. According to Section V, there are $N_U = \binom{N_t}{L}$ legitimate PA matrix candidates $\mathbf{P}_u(u = 1, \cdots, N_U)$, which can be obtained by using the method proposed in [29]. The complexity of computing each PA matrix is C_{PA} (Eq. (22) in [29]) flops. Hence, the associated complexity of the exhaustive-search based TAS&PA algorithm is $N_U C_{\text{PA}}$ flops. By contrast, the low-complexity TAS&PA algorithm first selects the optimal TA subset and then calculates the PA matrix for the selected set. Hence, the associated complexity order of the low-complexity TAS&PA algorithm is $C_{\text{TAS}} + C_{\text{PA}}$ flops, where C_{TAS} is the complexity of the TAS algorithm employed, i. e. C_{EVM} or C_{PQRD}.

REFERENCES

[1] R. Y. Mesleh, H. Haas, S. Sinanovic, C. W. Ahn, and S. Yun, "Spatial modulation," *IEEE Trans. Veh. Technol.*, vol. 57, no. 4, pp. 2228–2241, Jul. 2008.

[2] M. Di Renzo, H. Haas, A. Ghrayeb, S. Sugiura, and L. Hanzo, "Spatial modulation for generalized MIMO: Challenges, opportunities and implementation," *Proc. IEEE*, vol. 102, no. 1, pp. 56–103, Jan. 2014.

[3] S. Sugiura, S. Chen, and L. Hanzo, "A universal space-time architecture for multiple-antenna aided systems," *IEEE Commun. Surveys Tuts.*, vol. 14, no. 2, pp. 401–420, May 2012.

[4] M. Di Renzo, H. Haas, and P. M. Grant, "Spatial modulation for multiple-antenna wireless systems: A survey," *IEEE Commun. Mag.*, vol. 49, no. 12, pp. 182–191, Dec. 2011.

[5] A. Stavridis, S. Sinanovic, M. Di Renzo, and H. Haas, "Energy evaluation of spatial modulation at a multi-antenna base station," in *Proc. IEEE Veh. Technol. Conf.*, Barcelona, Spain, Sep. 2013, pp. 1–5.

[6] M. Di Renzo and H. Haas, "Bit error probability of SM-MIMO over generalized fading channels," *IEEE Trans. Veh. Technol.*, vol. 61, no. 3, pp. 1124–1144, Mar. 2012.

[7] P. Yang, M. Di Renzo, Y. Xiao, S. Li, and L. Hanzo, "Design guidelines for spatial modulation," *IEEE Commun. Surveys Tuts.*, vol. 17, no. 1, pp. 6–26, Mar. 2015.

[8] S. Sugiura and L. Hanzo, "On the joint optimization of dispersion matrices and constellations for near-capacity irregular precoded space-time shift keying," *IEEE Wireless Commun.*, vol. 12, no. 1, pp. 380–387, Jan. 2013.

[9] P. Yang, Y. Xiao, Y. Yi, and S. Li, "Adaptive spatial modulation for wireless MIMO transmission systems," *IEEE Commun. Lett.*, vol. 15, no. 6, pp. 602–604, Jun. 2011.

[10] P. Yang, Y. Xiao, L. Li, Q. Tang, Y. Yu, and S. Li, "Link adaptation for spatial modulation with limited feedback," *IEEE Trans. Veh. Technol.*, vol. 61, no. 8, pp. 3808–3813, Oct. 2012.

[11] M. Di Renzo and H. Haas, "Improving the performance of space shift keying (SSK) modulation via opportunistic power allocation," *IEEE Commun. Lett.*, vol. 14, no. 6, pp. 500–502, Jun. 2010.

[12] S. Sanayei and A. Nosratinia, "Antenna selection in MIMO systems," *IEEE Commun. Mag.*, vol. 42, no. 10, pp. 68–73, Oct. 2004.

[13] W. H. Chung, C. Y. Hung, Q. Zhang, and M. Gao, "Multi-antenna selection using space shift keying in MIMO systems," in *Proc. IEEE Veh. Technol. Conf.*, May 2012, pp. 1–5.

[14] B. Kumbhani and R. S. Kshetrimayum, "Outage probability analysis of spatial modulation systems with antenna selection," *Electron. Lett.*, vol. 50, no. 2, pp. 125–126, 2014.

[15] S. Sugiura, S. Chen, and L. Hanzo, "Coherent and differential space-time shift keying: A dispersion matrix approach," *IEEE Trans. Commun.*, vol. 58, no. 11, pp. 3219–3230, Nov. 2010.

[16] J Wang *et al.*, "Closed-loop spatial modulation with antenna selection," in *Proc. IEEE 11th Int. Conf. Signal Process.*, Oct. 2012, pp. 1291–1294.

[17] Z. Zhou, N. Ge, and X. Lin, "Reduced-complexity antenna selection schemes in spatial modulation," *IEEE Commun. Lett.*, vol. 18, no. 1, pp. 14–17, Jun. 2014.

[18] M. Maleki, H. R. Bahrami, and A. Alizadeh, "Adaptive antenna subset selection and constellation breakdown for spatial modulation," *IEEE Commun. Lett.*, vol. 18, no. 9, pp. 1649–1652, Sep. 2014.

[19] X. Wu, M. D. Renzo, and H. Haas, "Direct transmit antenna selection for transmit optimized spatial modulation," in *Proc. IEEE Veh. Technol. Conf. (VTC'13-Fall)*, Las Vegas, NV, USA, Sep. 2013, pp. 1–5.

[20] X. Wu, M. Di Renzo, and M. Haas, "Adaptive selection of antennas for optimum transmission in spatial modulation," *IEEE Trans. Wireless Commun.*, vol. 14, no. 7, pp. 3630–3641, Jul. 2015.

[21] R. Rajashekar, K. V. S. Hari, and L. Hanzo, "Antenna selection in spatial modulation systems," *IEEE Commun. Lett.*, vol. 17, no. 3, pp. 521–524, Mar. 2013.

[22] N. Pillay and H. Xu, "Comments on "Antenna selection in spatial modulation systems"," *IEEE Commun. Lett.*, vol. 17, no. 9, pp. 1681–1683, Sep. 2013.

[23] K. Ntontin, M. Di Renzo, A. Perez-Neira, and C. Verikoukis, "A low-complexity method for antenna selection in spatial modulation systems," *IEEE Commun. Lett.*, vol. 17, no. 12, pp. 2312–2315, Aug. 2013.

[24] N. Wang, W. Liu, H. Men, M. Jin, and H. Xu. "Further complexity reduction using rotational symmetry for EDAS in spatial modulation," *IEEE Commun. Lett.*, vol. 18, no. 10, pp. 1835–1838, Oct. 2014.

[25] J. Zheng and J. Chen, "Further complexity reduction for antenna selection in spatial modulation systems," *IEEE Commun. Lett.*, vol. 19, no. 6, pp. 937–940, Jun. 2015.

[26] R. Rajashekar, K. V. S. Hari, and L. Hanzo, "Quantifying the transmit diversity order of Euclidean distance based antenna selection in spatial modulation," *IEEE Commun. Lett.*, vol. 22, no. 9, pp. 1434–1437, Sep. 2015.

[27] N. Pillay and X. Hongjun, "Low-complexity transmit antenna selection schemes for spatial modulation," *IET Commun.*, vol. 9, no. 2, pp. 239–248, Jan. 2015.

[28] P. Yang, Y. Xiao, B. Zhang, S. Li, M. El-Hajjar, and L. Hanzo, "Power allocation aided spatial modulation for limited-feedback MIMO systems," *IEEE Trans. Veh. Technol.*, vol. 64, no. 5, pp. 2198–2204, May 2015.

[29] P. Yang, Y. Xiao, S. Li, and L. Hanzo, "A low-complexity power allocation algorithm for multiple-input multiple-output spatial modulation systems," *IEEE Trans. Veh. Technol.*, vol. 65, no. 3, pp. 1819–1825, Mar. 2016.

[30] M. Di Renzo and H. Haas, "Improving the performance of space shift keying (SSK) modulation via opportunistic power allocation," *IEEE Commun. Lett.*, vol. 14, no. 6, pp. 500–502, Jun. 2010.

[31] Y. Xiao, Q. Tang, L. Gong, P. Yang, and Z. Yang, "Power scaling for spatial modulation with limited feedback," *Int. J. Antennas Propag.*, vol. 2013 5 p., 2013.

[32] Z. Shi and H. Leib, "Transmit antenna selection V-BLAST systems with power allocation," *IEEE Trans. Veh. Technol.*, vol. 57, no. 4, pp. 2293–2304, Jul. 2008.

[33] R. Rajashekar, K. V. S. Hari, and L. Hanzo, "Reduced-complexity ML detection and capacity-optimized training for spatial modulation," *IEEE Trans. Commun.*, vol. 62, no. 1, pp. 112–125, Jan. 2014.

[34] S. Sugiura, C. Xu, S. X. Ng, and L. Hanzo, "Reduced complexity coherent versus non-coherent QAM-aided space time shift keying," *IEEE Trans. Commun.*, vol. 59, no. 11, pp. 3090–3101, Nov. 2011.

[35] A. Younis, S. Sinanovic, M. Di Renzo, R. Y. Mesleh, and H. Haas, "Generalised sphere decoding for spatial modulation," *IEEE Trans. Commun.*, vol. 61, no. 7, pp. 2805–2815, Jul. 2013.

[36] A. Goldsmith, *Wireless Communications*. Cambridge, U.K.: Cambridge Univ. Press, 2005.

[37] G. Golub and C. F. van Loan, *Matrix Computations*, 3 rd ed. Baltimore, MD, USA: The Johns Hopkins Univ. Press, 1996.

[38] J. K. Zhang, A. Kavcic, and K. M. Wong, "Equal-diagonal QR decomposition and its application to precoder design for successive-cancellation detection," *IEEE Trans. Inf. Theory*, vol. 51, no. 1, pp. 154–172, Jan. 2005.

[39] J. Lee, S. Y. Jung, and D. Park, "Simplified maximum-likelihood precoder selection for spatial multiplexing systems," *IEEE Trans. Veh. Technol.*, vol. 59, no. 9, pp. 4628–4634, Nov. 2010.

[40] Z. Chen, J. Yuan, and B. Vucetic, "Analysis of transmit antenna selection/maximal-ratio combining in Rayleigh fading channels," *IEEE Trans. Veh. Techol.*, vol. 54, no. 4, pp. 1312–1321, Jul. 2005.

[41] V. Raghavan, J. J. Choi, and D. J. Love, "Design guidelines for limited feedback in the spatially correlated broadcast channel," *IEEE Trans. Commun*, vol. 63, no. 7, pp. 2524–2540, Jul. 2015.

Ping Yang (SM'xx) received the Ph.D. degree from the University of Electronic Science and Technology of China (UESTC), Chengdu, China, in 2013. From September 2012 to September 2013, he was a Visiting Student at the School of Electronics and Computer Science, University of Southampton, Southampton, U.K. Since May 2014, he has been a Research Fellow in EEE of NTU, Singapore. Also, he is an Assistant Professor with UESTC. His research interests include MIMO/OFDM, machine learning, life science, and communication signal processing.

Yue Xiao (M'xx) received the Ph.D. degree in communication and information systems from the University of Electronic Science and Technology of China, Chengdu, China, in 2007. He is now a Full Professor with the University of Electronic Science and Technology of China. He has authored more than 30 international journals and been involved in several projects in Chinese Beyond 3G Communication R&D Program. His research interests include wireless and mobile communications.

Yong Liang Guan (M'xx) received the Ph.D. degree from the Imperial College of Science, Technology, and Medicine, University of London, London, U.K., in 1997, and the B.Eng. degree (with first class Hons.) from the National University of Singapore, Singapore, in 1991. He is now an Associate Professor with the School of Electrical and Electronic Engineering, Nanyang Technological University, Singapore. His research interests include modulation, coding and signal processing for communication, information security and storage systems.

Shaoqian Li (F'16) received the B.S.E. degree in communication technology from Northwest Institute of Telecommunication (Xidian University), Xi'an, China, in 1982, and the M.S.E. degree in communication system from the University of Electronic Science and Technology of China (UESTC), Chengdu, China, in 1984. He is a Professor, Ph.D. Supervisor, and the Director of the National Key Laboratory of Communication, UESTC, and member of the National High Technology R&D Program (863 Program) Communications Group. His research interests includes wireless communication theory, anti-interference technology for wireless communications, spread-spectrum and frequency-hopping technology, and mobile and personal communications.

Lajos Hanzo (F'xx) received the degree in electronics, in 1976, the doctorate degree, in 1983, and the D.Sc. degree. During his 37-year career in telecommunications, he has held various research and academic posts in Hungary, Germany, and the U.K. Since 1986, he has been with the School of Electronics and Computer Science, University of Southampton, Southampton, U.K., where he holds the chair in telecommunications. He has successfully supervised over 80 Ph.D. students, coauthored 20 John Wiley/IEEE Press books on mobile radio communications totalling in excess of 10 000 pages, published 1400+ research entries at IEEE Xplore, acted both as TPC and the General Chair of the IEEE conferences, presented keynote lectures and has been awarded a number of distinctions. Currently, he is directing a 100-strong academic research team, working on a range of research projects in the field of wireless multimedia communications sponsored by industry, the Engineering and Physical Sciences Research Council (EPSRC) U.K., the European Research Council's Advanced Fellow Grant and the Royal Society's Wolfson Research Merit Award. He is an enthusiastic supporter of industrial and academic liaison and offers a range of industrial courses. He is also a Governor of the IEEE VTS. From 2008 to 2012, he was the Editor-in-Chief of the IEEE Press and a Chaired Professor also at Tsinghua University, Beijing, China. His research is funded by the European Research Council's Senior Research Fellow Grant. He has more than 19 000 citations. In 2009, he was received the honorary doctorate "Doctor Honoris Causa" by the Technical University of Budapest, Budapest, Hungary. He is the fellow of the REng, IET, and EURASIP.

QUERIES

Q1: Please be advised that per instructions from the Communications Society this proof was formatted in Times Roman font and therefore some of the fonts will appear different from the fonts in your originally submitted manuscript. For instance, the math calligraphy font may appear different due to usage of the usepackage[mathcal]euscript. We are no longer permitted to use Computer Modern fonts.

Q2: Note that if you require corrections/changes to tables or figures, you must supply the revised files, as these items are not edited for you.

Q3: Please provide IEEE membership details of authors "Ping Yang, Yue Xiao, Yong Liang Guan, and Lajos Hanzo."

Transmit Antenna Selection for Multiple-Input Multiple-Output Spatial Modulation Systems

Ping Yang, *Senior Member, IEEE*, Yue Xiao, *Member, IEEE*, Yong Liang Guan, *Member, IEEE*, Shaoqian Li, *Fellow, IEEE*, and Lajos Hanzo, *Fellow, IEEE*

***Abstract*—The benefits of transmit antenna selection (TAS) invoked for spatial modulation (SM) aided multiple-input multiple-output (MIMO) systems are investigated. Specifically, we commence with a brief review of the existing TAS algorithms and focus on the recently proposed Euclidean distance-based TAS (ED-TAS) schemes due to their high diversity gain. Then, a pair of novel ED-TAS algorithms, termed as the improved QR decomposition (QRD)-based TAS (QRD-TAS) and the error-vector magnitude-based TAS (EVM-TAS) are proposed, which exhibit an attractive system performance at low complexity. Moreover, the proposed ED-TAS algorithms are amalgamated with the low-complexity yet efficient power allocation (PA) technique, termed as TAS-PA, for the sake of further improving the system's performance. Our simulation results show that the proposed TAS-PA algorithms achieve signal-to-noise ratio (SNR) gains of up to 9 dB over the conventional TAS algorithms and up to 6 dB over the TAS-PA algorithm designed for spatial multiplexing systems.**

***Index Terms*—Antenna selection, MIMO, power allocation, spatial modulation, link adaptation.**

I. Introduction

SPATIAL modulation (SM) and its variants constitute a class of promising low-complexity and low-cost multiple-input multiple-output (MIMO) transmission techniques [1]–[5]. However, the conventional SM schemes only achieve receiver-diversity, but no transmit diversity [6]. To circumvent this impediment, recently some SM solutions have been proposed [7]–[11] on how to glean a beneficial transmit-diversity gain both with the aid of open-loop as well as closed-loop transmit-symbol design techniques.

As an attractive closed-loop regime, transmit antenna selection (TAS) constitutes a promising technique of providing a high diversity potential as offered by the classic MIMO architectures. TAS has been lavishly researched in the context of spatial multiplexing systems [12]. As a new MIMO technique, SM can also be beneficially combined with TAS. Recently, several TAS algorithms have been conceived for the class of SM-MIMO systems with the goal of enhancing either its bit error rate (BER) or its capacity [13]–[20]. In [13], a norm-based TAS algorithm was proposed for providing diversity gain. In [14], a closed-form expression of the SM scheme's outage probability was derived for norm-based TAS. In [16], a two-stage TAS-based SM scheme was proposed for overcoming the specific constraint of SM, namely that the number of transmit antennas has to be a power of two. In [17], a novel TAS criterion was proposed for circumventing the detrimental effects of antenna correlation. In [18], the joint design of TAS and constellation breakdown was investigated and a graph-based search algorithm was proposed for reducing the search complexity imposed. In [19], a low-complexity TAS algorithm based on circle packing was proposed for a transmitter-optimized spatial modulation (TOSM) system, which trades off the spatial constellation size against the amplitude and phase modulation (APM) constellation size for improving the system's average bit error probability (ABEP). The adaptive TAS algorithm conceived for TOSM was further developed in [20], where a low-complexity two-stage optimization was proposed for selecting the best transmission mode.

More recently, the research of TAS-aided SM has been focused on the optimization of the Euclidean Distance (ED) of the received constellation points, since they achieve a high diversity gain at a moderate complexity compared to other TAS criteria [21]–[24]. Specifically, in [21] and [22] the ED-based TAS algorithm (ED-TAS) was compared to the signal-to-noise ratio (SNR)-optimized and capacity-optimized algorithms, and a low-complexity realization of ED-TAS, termed as the QR decomposition-based TAS (QRD-TAS) was proposed. The QRD-TAS algorithm constructs an ED-element matrix and exploits the QRD of the resultant matrix for reducing the imposed complexity. Moreover, in [24], the authors exploited the rotational symmetry of the APM adopted for the sake of reducing the complexity of QRD-TAS. Compared to directly optimizing the ED, in [23], Ntontin *et al*. proposed a low-complexity singular value decomposition-based TAS (SVD-TAS) algorithm for maximizing the lower bound of the ED. In [25], the complexity of SVD-TAS was reduced through an alternative computation of the singular value. In [26], the transmit diversity order of ED-TAS was quantified. In [27], the authors proposed several low-complexity TAS schemes relying

Manuscript received October 10, 2015; revised February 22, 2016; accepted March 24, 2016. This work was supported of the National Science Foundation of China under Grant 61501095, in part by the National High-Tech R&D Program of China ("863" Project under Grant 2014AA01A707), and in part by the European Research Council's Advanced Fellow Grant. The associate editor coordinating the review of this paper and approving it for publication was V. Raghavan.

P. Yang, Y. Xiao, and S. Li are with the National Key Laboratory of Science and Technology on Communications, University of Electronic Science and Technology of China, Sichuan 611731, China (e-mail: yplxw@163.com; xiaoyue@uestc.edu.cn; lsq@uestc.edu.cn).

Y. L. Guan is with the School of Electrical and Electronic Engineering, Nanyang Technological University, Singapore (e-mail: eylguan@ntu.edu.sg).

L. Hanzo is with the School of Electronics and Computer Science, University of Southampton, Southampton SO17 1BJ, U.K. (e-mail: lh@ecs.soton.ac.uk).

Color versions of one or more of the figures in this paper are available online at http://ieeexplore.ieee.org.

Digital Object Identifier 10.1109/TCOMM.2016.2547900

on exploiting the channel's amplitude, the antenna correlation, the ED between transmit vectors and their combinations for selecting the optimal TA subset for the sake of improving the system's reliability. However, as shown in [21]–[27], the QRD-TAS achieves an attractive BER performance at the cost of adopting high-complexity QRD operations, while the low-complexity SVD-TAS may suffer some performance loss.

On the other hand, power allocation (PA) is another promising link adaptation technique for MIMO systems. Recently, PA has been extended to SM systems [28]–[31]. For example, in [28], an adaptive PA algorithm based on maximizing the minimum ED was proposed, which is capable of improving the system's BER performance, while retaining all the single-RF benefits of SM. Subsequently, this attractive PA algorithm was further simplified in [29]. However, to the best of our knowledge, the potential benefits of TAS intrinsically amalgamated with PA have not been investigated in SM-MIMO systems.

Against this background, the contributions of this paper are:

1) We investigate the benefits of ED-TAS and propose a pair of novel ED-TAS schemes for SM-MIMO systems. In these schemes, we first classify the legitimate EDs into three specific subsets and then invoke a carefully designed upper bound as well as a set-reduction method for the most dominant set imposing a high complexity.
2) Specifically, we propose an improved QRD-TAS, where a tighter QRD-based lower bound of the ED is derived to replace the SVD-based bound of [23]. A low-complexity method is proposed for directly calculating the bound parameters, in order to avoid the high-complexity QRD or SVD operations of [21]–[24]. More importantly, compared to the conventional SVD-TAS of [25], the achieved QRD-based tighter bound can achieve a better BER performance.
3) Moreover, for striking a flexible tradeoff in terms of the BER attained and the complexity imposed, we propose an error-vector magnitude based TAS (EVM-TAS), which exploits the error vector selection probability to shrink the search space. The relevant optimization metrics of EVM-TAS are also derived for different PSK and QAM schemes.
4) Finally, we intrinsically amalgamate the proposed ED-TAS with the recently conceived PA technique of [29] for fully exploiting the MIMO channel's resources. A pair of different joint TAS-PA algorithms are conceived, which provide beneficial gains over both the conventional TAS algorithms and over the TAS-PA techniques designed for spatial multiplexing systems [32].

The organization of the paper is as follows. Section II introduces the system model of TAS-based SM, while Section III reviews the family of existing TAS algorithms designed for SM. In Section IV, we introduce the proposed QRD-TAS and EVM-TAS algorithms. In Section V, the joint design of the ED-TAS and PA algorithms is proposed. Then, we carry out their complexity analysis. Our simulation results and performance comparisons are presented in Section VI. Finally, Section VII concludes the paper.

Notation: $(\cdot)^*$, $(\cdot)^T$ and $(\cdot)^H$ denote conjugate, transpose, and Hermitian transpose, respectively. Furthermore, $\|\cdot\|_F$ stands for the Frobenius norm. $\mathbf{I}_b$ denotes a $(b \times b)$-element identity matrix and the operator diag$\{\cdot\}$ is the diagonal operator. $\mathfrak{R}\{\mathbf{x}\}$ and $\mathfrak{I}\{\mathbf{x}\}$ represent the real and imaginary parts of $\mathbf{x}$, respectively.

II. System Model

Consider a SM system having N_t transmit and N_r receive antennas, as depicted in Fig. 1. The frequency-flat quasi-static fading MIMO channel is represented by $\mathbf{H} = [\mathbf{h}(1), \mathbf{h}(2), \cdots, \mathbf{h}(N_t)] \sim \mathcal{CN}(0, \mathbf{I}_{N_r \times N_t})$, where $\mathbf{h}(1), \mathbf{h}(2), \cdots, \mathbf{h}(N_t)$ are the column vectors corresponding to each transmit antenna (TA) in $\mathbf{H}$. The receiver first selects L TAs according to a specific selection criterion. Then, the receiver sends this information to the transmitter via a feedback link. As shown in [23], let U_u denote the uth legitimate TA subset, where we have

$$\begin{aligned} &U_1 = \{1, 2, \cdots, L\},\\ &U_2 = \{1, 2, \cdots, L-1, L+1\},\\ &\vdots\\ &U_{N_U} = \{N_t - L + 1, \cdots, N_t\}. \end{aligned} \tag{1}$$

In Eq. (1), there are $N_U = \binom{N_t}{L}$ possible TA subsets, each of which corresponds to an $(N_r \times L)$-element MIMO channel. As shown in Fig. 1, $\mathbf{b} = [b_1, \ldots, b_L]$ is the transmit bit vector in each time slot, which contains $m = \log_2(LM)$ bits, where M is the size of the APM constellation. In SM, the input vector $\mathbf{b}$ is partitioned into two sub-vectors of $\log_2(L)$ and $\log_2(M)$ bits, denoted as $\mathbf{b}_1$ and $\mathbf{b}_2$, respectively. The bits in $\mathbf{b}_1$ are used for selecting a unique TA index q for activation, while the bits of $\mathbf{b}_2$ are mapped to a Gray-coded APM symbol $s_l^q \in \mathbb{S}$. Then, the SM symbol $\mathbf{x} \in \mathbb{C}^{L\times 1}$ is formulated as

$$\mathbf{x} = s_l^q \mathbf{e}_q = [0, \cdots, \overset{\downarrow\, qth}{s_l^q}, \cdots, 0]^T, \tag{2}$$

where $\mathbf{e}_q (1 \le q \le L)$ is selected from the L-dimensional basis vectors (as exemplified by $\mathbf{e}_1 = [1, 0, \cdots, 0]^T$). In the scenario that U_u is selected, the signal observed at the N_r receive antennas is given by

$$\mathbf{y} = \mathbf{H}_u \mathbf{x} + \mathbf{n}, \tag{3}$$

where $\mathbf{H}_u$ is the $(N_r \times L)$-element TAS matrix corresponding to the selected TA set U_u, and $\mathbf{n}$ is the $(N_r \times 1)$-element noise vector. The elements of the noise vector $\mathbf{n}$ are complex Gaussian random variables obeying $\mathcal{CN}(0, N_0)$.

The receiver performs maximum-likelihood (ML) detection over all legitimate SM symbols $\mathbf{x} \in \mathbb{C}^{L\times 1}$ to obtain

$$\hat{\mathbf{x}} = \arg\min_{\mathbf{x}\in\mathbb{X}} \|\mathbf{y} - \mathbf{H}_u\mathbf{x}\|_F^2 = \arg\min_{\mathbf{x}\in\mathbb{X}} \left\|\mathbf{y} - \mathbf{h}_u(q) s_l^q\right\|_F^2, \tag{4}$$

where $\mathbb{X}$ is the set of all legitimate transmit symbols and $\mathbf{h}_u(q)$ is the qth column of the equivalent channel matrix $\mathbf{H}_u$. The complexity of the single-stream ML detection of Eq. (4) is low, since a single TA is activated during any time slot [34], [35].

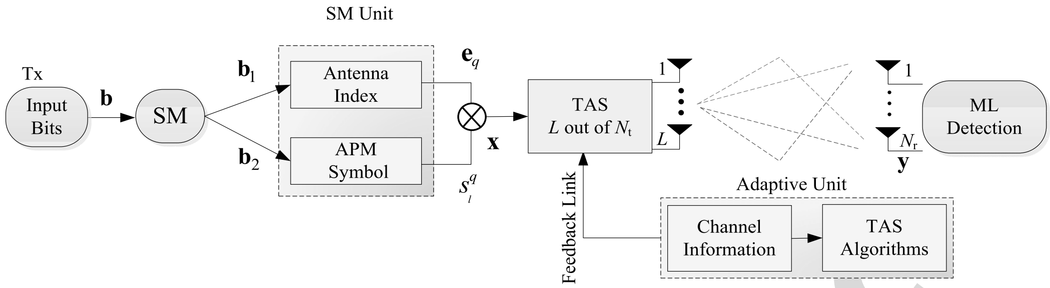

Q1

Fig. 1. The system model of the TAS-based SM system.

III. Conventional TAS Algorithms

This section offers a brief state-of-the-art review of the existing TAS algorithms proposed for SM systems.

A. *The Maximum-Capacity and The Maximum-Norm Based TAS Algorithms*

The capacity C_u of the SM-aided MIMO system depends on the classic transmitted signal s_l^q and the TA index signal $\mathbf{e}_q$. As shown in [21], [33], the capacity C_s relying on the signal s_l^q and the channel $\mathbf{H}_u$ is lower bounded by

$$\alpha = \frac{1}{L}\sum\nolimits_{i=1}^{L} \log_2(1+\rho\,\|\mathbf{h}_u(i)\|_F^2) \le C_\mathrm{s}, \tag{5}$$

where $\mathbf{h}_u(i)$ is the ith column of $\mathbf{H}_u$ and ρ is the average SNR at the receiver. Moreover, the capacity C_{TA} relying on the signal $\mathbf{e}_q$ is bounded by $C_{\mathrm{TA}} \le \log_2(L)$ [33]. It is proved in [33] that the total capacity $C_u = C_{\mathrm{TA}} + C_\mathrm{s}$ is bounded by

$$\alpha \le C_u \le \alpha + \log_2(L), \tag{6}$$

Based on the bound of Eq. (6), a maximum-capacity based TAS algorithm was formulated in [21] as

$$\mathbf{H}_{\hat{u}} = \arg \max_{u\in\{1,\cdots,N_U\}} \alpha. \tag{7}$$

Based on Eq. (5), the optimization objective α of Eq. (7) is maximized by selecting the L TAs associated with the largest channel norms out of the N_t TAs, which is equivalent to the maximum-norm based TAS [13] given by

$$\mathbf{H}_{\hat{u}} = \arg \max_{u\in\{1,\cdots,N_U\}} \|\mathbf{H}_u\|_F^2 . \tag{8}$$

B. *The Exhaustive Max-$d_{\min}$ Based ED-TAS*

In order to improve the BER performance of SM, the free distance (FD) $d_{\min}$ was optimized in [21]. For a given channel $\mathbf{H}_u$, its FD can be formulated as

$$\begin{aligned} d_{\min}(\mathbf{H}_u) &= \min_{\substack{\mathbf{x}_i,\mathbf{x}_j\in\mathbb{X}\\ \mathbf{x}_i\neq\mathbf{x}_j}} \left\|\mathbf{H}_u(\mathbf{x}_i-\mathbf{x}_j)\right\|_F^2 \\ &= \min_{\mathbf{e}_{ij}\in\mathbb{E}} \left\|\mathbf{H}_u\mathbf{e}_{ij}\right\|_F^2 = \min_{\mathbf{e}_{ij}\in\mathbb{E}} \mathbf{e}_{ij}^H\mathbf{H}_u^H\mathbf{H}_u\mathbf{e}_{ij}, \end{aligned} \tag{9}$$

where we have the error vector $\mathbf{e}_{ij} = \mathbf{x}_i - \mathbf{x}_j$, $\mathbf{x}_i, \mathbf{x}_j \in \mathbb{X}$. In [21], the max-$d_{\min}$ aided ED-TAS algorithm is defined as

$$\mathbf{H}_{\hat{u}} = \arg \max_{u\in\{1,\cdots,N_U\}} d_{\min}(\mathbf{H}_u). \tag{10}$$

The optimum solution obeying the objective function of Eq. (10) can be found by an exhaustive search over all possible $\binom{N_t}{L}$ candidate channel matrices and all the different error vectors, which imposes a complexity order of $\mathcal{O}(N_t^2M^2)$. This results in an excessive complexity, when high data rates are required.

C. *The Conventional QRD-Based ED-TAS*

In order to reduce the complexity of the exhaustive ED-TAS of Eq. (10), in [21] an ED-TAS based on an equivalent decision metric $\mathbf{D}(u)$ was formulated as:

$$\mathbf{H}_{\hat{u}} = \arg \max_{u\in\{1,\cdots,N_U\}} \{\min[\mathbf{D}(u)]\}, \tag{11}$$

where $\mathbf{D}(u)$ is an $(L\times L)$-element sub-matrix of an upper triangular $(N_t\times N_t)$-element matrix $\mathbf{D}$ obtained by deleting the specific rows and columns that are absent in u, while $\min[\mathbf{D}(u)]$ is the minimum non-zero value of $\mathbf{D}(u)$. Here, the $(i,j)-th$ element of $\mathbf{D}$ can be expressed as

$$\begin{aligned} \mathbf{D}_{ij} &= \min_{s_1,s_2\in\mathbb{S}} \left\|\mathbf{H}(s_1\mathbf{e}_i - s_2\mathbf{e}_j)\right\|_F^2 \\ &= \min_{s_1,s_2\in\mathbb{S}} \|\mathbf{h}(i)s_1 - \mathbf{h}(j)s_2\|_F^2 , \end{aligned} \tag{12}$$

where s_1 and s_2 are M-ary APM constellation points, while $\mathbf{h}(i)$ and $\mathbf{h}(j)$ are the ith and jth columns of $\mathbf{H}$. Provided that we have $i=j$ in Eq. (12), the corresponding element becomes $\mathbf{D}_{ii} = \min_{s_1,s_2\in\mathbb{S}}(\|\mathbf{h}(i)\|_F^2\,|s_1-s_2|^2) = d_{\min}^{\mathrm{APM}}\,\|\mathbf{h}(i)\|_F^2$, where $d_{\min}^{\mathrm{APM}}$ is the minimum distance of the APM constellation. For the case of $i\neq j$, $\mathbf{D}_{ij}$ is re-formulated in the real-valued representation of the QRD as

$$\mathbf{D}_{ij} = \min_{\substack{s_{1I},s_{2I}\in\mathcal{R}\{\mathbb{S}\},\\ s_{1Q},s_{2Q}\in\mathcal{I}\{\mathbb{S}\}}} \left\|\mathbf{R}[s_{1I}, s_{1Q}, -s_{2I}, -s_{2Q}]^T\right\|_F^2, \tag{13}$$

where we have $s_{nI} = \mathcal{R}\{s_n\}$ and $s_{nQ} = \mathcal{I}\{s_n\}$ for $n = 1, 2$, while $\mathbf{R}$ is a (4×4)-element upper triangular matrix created by the QRD of the resultant channel matrix [21]. As shown in [21], the complexity order of this QRD-TAS is $\mathcal{O}(N_t^2M)$, which increases only linearly with the modulation order M. In [22] and [24], both the modulus and the symbol set symmetry of the APM constellations were exploited for further reducing the complexity of this algorithm.

D. The Conventional SVD-Based ED-TAS

Although the QRD-based ED-TAS of Eq. (13) is capable of finding the optimal solution, its complexity imposed is a function of the modulation order M. Moreover, the high-complexity QRD has to be applied to the $(2N_r \times 4)$-element channel matrices [21], [22], [24]. Hence, the complexity of this TAS remains high. This problem was circumvented in [23], where the ED was classified into three categories as follows

$$d_{\min}(\mathbf{H}_u) = \min\left\{d_{\min}^{\text{signal}}, d_{\min}^{\text{spatial}}, d_{\min}^{\text{joint}}\right\}, \tag{14}$$

where we have

$$\begin{aligned} d_{\min}^{\text{signal}} &= \min_{i=1,\cdots,L} \|\mathbf{h}_u(i)\|_F^2 \min\nolimits_{s_a \neq s_b \in \mathbb{S}} |s_a - s_b|^2 \\ &= d_{\min}^{\text{APM}} \min_{i=1,\cdots,L} \|\mathbf{h}_u(i)\|_F^2 , \end{aligned} \tag{15}$$

$$\begin{aligned} d_{\min}^{\text{spatial}} &= \min_{\substack{i,j=1,\cdots,L \\ i\neq j}} \|\mathbf{h}_u(i) - \mathbf{h}_u(j)\|_F^2 \min\nolimits_{s_l \in \mathbb{S}} |s_l|^2 \\ &= d_{\min}^{\text{Modulus}} \min_{\substack{i,j=1,\cdots,L \\ i\neq j}} \|\mathbf{h}_u(i) - \mathbf{h}_u(j)\|_F^2 , \end{aligned} \tag{16}$$

$$d_{\min}^{\text{joint}} = \min_{\substack{i,j=1,\cdots,L, i\neq j \\ s_a, s_b, \in \mathbb{S}, a\neq b}} \|\mathbf{h}_u(i)s_a - \mathbf{h}_u(j)s_b\|_F^2 . \tag{17}$$

In Eq. (16), the term $d_{\min}^{\text{Modulus}} = \min_{s_l \in \mathbb{S}} |s_l|^2$ is the minimum squared modulus value of the APM constellation. Since the calculations of $d_{\min}^{\text{signal}}$ and $d_{\min}^{\text{spatial}}$ in Eqs. (15) and (16) do not depend on the size of APM constellation and the corresponding complexity is low, the complexity of computing the FD of Eq. (14) is dominated by the computation of $d_{\min}^{\text{joint}}$ in Eq. (17). To reduce this complexity, in [23] the Rayleigh-Ritz theorem was utilized for driving a lower bound of $d_{\min}^{\text{joint}}$ as

$$\begin{aligned} d_{\min}^{\text{joint}} &= \min_{\substack{i,j=1,\cdots,L, i\neq j \\ s_a, s_b \in \mathbb{S}, a\neq b}} \left\| [\mathbf{h}_u(i), -\mathbf{h}_u(j)][s_a, s_b]^T \right\|_F^2 \\ &\geq d_{\min}^{\text{SVD-bound}} \\ &= \min_{i,j=1,\cdots,L,i\neq j} \lambda_{\min}^2(\mathbf{H}_{u,ij}) \min_{s_a,s_b \in \mathbb{S}} \left\| [s_a, s_b]^T \right\|_F^2 \\ &= \min_{i,j=1,\cdots,L,i\neq j} \lambda_{\min}^2(\mathbf{H}_{u,ij}) d_{\min}^{\text{all}} \end{aligned} , \tag{18}$$

where we have $d_{\min}^{\text{all}} = \min_{s_a,s_b \in \mathbb{S}} \left\| [s_a, s_b]^T \right\|_F^2$ and $\mathbf{H}_{u,ij} = [\mathbf{h}_u(i), -\mathbf{h}_u(j)]$ is an $(N_r \times 2)$-element matrix. Here, $\lambda_{\min}^2(\mathbf{H}_{u,ij})$ is the minimum squared singular value of the submatrix $\mathbf{H}_{u,ij}$. Upon exploiting Eq. (18), the distance $d_{\min}(\mathbf{H}_u)$ of Eq. (14) is bounded by

$$d_{\min}^{\text{SVD}}(\mathbf{H}_u) = \min\{d_{\min}^{\text{signal}}, d_{\min}^{\text{spatial}}, d_{\min}^{\text{SVD-bound}}\}. \tag{19}$$

Based on Eq. (19), the SVD-TAS algorithm is given by

$$\mathbf{H}_{\hat{u}} = \arg \max_{u \in \{1,\cdots,N_U\}} d_{\min}^{\text{SVD}}(\mathbf{H}_u). \tag{20}$$

Compared to the conventional QRD-based TAS, this bound-aided algorithm has the following advantages:

- Using the SVD-based bound of Eq. (18), the calculation of the distance $d_{\min}^{\text{joint}}$ is independent of the APM modulation order;
- Moreover, the SVD operation of Eq. (18) is performed on the smaller channel matrices of size $(N_r \times 2)$ compared to the QRD-based ED-TAS, which is performed on $(2N_r \times 4)$-element matrices. In [25], the complexity of SVD-TAS [23] was further reduced through an alternative computation of the singular value.

IV. The Proposed Low-Complexity ED-TAS

As shown in subsection III, the conventional QRD-based ED-TAS is capable of achieving the optimal BER, but it imposes high complexity. In contrast, the SVD-based ED-TAS imposes a lower complexity at the cost of a BER performance degradation, because the derived bound may be loose and the corresponding TAS results may be suboptimal.

To circumvent this problem, in this section, a pair of ED-TAS algorithms are proposed. Specifically, an improved QRD-TAS is proposed, where a tighter QRD-based lower bound of the ED is found for replacing the SVD-based bound of [23], while the sparse nature[1] of the error vectors of SM is exploited to avoid the full-dimensional QRD operation. Then, for striking a further flexible BER vs complexity tradeoff, we propose an EVM-based ED-TAS algorithm, which exploits the error vector selection probability to shrink the search space.

A. The Proposed QRD-Based ED-TAS

1) The QRD-Based Bounds: To evaluate the value of $d_{\min}^{\text{joint}}$ more accurately, in this paper, we apply the QRD-based bound to replace the SVD-bound of Eq. (18). Specifically, the submatrix $\mathbf{H}_{u,ij}$ of Eq. (18) is first subjected to the QRD [38], yielding $\mathbf{H}_{u,ij} = \tilde{\mathbf{Q}}\tilde{\mathbf{R}}$, where $\tilde{\mathbf{Q}}$ is an $(N_r \times 2)$ column-wise orthonormal matrix and $\tilde{\mathbf{R}}$ is a (2×2) upper triangular matrix with positive real-valued diagonal entries formulated as

$$\tilde{\mathbf{R}} = \begin{bmatrix} \tilde{R}_{1,1} & \tilde{R}_{1,2} \\ 0 & \tilde{R}_{2,2} \end{bmatrix}. \tag{21}$$

Let $[\tilde{\mathbf{R}}]_k = \tilde{R}_{k,k}$ denote the kth diagonal entry of $\tilde{\mathbf{R}}$. Based on this decomposition, another lower bound of the distance $d_{\min}^{\text{joint}}$ in Eq. (18) can be formulated as

$$\begin{aligned} d_{\min}^{\text{joint}} &\geq d_{\min}^{\text{QRD-bound}} \\ &= \min_{i,j=1,\cdots,L,i\neq j} \{[\tilde{\mathbf{R}}]_{\min}^2\} \min_{s_a \neq s_b \in \mathbb{S}} \|[s_a, s_b]\|_F^2 , \\ &= \min_{i,j=1,\cdots,L,i\neq j} \{[\tilde{\mathbf{R}}]_{\min}^2\} d_{\min}^{\text{all}} \end{aligned} \tag{22}$$

[1] In SM, the transmit vector $\mathbf{x}$ only has a single non-zero element, hence the number of non-zero elements of the error vectors $\mathbf{e}_{ij}$ of SM is no more than 2.

where $[\tilde{\mathbf{R}}]^2_{\min}$ is the minimum squared nonzero diagonal entry of the upper matrix $\tilde{\mathbf{R}}$, given by

$$\left[\tilde{\mathbf{R}}\right]_{\min} = \min\{\tilde{R}_{1,1}, \tilde{R}_{2,2}\}. \tag{23}$$

Lemma 1: For an $(N_r \times 2)$-element full column-rank matrix $\mathbf{H}_{u,ij}$ associated with its minimum squared singular non-zero value $\lambda^2_{\min}(\mathbf{H}_{u,ij})$ for SVD and its minimum squared diagonal non-zero entry $[\tilde{\mathbf{R}}]^2_{\min}$ of $\tilde{\mathbf{R}}$ for QRD, respectively, the inequality $[\tilde{\mathbf{R}}]^2_{\min} \geq \lambda^2_{\min}(\mathbf{H}_{u,ij})$ is satisfied.

According to the analysis process in Section III of [38], the formulation of Lemma 1 is straightforward. As a result, the lower bound of Eq. (22) achieved by the QRD is tighter than that of the SVD algorithm in Eq. (18).

To derive an even tighter upper QRD bound than that of Eq. (22), the permutation matrix $\mathbf{\Pi}_m$ can be invoked for calculating $d^{\text{joint}}_{\min}$ of Eq. (22) as

$$d^{\text{joint}}_{\min} = \min_{\substack{i,j=1,\cdots,L,\\ i\neq j, s_a, s_b \in \mathbb{S}}} \left\| [\mathbf{h}_u(i), -\mathbf{h}_u(j)]\mathbf{\Pi}_m \mathbf{\Pi}_m^{-1}[s_a, s_b]^T \right\|^2_F, \tag{24}$$

where $\mathbf{\Pi}_m$ is an orthogonal matrix satisfying $\mathbf{\Pi}_m^{-1} = \mathbf{\Pi}_m^T$. Since the size of the channel matrix $\mathbf{H}_{u,ij} = [\mathbf{h}_u(i), -\mathbf{h}_u(j)]$ is $N_r \times 2$, we only have two legitimate permutation matrices $\mathbf{\Pi}_m \in \mathbb{C}^{2\times 2}$, $m = 1, 2$, namely

$$\mathbf{\Pi}_1 = \begin{bmatrix} 1 & 0 \\ 0 & 1 \end{bmatrix} \text{ and } \mathbf{\Pi}_2 = \begin{bmatrix} 0 & 1 \\ 1 & 0 \end{bmatrix}. \tag{25}$$

For each matrix $\mathbf{\Pi}_m$, similar to Eq. (22), the corresponding QRD-based bound is

$$\begin{aligned} d^{\text{joint}}_{\min} &\geq \min_{i,j=1,\cdots,L, i\neq j} \left\{ \left[\tilde{\mathbf{R}}_m\right]^2_{\min} \right\} \min_{s_a, s_b \in \mathbb{S}} \left\| \mathbf{\Pi}_m^T [s_a, s_b]^T \right\|^2_F \\ &= \left[\tilde{\mathbf{R}}_m\right]^2_{\min} d^{\text{all}}_{\min}, \end{aligned} \tag{26}$$

where $\tilde{\mathbf{R}}_m$ is the upper triangular part of the QRD of the equivalent matrix $\mathbf{H}_{u,ij}\mathbf{\Pi}_m$. Note in Eq. (26) that the permutation matrix does not change the distance of $\left\|\mathbf{\Pi}_m^T[s_a, s_b]\right\|^2_F$ and we have $\min_{s_a,s_b\in\mathbb{S}} \left\|\mathbf{\Pi}_m^T[s_a, s_b]^T\right\|^2_F = \min_{s_a,s_b\in\mathbb{S}} \left\|[s_a, s_b]^T\right\|^2_F = d^{\text{all}}_{\min}$. For the permutation matrices given in Eq. (25), we can obtain two different values $[\tilde{\mathbf{R}}_m]_{\min}$, $(m = 1, 2)$, which are given by $[\tilde{\mathbf{R}}_1]_{\min} = \min\{\tilde{R}_{1,1}(\mathbf{\Pi}_1), \tilde{R}_{2,2}(\mathbf{\Pi}_1)\}$ and $[\tilde{\mathbf{R}}_2]_{\min} = \min\{\tilde{R}_{1,1}(\mathbf{\Pi}_2), \tilde{R}_{2,2}(\mathbf{\Pi}_2)\}$. Here, $\tilde{R}_{1,1}(\mathbf{\Pi}_m)$ and $\tilde{R}_{2,2}(\mathbf{\Pi}_m)$, $m = 1, 2$ are the diagonal elements of $\tilde{\mathbf{R}}_m$.

Remark: The bound of Eq. (22) constitutes a special case of the bound of Eq. (26), which can be obtained by setting $m = 1$.

Based on Eq. (26), an improved QRD-based upper bound of the distance $d^{\text{joint}}_{\min}$ is given by

$$\begin{aligned} d^{\text{joint}}_{\min} &\geq d^{\text{QRD-bound\_P}}_{\min} \\ &= \min_{i,j=1,\cdots,L, i\neq j} \{[\tilde{\mathbf{R}}_{QRQ\_P}]^2_{\min}\} d^{\text{all}}_{\min}. \end{aligned} \tag{27}$$

where we have $[\tilde{\mathbf{R}}_{QRQ\_P}]^2_{\min} = \max\{[\tilde{\mathbf{R}}_1]^2_{\min}, [\tilde{\mathbf{R}}_2]^2_{\min}\}$.

Lemma 2: For an $(N_r \times 2)$-element full column-rank matrix $\mathbf{H}_{u,ij}$ having a minimum squared diagonal non-zero entry $[\tilde{\mathbf{R}}]^2_{\min}$ for its QRD and a value of $[\tilde{\mathbf{R}}_{QRQ\_P}]^2_{\min} = \max\{[\tilde{\mathbf{R}}_1]^2_{\min}, [\tilde{\mathbf{R}}_2]^2_{\min}\}$ based on the pair of legitimate permutation matrices $\mathbf{\Pi}_m \in \mathbb{C}^{2\times 2}$, $m = 1, 2$, respectively, the inequality $[\tilde{\mathbf{R}}_{QRQ\_P}]^2_{\min} \geq [\tilde{\mathbf{R}}]^2_{\min}$ is satisfied.

Since we have $[\tilde{\mathbf{R}}]^2_{\min} = [\tilde{\mathbf{R}}_1]^2_{\min}$, Lemma 2 can be obtained.

2) The Proposed QRD-Based ED-TAS: According to Lemma 2, the QRD bound of Eq. (27) is tighter than that of Eq. (22). Hence, we use this tighter bound to derive the proposed QRD-based ED-TAS as

$$\mathbf{H}_{\hat{u}} = \arg \max_{u\in\{1,\cdots,N_U\}} \left\{ d^{\text{signal}}_{\min}, d^{\text{spatial}}_{\min}, d^{\text{QRD-bound\_P}}_{\min} \right\}. \tag{28}$$

Note that the complexity of the QRD-based TAS is dominated by the computation of $[\tilde{\mathbf{R}}_m]_{\min}$. In general, the full QRD can be adopted in Eq. (26) for solving Eq. (27). However, this may impose a high complexity. In order to reduce this complexity, for a fixed channel $\mathbf{H}_{u,ij}$, we found that the value of $[\tilde{\mathbf{R}}_m]_{\min}$ only depends on the diagonal entries of $\tilde{\mathbf{R}}_m$, namely $\tilde{R}_{k,k}(\mathbf{\Pi}_m)(k = 1, 2)$, which can be directly calculated as [38]

$$[\tilde{\mathbf{R}}_m]_k = \tilde{R}_{k,k}(\mathbf{\Pi}_m) = \sqrt{\frac{\det[(\mathbf{G}(1:k))^H \mathbf{G}(1:k)]}{\det[(\mathbf{G}(1:k-1))^H \mathbf{G}(1:k-1)]}}, \tag{29}$$

where $\mathbf{G}(1:k)$ denotes a matrix consisting of the first k columns of $\mathbf{H}_{u,ij}\mathbf{\Pi}_m$. In the classic V-BLAST systems, the calculation of Eq. (29) suffers from the problem of having a high complexity [38]. In SM, the number of non-zero elements of the error vectors of SM is up to 2. This sparse character leads to the simple sub-matrix $\mathbf{H}_{u,ij} = [\mathbf{h}_u(i), -\mathbf{h}_u(j)] \in \mathbb{C}^{N_r\times 2}$ and hence the values of $\tilde{R}_{k,k}(\mathbf{\Pi}_m)(m = 1, 2, k = 1, 2)$ are given by

$$\tilde{R}_{1,1}(\mathbf{\Pi}_1) = \sqrt{\|\mathbf{h}_u(i)\|^2_F}, \tag{30}$$

$$\tilde{R}_{2,2}(\mathbf{\Pi}_1) = \sqrt{\frac{\|\mathbf{h}_u(i)\|^2_F + \|\mathbf{h}_u(j)\|^2_F - 2\Re\{\mathbf{h}_u(i)^H \mathbf{h}_u(j)\}}{\|\mathbf{h}_u(i)\|^2_F}} \tag{31}$$

$$\tilde{R}_{1,1}(\mathbf{\Pi}_2) = \sqrt{\|\mathbf{h}_u(j)\|^2_F} \tag{32}$$

and

$$\tilde{R}_{2,2}(\mathbf{\Pi}_2) = \sqrt{\frac{\|\mathbf{h}_u(i)\|^2_F + \|\mathbf{h}_u(j)\|^2_F - 2\Re\{\mathbf{h}_u(i)^H \mathbf{h}_u(j)\}}{\|\mathbf{h}_u(j)\|^2_F}} \tag{33}$$

The complexity of our proposed QRD-TAS of Eq. (28) is dominated by the computation of $\tilde{R}_{k,k}(\mathbf{\Pi}_m)$, $m = 1, 2$. In SM, these values only depend on the values of $\|\mathbf{h}_u(i)\|^2_F$, $\|\mathbf{h}_u(j)\|^2_F$ and $\mathbf{h}_u(i)^H\mathbf{h}_u(j)$, which are elements of the matrix $\mathbf{H}^H\mathbf{H}$, as shown in Eqs. (30)-(33). Based on this observation, we can calculate the values of $\tilde{R}_{k,k}(\mathbf{\Pi}_m)$, $m = 1, 2$ by reusing these elements for the different TAS candidates $\mathbf{H}_u$,

TABLE I
COMPLEXITY COMPARISON OF DIFFERENT TAS ALGORITHMS FOR SM SYSTEMS

TAS algorithm	ED Optimality	Computational complexity
Exhaustive ED-TAS [13]	optimal	$\frac{N_t(N_t-1)}{2}(5N_r-1)M^2$
Maximum-norm based TAS of [21]	sub-optimal	$2N_tN_r - N_t$
Minimum-correlation based TAS of [15]	sub-optimal	$2N_t^2N_r - N_t^2 + \frac{3}{2}N_t(N_t-1)$
Conventional QRD-based ED-TAS of [24]	optimal	$2N_tN_r - N_t + 32N_t(N_t-1)(N_r-\frac{2}{3})\frac{M}{N_{APM}}$ ($N_{APM}=M$ for PSK, $N_{APM}=4$ for QAM)
Conventional SVD-based ED-TAS of [23]	sub-optimal	$2N_tN_r - N_t + \frac{19}{2}N_t(N_t-1)(N_r-\frac{1}{3})$
Simplified SVD-TAS [25]	sub-optimal	$\frac{N_t(N_t-1)}{2}(2N_r+11) + N_t(2N_r-1)$
Proposed QRD-based ED-TAS	sub-optimal	$2N_t^2N_r + \frac{3}{2}N_t(N_t-1)$
Proposed EVM-based ED-TAS	M-PSK: optimal	$2N_t^2N_r - N_t^2 + \frac{1}{2}N_t(N_t-1)(M+7)$
	$M-\text{QAM}\begin{cases}\text{sub-optimal}, & K<\upsilon\\ \text{optimal}, & K=\upsilon\end{cases}$	$2N_t^2N_r - N_t^2 + \frac{15}{2}GN_t(N_t-1)$
Exhaustive TAS&PA	——	$\binom{N_t}{L}C_{\text{PA}}$
Low-complexity TAS&PA	——	$C_{\text{TAS}} + C_{\text{PA}} = \begin{cases}C_{\text{PQRD}} + C_{\text{PA}}\\ C_{\text{EVM}} + C_{\text{PA}}\end{cases}$

hence the resultant complexity is considerably reduced compared to the conventional QRD-based ED-TAS, as will show in Table I.

To confirm the benefits of the QRD-based bound derived in Eq. (27), Fig. 2 shows the BER performance of the proposed QRD-based ED-TAS algorithm in contrast to the existing SVD-based ED-TAS of [23]. Moreover, we add the performance of the norm-based TAS of [13] and of the exhaustive-search based optimal ED-TAS of [21] as benchmarks. In Fig. 2, the number of TAs is set to $N_t = 4$, where $L = 2$ out of $N_t = 4$ TAs were selected in these TAS algorithms. As expected, since the proposed QRD-based ED-TAS has a tighter bound, in Fig. 2 it performs better than the SVD-based ED-TAS. Quantitatively, observe in Fig. 2 that this scheme provides an SNR gain of about 1.2 dB over the SVD-based ED-TAS at the BER of 10^{-5}. In Fig. 2, we also observe that the QRD-based ED-TAS achieves a near-optimum performance, where the performance gap between the proposed QRD-based ED-TAS and the exhaustive-search-based optimal ED-TAS is only about 0.2 dB. We will provide more detailed comparisons about the BER and the complexity issues in Section VI.

B. The Proposed EVM-Based ED-TAS

In this section, for striking a further flexible tradeoff in terms of the BER attained and the complexity imposed, we propose an EVM-based ED-TAS algorithm. The proposed EVM-TAS directly calculates the value of $d_{\min}(\mathbf{H}_u)$ for the specific TAS candidate $\mathbf{H}_u$, rather than exploiting the equivalent decision metric of Eq. (13) or the estimated bound of (18). Specifically, we will derive simple optimization metrics for both PSK and QAM constellations, where the error-vector selection probability is exploited for reducing the search space.

1) The Calculation of $d_{\min}(\mathbf{H}_u)$ in EVM-Based ED-TAS: Specifically, the M-PSK constellation can be expressed as $\mathbb{S}_{PSK} = \{e^{j\frac{2m\pi}{M}}, m = 0, \cdots, M-1\}$, and the symbols of the rectangular $M = 4^k$ QAM constellation belong to the set of [36]

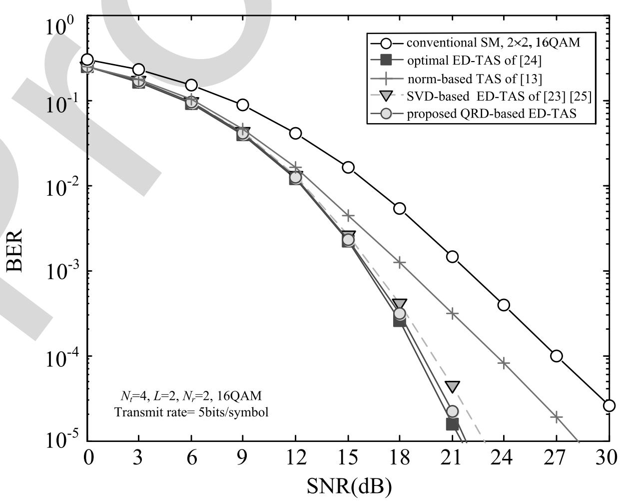

Fig. 2. BER performance comparison of the existing TAS algorithms and the proposed QRD-based ED-TAS algorithm. The setup of the simulation is based on $N_t = 4$, $N_r = 2$, $L = 2$ and 16-QAM. The transmit rate is 5 bits/symbol.

$$\mathbb{S}_{QAM} = \frac{1}{\sqrt{\beta_k}}\{a+bj, a-bj, -a+bj, -a-bj\}, \qquad (34)$$

where we have $\beta_k = \frac{2}{3}(4^k - 1)$ and $a, b \in \{1, 3, \cdots, 2^k - 1\}$. Similar to Eq. (14), the calculation of $d_{\min}(\mathbf{H}_u)$ is partitioned into three cases: $d_{\min}^{\text{signal}}$, $d_{\min}^{\text{spatial}}$ and $d_{\min}^{\text{joint}}$. As shown in Eqs. (15)-(16), $d_{\min}^{\text{signal}}$ depends the minimum distance of the APM $d_{\min}^{\text{APM}}$ as [39]

$$d_{\min}^{\text{APM}} = \begin{cases} 4\sin^2(\pi/M) & \text{for} \quad M-\text{PSK} \\ \frac{4}{\beta_k} & \text{for} \quad M-\text{QAM} \end{cases}, \qquad (35)$$

while $d_{\min}^{\text{spatial}}$ relies on the minimum squared modulus value $d_{\min}^{\text{Modulus}}$ of the APM constellation as

$$d_{\min}^{\text{Modulus}} = \begin{cases} 1 & \text{for} \quad M-\text{PSK} \\ \frac{2}{\beta_k} & \text{for} \quad M-\text{QAM} \end{cases}. \qquad (36)$$

Based on Eqs. (35) and (36), the complexity of computing the values of $d_{\min}^{\text{signal}}$ and $d_{\min}^{\text{spatial}}$ in Eqs. (15)-(16) may be deemed negligible. Hence, we only have to reduce the complexity of computing $d_{\min}^{\text{joint}}$, which can be achieved as follows:

$$\begin{aligned} d_{\min}^{\text{joint}-EVM} &= \min_{\substack{i,j=1,\cdots,L, i\neq j\\ s_a,s_b\in\mathbb{S}}} \|\mathbf{h}_u(i)s_a - \mathbf{h}_u(j)s_b\|_F^2 \\ &= \min_{\substack{i,j=1,\cdots,L,\\ i\neq j, s_a,s_b\in\mathbb{S}}} |s_a|^2 \|\mathbf{h}_u(i)\|_F^2 + |s_b|^2 \|\mathbf{h}_u(j)\|_F^2 - 2m_{\text{APM}}, \end{aligned} \tag{37}$$

where we have $m_{\text{APM}} = \mathcal{R}\{s_a^H s_b \mathbf{h}_u(i)^H \mathbf{h}_u(j)\}$, which relies on the specific APM scheme adopted. Next, we will derive the simplified metrics $d_{\min}^{\text{joint}-EVM}$ for the general family of M-PSK and M-QAM modulated SM systems.

2) Simplification for M-PSK Schemes: For a pair of M-PSK symbols $s_a = e^{j\frac{2a\pi}{M}}$ and $s_b = e^{j\frac{2b\pi}{M}}$, the possible values of $s_a^H s_b$ obey $e^{j\frac{2(b-a)\pi}{M}}$, $(b-a) \in \{-(M-1), \cdots, (M-1)\}$. As a result, m_{APM} of the general M-PSK scheme obeys:

$$m_{\text{APM}} \in \{\mathcal{R}\{\mathbf{h}_u(i)^H \mathbf{h}_u(j)\}\cos\theta_n - \mathcal{J}\{\mathbf{h}_u(i)^H \mathbf{h}_u(j)\}\sin\theta_n\}, \tag{38}$$

where $\theta_n = \frac{2n\pi}{M}$, $n = -(M-1), \cdots, (M-1)$. Since the minimum ED is considered in Eq (37), only the maximum value of m_{APM} needs to be considered, which is given by Eq. (39), shown at the bottom of the page. As shown in Eq. (39), the number of possible θ_n values is reduced from $2M-1$ to $\frac{M}{4}+1$. According to Eq. (39), $|s_a|^2 = 1$ and $|s_b|^2 = 1$, the distance $d_{\min}^{\text{joint}-EVM}$ of Eq. (37) is simplified for M-PSK as follows:

$$d_{\min}^{\text{joint}-EVM} = \min_{\substack{i,j=1,\cdots,L,\\ i\neq j}} \|\mathbf{h}_u(i)\|_F^2 + \|\mathbf{h}_u(j)\|_F^2 - 2m_{M\text{-PSK}}(\mathbf{H}_u). \tag{40}$$

Example: The constellation points s_a and s_b of BPSK and QPSK modulation schemes belong to the set $\mathbb{S}_{\text{BPSK}} = \{\pm 1\}$ and $\mathbb{S}_{\text{QPSK}} = \{\pm 1, \pm j\}$, respectively. Based on Eq. (39), the corresponding optimized metrics $m_{M-\text{PSK}}(\mathbf{H}_u) = \max m_{\text{APM}}$ are simplified to $m_{2-\text{PSK}}(\mathbf{H}_u) = |\mathcal{R}\{\mathbf{h}_u(i)^H \mathbf{h}_u(j)\}|$ and $m_{4-\text{PSK}}(\mathbf{H}_u) = \max\{|\mathcal{R}\{\mathbf{h}_u(i)^H \mathbf{h}_u(j)\}|, |\mathcal{J}\{\mathbf{h}_u(i)^H \mathbf{h}_u(j)\}|\}$, respectively.

As shown in Eqs. (37)-(40), since we have $|s_a|^2 = 1$, $|s_b|^2 = 1$ and a reduced set $s_a^H s_b$ for M-PSK constellation, the complexity of calculating $d_{\min}^{\text{joint}-EVM}$ is low, as it will be shown in Table I.

3) Simplification for M-QAM Schemes: When M-QAM constellations are considered, the calculation of $d_{\min}^{\text{joint}-EVM}$ in Eq. (37) becomes substantially complicated, because there are many combinations of the values of $|s_a|^2$, $|s_b|^2$ and $s_a^H s_b$ in Eq. (37), which lead to different received SM-symbol distances. To derive a simplified optimized metrics for M-QAM, we first introduce the following Lemma.

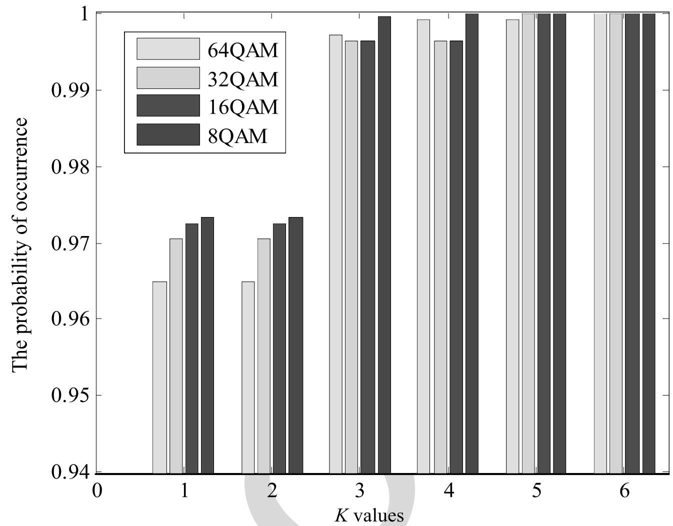

Fig. 3. The statistical probability of the norm error vectors relying on K minimum moduli, yielding the optimal ED-TAS solution, where the system setup is $N_t = 4$, $N_r = 2$ and $L = 2$.

Lemma 3: It is highly likely that an error vector associated with a small norm value yields the FD value of Eq. (9). Thus, the search space to be evaluated for finding the FD can be reduced to a few dominant error vectors having small norm values.

Proof: Based on the Rayleigh-Ritz theorem of [37], for a fixed channel matrix $\mathbf{H}_{u,ij}$ and a given error vector $\mathbf{e}_{ij}$, the distance amongst the received symbols is bounded by $\lambda_{\max}^2(\mathbf{H}_{u,ij})\,\|\mathbf{e}_{ij}\|^2 \geq \|\mathbf{H}_u\mathbf{e}_{ij}\|^2 \geq \lambda_{\min}^2(\mathbf{H}_{u,ij})\,\|\mathbf{e}_{ij}\|^2$, where $\lambda_{\max}^2(\mathbf{H}_{u,ij})$ is the maximum squared singular value of the submatrix $\mathbf{H}_{u,ij} = [\mathbf{h}_u(i), -\mathbf{h}_u(j)]$. It may be readily shown that the values of $\lambda_{\max}^2(\mathbf{H}_{u,ij})$ and $\lambda_{\min}^2(\mathbf{H}_{u,ij})$ are constants for a fixed channel realization $\mathbf{H}_{u,ij}$, while the value of $\|\mathbf{e}_{ij}\|^2$ depends on the specific APM constellation points. Based on the bound above, it is highly likely that an $\mathbf{e}_{ij}$ with a small norm yields low upper bound and lower bound. Hence it has a high probability of generating the FD value, as it will be exemplified in Fig. 3. ■

Based on Lemma 3, for the sake of striking a beneficial trade-off between the BER performance and complexity for M-QAM, the search space is limited to the error vectors having small modulus values and only these vectors are utilized to compute the FD metric. Specifically, we first evaluate all possible modulus values $T_1, T_2, T_3, \cdots, T_v$ of all the legitimate error vectors $\mathbf{e}_{ij}$, then we find the K smallest T_K from the full set of $\{T_1, T_2, T_3, \cdots, T_v\}$ and only consider the set of $\mathbf{e}_{ij}$ having moduli lower than T_K to compute $d_{\min}(\mathbf{H}_u)$. In this process, the error vectors can be divided into the pair of sub-sets $\mathbb{D}_1$ and $\mathbb{D}_2$ based on their sparsity, where $\mathbb{D}_1$ contains the error vectors, which have only a single non-zero element, while $\mathbb{D}_2$ contains

$$\begin{aligned} m_{M-\text{PSK}}(\mathbf{H}_u) = \max_n m_{\text{APM}} &= \max_{n\in\{-(M-1),\cdots,M-1\}} \{\mathcal{R}\{\mathbf{h}_u(i)^H \mathbf{h}_u(j)\}\cos\theta_n - \mathcal{J}\{\mathbf{h}_u(i)^H \mathbf{h}_u(j)\}\sin\theta_n\} \\ &= \max_{n\in\{0,\cdots,M/4\}} \{|\mathcal{R}\{\mathbf{h}_u(i)^H \mathbf{h}_u(j)\}\cos\theta_n - \mathcal{J}\{\mathbf{h}_u(i)^H \mathbf{h}_u(j)\}\sin\theta_n|\}. \end{aligned} \tag{39}$$

the error vectors, which have two non-zero elements. As will be shown in our simulation results, $K = 3$ is a good choice for diverse configurations, hence we only provide the simplified expressions of $d_{\min}^{\text{joint}-EVM}$ for $K \leq 3$ as follows.

For $K = 1$, according to the M-QAM constellation of Eq. (34), only error vectors having $T_1 = \sqrt{\frac{4}{\beta_k}}$ are considered and the associated sets $\mathbb{D}_1$ and $\mathbb{D}_2$ are given by $\mathbb{D}_1 = \frac{1}{\sqrt{\beta_k}}\{\pm 2\mathbf{e}_i, \pm 2\text{j}\mathbf{e}_i\}, i = 1, \cdots, L$ and $\mathbb{D}_2 = \frac{1}{\sqrt{\beta_k}}\{(\pm 1 \pm 1\text{j})\mathbf{e}_i - (\pm 1 \pm 1\text{j})\mathbf{e}_j\}, i, j = 1, \cdots, L, i \neq j$, respectively, where $\mathbf{e}_i$ and $\mathbf{e}_j$ are the active TA selection vectors in Eq. (2). Since only the minimum ED is considered, the set $\mathbb{D}_1$ can be reduced to $\mathbb{D}_1 = \frac{1}{\sqrt{\beta_k}}\{2\mathbf{e}_i\}, i = 1, \cdots, L$. Moreover, based on the set $\mathbb{D}_2$, it is find that the elements s_a and s_b belong to the reduced set $\frac{1}{\sqrt{\beta_k}}\{\pm 1 \pm 1\text{j}\}$ and we have $|s_a|^2 = \frac{2}{\beta_k}$, $|s_b|^2 = \frac{2}{\beta_k}$ and $s_a^H s_b \in \frac{2}{\beta_k}\{\pm 1, \pm 1\text{j}\}$. Substituting these values into Eq. (37), we get the simplified optimized metric for $K = 1$ as

$$d_{\min, K=1}^{\text{joint}-EVM} = \min_{\substack{i,j=1,\cdots,L,\\ i \neq j,}} \frac{2}{\beta_k}\|\mathbf{h}_u(i)\|_F^2 + \frac{2}{\beta_k}\|\mathbf{h}_u(j)\|_F^2 - 2m_{M-QAM}^{K=1}, \tag{41}$$

where we have

$$\begin{aligned} m_{M-QAM}^{K=1} &= \max m_{\text{APM}} \\ &= \max\left\{\frac{2}{\beta_k}\left|\mathcal{R}\{\mathbf{h}_u(i)^H\mathbf{h}_u(j)\}\right|, \frac{2}{\beta_k}\left|\mathcal{I}\{\mathbf{h}_u(i)^H\mathbf{h}_u(j)\}\right|\right\}. \end{aligned} \tag{42}$$

For the case of $K = 2$, all the error vectors $\mathbf{e}_{ij}$ having moduli lower than T_2 are used for FD calculation. Compared to $K = 1$, we have to consider the added error vectors $\frac{1}{\sqrt{\beta_k}}\{\pm 2 \pm 2\text{j}\mathbf{e}_i\} (i = 1, \cdots, L)$ having $T_2 = \sqrt{\frac{8}{\beta_k}}$, which belong to $\mathbb{D}_1$ and do not change the set $\mathbb{D}_2$. After eliminating all collinear elements, the set $\mathbb{D}_1$ of $K = 2$ is reduced to $\frac{1}{\sqrt{\beta_k}}\{2\mathbf{e}_i, \pm 2 \pm 2\text{j}\mathbf{e}_i\}, i = 1, \cdots, L$. Moreover, since only the minimum distance is investigated, the set is further reduced to $\mathbb{D}_1 = \frac{1}{\sqrt{\beta_k}}\{2\mathbf{e}_i\}, i = 1, \cdots, L$, which is the same as that of $K = 1$. Therefore, the setups of $K = 1$ and $K = 2$ will provide the same FD $d_{\min}(\mathbf{H}_u)$.

Moreover, for the case of $K = 3$, besides the error vectors $\mathbf{e}_{ij}$ for $K = 2$, the error vectors having $T_3 = \sqrt{\frac{10}{\beta_k}}$ should be considered, which are given by $\frac{1}{\sqrt{\beta_k}}\{(\pm 3 \pm 1\text{j})\mathbf{e}_i - (\pm 1 \pm 1\text{j})\mathbf{e}_j, (\pm 1 \pm 3\text{j})\mathbf{e}_i - (\pm 1 \pm 1\text{j})\mathbf{e}_j\}$, $i, j = 1, \cdots, L, i \neq j$. For these added error vectors, we have $s_a^H s_b \in \frac{1}{\beta_k}\{\pm 2 \pm 4\text{j}, \pm 4 \pm 2\text{j}\}$ and two legitimate combinations of the values of $|s_a|^2$ and $|s_b|^2$ as: (1) $|s_a|^2 = \frac{2}{\beta_k}$, $|s_b|^2 = \frac{10}{\beta_k}$ and (2) $|s_a|^2 = \frac{10}{\beta_k}$, $|s_b|^2 = \frac{2}{\beta_k}$. For each combination, similar to the process of Eqs. (41)-(42), we can substitute the values of $|s_a|^2$, $|s_b|^2$ and $s_a^H s_b$ into Eq. (37) and get the simplified optimized metric for $K = 3$ as

$$d_{\min, K=3}^{\text{joint}-EVM} = \min\{d_{\min, K=1}^{\text{joint}-EVM}, d_{\min,(1)}^{\text{joint}-EVM}, d_{\min,(2)}^{\text{joint}-EVM}\} \tag{43}$$

where $d_{\min,(1)}^{\text{joint}-EVM}$ and $d_{\min,(2)}^{\text{joint}-EVM}$ are the simplified ED for the above-mentioned two combinations, given by Eq. (44), shown at the bottom of the page.

4) The Proposed EVM-Based ED-TAS: Based on the simplified versions of $d_{\min}^{\text{joint}-EVM}$ for M-PSK and M-QAM schemes derived in Eqs. (41) and (43), the solution of our EVM-based ED-TAS algorithm is given by

$$\mathbf{H}_{\hat{u}} = \arg\max_{u \in \{1, \cdots, N_U\}} \left\{d_{\min}^{\text{signal}}, d_{\min}^{\text{spatial}}, d_{\min}^{\text{joint}-EVM}\right\}. \tag{45}$$

Note that similar to the proposed QRD-TAS, the terms $\|\mathbf{h}_u(i)\|_F^2$, $\|\mathbf{h}_u(j)\|_F^2$ and $\mathbf{h}_u(i)^H\mathbf{h}_u(j)$ in Eqs. (40)-(44) are elements of the matrix $\mathbf{H}^H\mathbf{H}$. Then, we can find the solution of Eq. (45) by reusing these elements for different TAS candidates $\mathbf{H}_u$.

Fig. 3 shows the probability that the error vectors having the minimum norm do result in finding the optimal ED-TAS solution as a function of K. For example, we have a probability of 97% for 16-QAM modulated SM for $K = 1$ using $N_t = 4$, $L = 2$ and $N_r = 2$. Moreover, it is observed from Fig. 3 that this probability is also high for other QAM schemes; hence the EVM-based ED-TAS can be readily used in diverse scenarios. In general, for striking a flexible BER vs complexity tradeoff, we can adjust the parameter K to reduce the search space to a subset of the error vectors that may yield the optimal ED-TAS solution with a high probability.

Note that in [17] a PEP-based TAS (PEP-TAS) algorithm was proposed, which was based on a different search set reduction. The main differences of the proposed EVM-TAS and the PEP-TAS of [17] are:

- The PEP-TAS is based on the assumption that a smaller APM symbol amplitude leads to a smaller distance $d_{\min}^{\text{joint}}$, whereas based on our analysis it is highly likely that an error vector with a small norm yields the distance $d_{\min}^{\text{joint}}$.
- Moreover, in EVM-TAS, we propose to use the parameter K for striking a flexible tradeoff between the conflicting factors of the computational complexity imposed and the attainable BER.

Remark: Compared to the EVM-TAS, the PEP-TAS considers only the error vectors generated by M-QAM symbols having the minimum amplitude. It can be shown that the non-linear error vectors of the PEP-TAS are the same as those of the

$$\begin{cases} d_{\min,(1)}^{\text{joint}-EVM} = \min\limits_{\substack{i,j=1,\cdots,L\\ i \neq j}} \frac{2}{\beta_k}\|\mathbf{h}_u(i)\|_F^2 + \frac{10}{\beta_k}\|\mathbf{h}_u(j)\|_F^2 - 2m_{M-QAM}^{K=3} \\ d_{\min,(2)}^{\text{joint}-EVM} = \min\limits_{\substack{i,j=1,\cdots,L\\ i \neq j}} \frac{10}{\beta_k}\|\mathbf{h}_u(i)\|_F^2 + \frac{2}{\beta_k}\|\mathbf{h}_u(j)\|_F^2 - 2m_{M-QAM}^{K=3} \\ m_{M-QAM}^{K=3} = \max \frac{1}{\beta_k}\left\{\left|2\mathcal{R}\{\mathbf{h}_u(i)^H\mathbf{h}_u(j)\}\right| + \left|4\mathcal{I}\{\mathbf{h}_u(i)^H\mathbf{h}_u(j)\}\right|, \left|4\mathcal{R}\{\mathbf{h}_u(i)^H\mathbf{h}_u(j)\}\right| + \left|2\mathcal{I}\{\mathbf{h}_u(i)^H\mathbf{h}_u(j)\}\right|\right\} \end{cases} \tag{44}$$

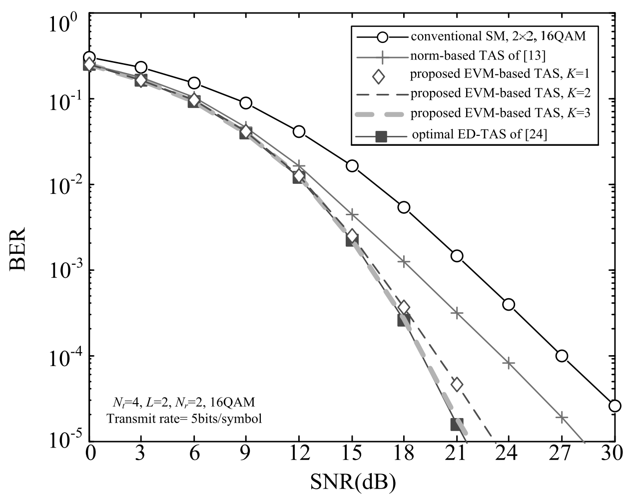

Fig. 4. BER performance comparison of the existing TAS algorithms and the proposed EVM-based TAS algorithm for $N_t = 4$, $N_r = 2$, 16QAM and $L = 2$. The transmit rate is 5 bits/symbol.

EVM-TAS associated with $K = 1$. Therefore, it can be viewed as a special case of EVM-TAS by setting $K = 1$.

Fig. 4 shows our BER comparison for the existing TAS algorithms and the proposed EVM-TAS algorithm. The simulation parameters are the same as those of Fig. 2. Firstly, as proved in Section IV-B and observed in Fig. 3, the probability that the error vectors do indeed result in the optimal ED-TAS solution is the same for the cases of $K = 1$ and $K = 2$. Hence, they provide the same BER performance, as shown in Fig. 4. Furthermore, we observe in Fig. 3 that this probability is increased from 0.975 to 0.998 upon increasing K from 1 to 3. As a result, in Fig. 4 the performance of the EVM-based ED-TAS associated with $K = 3$ is improved compared to that scheme with $K = 1$. Moreover, compared the results in Figs. 2 and 4, the EVM-based ED-TAS outperforms the SVD-based ED-TAS for $K = 3$.

V. Joint TAS and PA Algorithms for SM

Similar to the TAS technique, PA is another attractive link adaptation technique conceived for SM, which has been advocated in [7], [11], [28], [29]. The process of PA can be modeled by the PA matrix $\mathbf{P}$, which is given by

$$\mathbf{P} = \mathrm{diag}\{p_1, \cdots, p_q, \cdots, p_L\}, \tag{46}$$

where p_q controls the channel gain of the qth TA. Here, we let $\sum_{q=1}^{L} p_q^2 = 1$ for normalizing the transmit power. Based on our TAS algorithms, we propose a pair of combined algorithms for jointly considering the PA and TAS as follows:

1) **TAS&PA**

- *Step 1*: Each $(N_r \times N_t)$ channel matrix $\mathbf{H}$ has $N_U = \binom{N_t}{L}$ possible subchannel matrices $\mathbf{H}_u$, each of which corresponds to a specifically selected $(N_r \times L)$ MIMO channel. For each $\mathbf{H}_u$, we calculate the corresponding PA matrix $\mathbf{P}_u$ and its FD with the aid of the algorithm of [29].
- *Step 2*: The particular combinations of $\mathbf{H}_u\mathbf{P}_u (u = 1, \cdots, N_U)$ constitute the legitimate TAS&PA candidates. Let us interpret the matrices $\mathbf{H}_u\mathbf{P}_u$ $(u = 1, \cdots, N_U)$ as being the equivalent channel matrices of Section IV and select the specific candidate with the maximum free distance as the final solution.

Since for each channel realization $\mathbf{H}$, there are N_U possible PA matrices $\mathbf{P}_u (u = 1, \cdots, N_U)$, we have a high computational complexity if N_U is high. Next, we introduce a lower-complexity solution for this joint TAS and PA algorithm.

2) **Low-complexity TAS&PA**

- *Step 1*: Assume $\mathbf{P}_u = \mathbf{I}_L (u = 1, \cdots, N_U)$ and use the proposed low-complexity QRD-based ED-TAS or the EVM-based ED-TAS algorithm to select a particular subset of TAs from the set of options, which corresponds to $\mathbf{H}_{\hat{u}}$.
- *Step 2*: Calculate the power weights for the selected TAs, which can be represented by the PA matrix $\mathbf{P}_{\hat{u}}$. During this step, the low-complexity PA algorithm of [29] can be invoked. In the simple TAS&PA, the PA matrix only has to be calculated once, hence the associated complexity is low.

VI. Simulation Results

In this section, we provide simulation results for further characterizing the proposed QRD-based ED-TAS, EVM-based ED-TAS and TAS&PA schemes for transmission over frequency-flat fading MIMO channels. For comparison, these performance results are compared to various existing TAS-SM schemes of [13], [21], [23], [25], to the classic TAS/maximal-ratio combining (TAS/MRC) schemes of [40], as well as to the TAS&PA aided V-BLAST of [32]. In our simulations, the single-stream ML detector of [34], [35] is utilized.

A. BER Comparisons of Different TAS Algorithms for SM

In Fig. 5, we compare the BER performance of various TAS-SM schemes for 4 bits/symbol associated with $N_t = 8$, $L = 4$, $N_r = 4$ and QPSK. We also considered the conventional single-RF based TAS/MRC arrangement of [40] as benchmarker. As seen from Fig. 5, the proposed QRD-based ED-TAS outperforms the conventional SVD-based ED-TAS of [23], as also formally shown in Fig. 2. Moreover, as expected, in Fig. 5 the EVM-based TAS is capable of achieving the same performance as the optimal ED-TAS of [21]. We also confirm that our proposed EVM-based ED-TAS schemes outperform the norm-based TAS of [13] and the QRD-based ED-TAS proposed for PSK modulation. These results are consistent with the analysis results in Section IV, where the EVM-based TAS has considered all legitimate error vectors for simplifying $d_{\min}^{\text{joint}}$ in Eq. (40), while the QRD-based ED-TAS may achieve uncorrect estimation of $d_{\min}^{\text{joint}}$ due to the employment of lower bound of Eq. (27).

Fig. 5 also shows that our new TAS-SM schemes outperform the TAS/MRC scheme of [40]. The main reason behind the poorer performance of TAS/MRC is the employment of a higher modulation order required for achieving the same

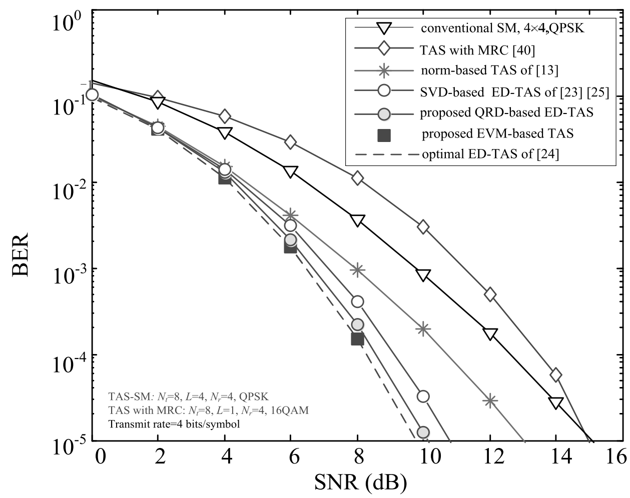

Fig. 5. BER comparison at $m = 4$ bits/symbol for the proposed TAS-SM schemes, the existing TAS-SM schemes and the classic TAS/MRC scheme having $N_t = 8$ and $L = 4$.

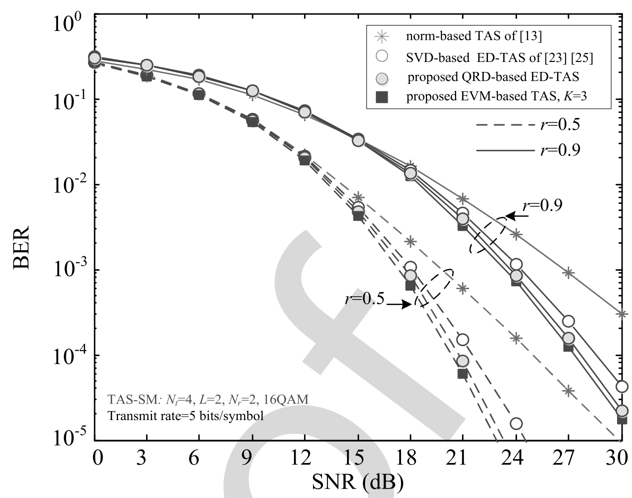

Fig. 7. BER comparison of different TAS algorithms for SM systems in correlated Rayleigh fading channels.

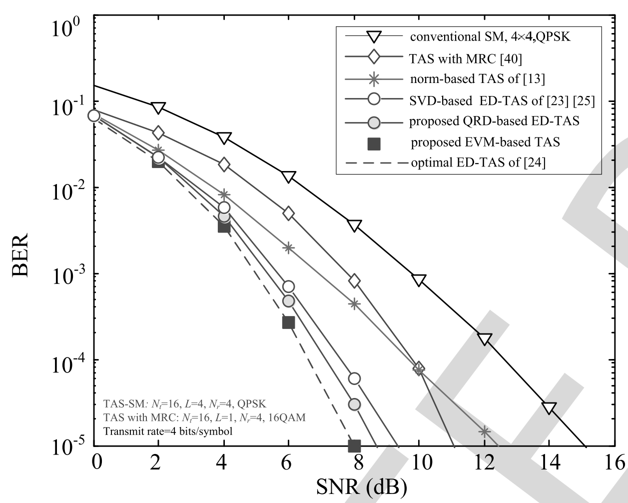

Fig. 6. BER comparison at $m = 4$ bits/symbol for the proposed TAS-SM schemes, the existing TAS-SM schemes and the classic TAS/MRC scheme having $N_t = 16$ and $L = 4$.

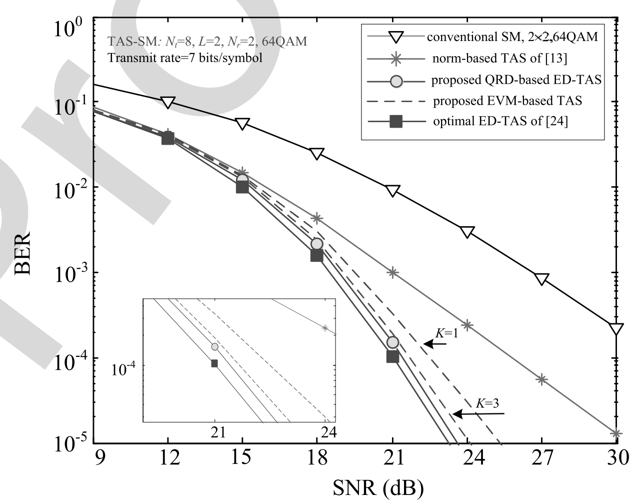

Fig. 8. BER comparison at $m = 7$ bits/symbol for the proposed QRD-based ED-TAS and EVM-based ED-TAS with 64-QAM.

throughput as our SM-based schemes. Note that this benefit depends on the particular MIMO setups. To be specific, as noted in [23], the TAS-SM and the TAS/MRC schemes exhibit different BER advantages for different system setups. However, similar to the results achieved in [23], our new TAS-SM schemes strike an attractive tradeoff between the complexity and the BER attained. The above-mentioned trends of these proposed TAS-SM schemes are also confirmed in Fig. 6, where the number N_t of TAs increases from 8 to 16.

In Fig. 7, a spatially correlated MIMO channel model characterized by $\mathbf{H}^{corr} = \mathbf{R}_r^{1/2}\mathbf{H}\mathbf{R}_t^{1/2}$ [24], [41] is considered for the proposed QRD-based ED-TAS and EVM-based TAS ($K = 3$) schemes, where $\mathbf{R}_t = [r_{ij}]_{N_t \times N_t}$ and $\mathbf{R}_r = [r_{ij}]_{N_r \times N_r}$ are the positive definite Hermitian matrices that specify the transmit and receive correlations, respectively. In Fig. 7, the components of $\mathbf{R}_t$ and $\mathbf{R}_r$ are calculated as $r_{ij} = r_{ji}^* = r^{j-i}$ for $i \leq j$, where r is the correlation coefficient ($0 \leq r \leq 1$). Here, the simulation parameters are the same as those of Figs. 2 and 4 for 5 bits/symbol transmissions. We found that the BER curves of the EVM-based TAS schemes and of the optimal ED-TAS are almost overlapped (similar to the results seen in Fig. 4), hence for clarity in Fig. 7 we simply provide the BER curves for the EVM-based TAS schemes only. Compared to the BER curves in Figs. 2 and 4 for the correlation coefficient $r = 0$, we observe in Fig. 7 that the BER performance of all schemes is substantially degraded by these correlations. However, the proposed schemes remain capable of operating efficiently for the correlated channels.

In Fig. 8, we further compare the proposed QRD-based ED-TAS scheme and the proposed EVM-based TAS schemes for a higher modulation order, where the 64-QAM scheme is employed. Observe in Fig. 8 that the proposed QRD-based ED-TAS scheme outperforms the EVM-based TAS scheme in conjunction with $K = 1$ and the corresponding performance gain is seen to be about 1 dB. Similar to the results in Figs. 2 and 4, the EVM-based TAS associated with $K = 3$ provide an improved BER compared to that scheme with $K = 1$. At

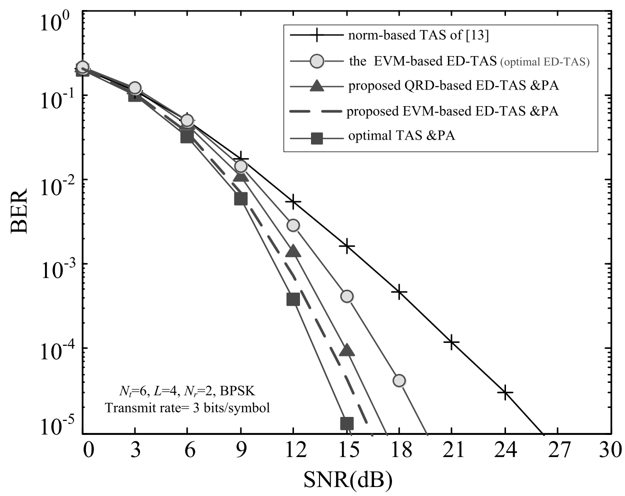

Fig. 9. BER performance comparison of the TAS algorithms and of the proposed TAS &PA algorithms in SM systems, having the transmit rate of 3 bits/symbol.

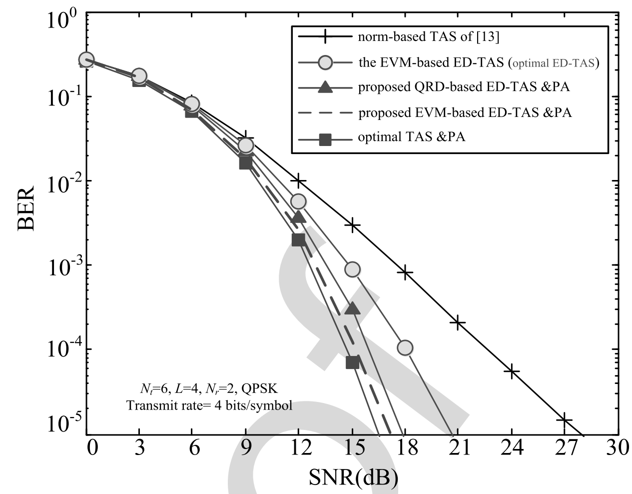

Fig. 10. BER performance comparison of the TAS algorithms and of the proposed TAS &PA algorithms in SM systems, having the transmit rate of 4 bits/symbol.

BER=10^{-5}, the performance gap between the proposed EVM-based TAS with $K = 3$ and the proposed QRD-based ED-TAS becomes negligible.

The main conclusions observed from Figs. 2, 4 and 5–8 are: (1) the proposed EVM-based TAS and QRD-based ED-TAS schemes exhibit different BER advantages for different system setups; (2) the proposed QRD-based ED-TAS is preferred to the QAM-modulated SM schemes, since its complexity is independent of the modulation order; (3) The proposed EVM-based TAS is preferred to the PSK-modulated SM schemes, since it can achieve the performance of optimal ED-TAS at the reduced error vector set. (4) For the QAM-modulated SM schemes, the parameter K of the proposed EVM-based TAS can be flexibly selected for striking a beneficial trade-off between the complexity imposed and the BER attained.

B. BER Comparisons of TAS Algorithms and TAS &PA Algorithms for SM

In this subsection, we focus our attention on studying the BER performance of our TAS&PA algorithms. Here, for the low-complexity TAS&PA, the proposed QRD-based ED-TAS as well as the EVM-based ED-TAS algorithms are utilized and the corresponding algorithms are termed as the QRD-based ED-TAS &PA and the EVM-based ED-TAS &PA, respectively. Note that the EVM-based ED-TAS achieves the same performance as the optimal ED-TAS for the PSK-modulated SM schemes. The BER performances of other TAS algorithms are similar to the results seen in Figs. 2, 4 and 5–8. Hence, for clarity, when only pure TAS is considered, we simply provide the corresponding BER curves of the proposed EVM-based ED-TAS and of the conventional norm-based TAS as benchmarkers.

Fig. 9 compares the BER performance of the proposed TAS&PA arrangement to that of other SM-based schemes. In Fig. 9, the parameter setup is $N_t = 6$, $L = 4$, $N_r = 2$ and $M = 2$. It becomes clear from Fig. 9 that the TAS&PA algorithms advocated outperform both the EVM-based ED-TAS and the norm-based ED-TAS. At a BER of 10^{-5}, the exhaustive-search based optimal TAS&PA provides 9.5 dB and 4 dB SNR gains over the norm-based ED-TAS and over the EVM-based ED-TAS, respectively. Moreover, the low-complexity QRD-based ED-TAS &PA provides about 4 dB SNR gain over the EVM-based TAS operating without PA.

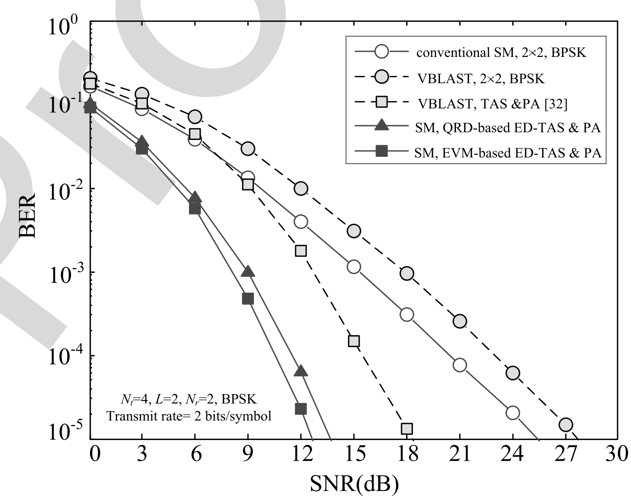

Fig. 11. BER performance comparison of the proposed TAS &PA algorithms in SM systems and the conventional identical-throughput TAS&TA algorithm in V-BLAST systems, where the throughput is 2 bits/symbol ($N_t = 4$, $N_r = 2$, $L = 2$).

Fig. 9 also shows that the EVM-based ED-TAS &PA outperforms the QRD-based ED-TAS&PA and is capable of achieving almost the same BER performance as the optimal TAS&PA. The performance advantages of our schemes are attained as a result of exploiting all the benefits of MIMO channels. The above-mentioned trends of these TAS&PA algorithms recorded for SM are also visible in Fig. 10, where a SM system using $N_t = 6$, $L = 4$, $N_r = 2$ and QPSK modulation is considered.

In Fig. 11, the BPSK-modulated V-BLAST scheme and its TAS&PA-aided counterpart [32] associated with zero-forcing successive interference cancellation (ZF-SIC) are compared to

TABLE II
COMPLEXITY COMPARISON OF DIFFERENT TAS-SM ALGORITHMS IN DIVERSE CONFIGURATIONS

TAS algorithm	Configuration 1 ($N_t = 4$, $N_r = 2$ $L = 2$, 16QAM)	Configuration 2 ($N_t = 8$, $N_r = 4$ $L = 4$, QPSK)	Configuration 3 ($N_t = 8$, $N_r = 2$ $L = 2$, 64-QAM)
Exhaustive ED-TAS [13]	13824	8512	1032192
Maximum-norm based TAS [21]	12	56	24
Conventional QRD-based ED-TAS [24]	2060	6029	38253
SVD-based ED-TAS [25]	102	588	444
Proposed QRD-based ED-TAS	82	596	340
Proposed EVM-based ED-TAS	84, $K = 1$; 180, $K = 3$	756	360, $K = 1$; 808, $K = 3$
Exhaustive TAS&PA	4626	46340	256788
Proposed QRD-based ED-TAS&PA	853	1004	9511
Proposed EVM-based ED-TAS&PA	855, $K = 1$; 951, $K = 3$	1164	9531, $K = 1$; 9979, $K = 3$

our TAS&PA based schemes. For maintaining an identical-throughput, in Fig. 11 we let $N_t = 4$, $N_r = 2$, $L = 2$ and use BPSK for all schemes. Observe in Fig. 11 that our TAS&PA based SM schemes outperform the TAS&PA aided V-BLAST schemes by about 5-6 dB SNR at the BER of 10^{-5}.

C. Complexity Comparison

Table I shows the complexity comparison of various TAS algorithms conceived for SM, where the total number of floating point operations is considered. The Appendix provides the details of our computational complexity evaluations for the proposed TAS algorithms list in Table I. The complexity estimation of the existing TAS algorithms can be found in [15], [23] and [24]. Moreover, our complexity analysis is similar to that of [23] and [24].

Explicitly, in Table II, the quantified complexity of different TAS algorithms for some specific configurations are provided. As shown in Table I, the proposed QRD-based ED-TAS has a similar complexity order to that of the low-complexity SVD-based ED-TAS of [23], while exhibiting a lower complexity compared to the conventional QRD-based ED-TAS of [24]. For example, the proposed QRD-based ED-TAS imposes an approximately 168 times and 25 times lower complexity than the exhaustive ED-TAS and the conventional QRD-based ED-TAS for configuration 1. This is due to the fact that it is capable of avoiding the high-complexity QRD operation by directly computing the bound parameters of Eq. (27). Moreover, as shown in Tables I-II and Figs. 4-8, the EVM-based ED-TAS advocated is capable of striking a flexible BER vs complexity trade-off by employing the parameter K for diverse M-QAM schemes. Furthermore, the proposed low-complexity TAS&PA schemes impose a lower complexity than the exhaustive-search based TAS&PA and only impose a slightly increased complexity compared to the proposed EVM-based TAS and QRD-based TAS schemes. By considering the BER vs complexity results of Tables I-II and Figs. 9-11, the proposed low-complexity TAS&PA is seen to provide an improved BER performance at a modest complexity cost.

VII. CONCLUSIONS

In this paper, we have investigated TAS algorithms conceived for SM systems. Firstly, a pair of low-complexity ED-TAS algorithms, namely the QRD-based ED-TAS and the EVM-based ED-TAS, were proposed. The theoretical analysis and simulation results indicated that the QRD-based ED-TAS exhibits a better BER performance compared with the conventional SVD-based ED-TAS, while the EVM-based ED-TAS is capable of striking a flexible BER vs complexity trade-off. To further improve the attainable performance, the proposed TAS algorithms were amalgamated with PA. A pair of beneficial joint TAS-PA algorithms were proposed and our simulation results demonstrated that they outperform both the pure TAS algorithms and the TAS&PA algorithm designed for spatial multiplexing systems.

APPENDIX

Computational complexity of the proposed TAS algorithms designed for SM systems.

A. The Proposed QRD-Based ED-TAS

As detailed in Section IV-A, the calculation of the QRD-based bound of Eq. (27) only depends on the elements of the matrix $\mathbf{H}^H\mathbf{H}$, which incurs a complexity in the order of $comp(\mathbf{H}^H\mathbf{H}) = 2N_t^2N_r - N_t^2$. Then, we can calculate the values of $\tilde{R}_{k,k}(\mathbf{\Pi}_m), (m = 1, 2,\ \ k = 1, 2)$ in Eqs. (30)-(33) by reusing these elements for the different TAS candidates $\mathbf{H}_u$. Specifically, the calculation of $\sqrt{\|\mathbf{h}_u(j)\|_F^2}$, $j = 1, \cdots, N_t$ for estimating $\tilde{R}_{1,1}(\mathbf{\Pi}_m), m = 1, 2$ in Eqs. (30) and (32) requires N_t flops. Moreover, to calculate the values of $\tilde{R}_{2,2}(\mathbf{\Pi}_m), m = 1, 2$ in Eqs. (31) and (33), we have to consider $\binom{N_t}{2}$ possible combinations (i, j) for computing the value of $\sqrt{\frac{\|\mathbf{h}_u(i)\|_F^2 + \|\mathbf{h}_u(j)\|_F^2 - 2\mathcal{R}\{\mathbf{h}_u(i)^H\mathbf{h}_u(j)\}}{\|\mathbf{h}_u(j)\|_F^2}}$. For each combination, the complexity imposed is 5 flops. Hence, the complexity of computing $\tilde{R}_{2,2}(\mathbf{\Pi}_m), m = 1, 2$ is $5\binom{N_t}{2}$ flops. The overall complexity of the proposed QRD-based ED-TAS is

$$\begin{aligned} C_{\text{PQRD}} &= 2N_t^2N_r - N_t^2 + N_t + 5\tbinom{N_t}{2} \\ &= 2N_t^2N_r + \tfrac{3}{2}N_t(N_t - 1). \end{aligned} \tag{47}$$

Note that based on Eq. (28), $d_{\min}^{\text{Modulus}}$, $d_{\min}^{\text{APM}}$ and $d_{\min}^{\text{all}}$ are constants for a specific APM scheme and the calculation of $d_{\min}^{\text{signal}}$ and $d_{\min}^{\text{spatial}}$ can also exploit the common elements, such as $\|\mathbf{h}_u(i)\|_F^2 + \|\mathbf{h}_u(j)\|_F^2 - 2\mathcal{R}\{\mathbf{h}_u(i)^H\mathbf{h}_u(j)\}$, $\|\mathbf{h}_u(i)\|_F^2$, in the calculation of the bound of $d_{\min}^{\text{joint}}$, as shown in Eqs. (15) and (16). Hence, the complexity imposed can be deemed negligible.

B. The Proposed EVM-Based ED-TAS

Similar to the proposed QRD-based ED-TAS, the computational complexity of EVM-based ED-TAS is also dominated by computing $d_{\min}^{\text{joint}}$. Specifically, we also first have to evaluate the elements $\|\mathbf{h}_u(i)\|_F^2$, $\|\mathbf{h}_u(j)\|_F^2$ and $\mathbf{h}_u(i)^H\mathbf{h}_u(j)$, which incurs a complexity of $2N_t^2N_r - N_t^2$ flops. Then, for M-PSK, the simplified version of $d_{\min}^{\text{joint}}$ is given in Eq. (40), which has to consider $\binom{N_t}{2}$ legitimate TA combination (i, j). For each combination (i, j), the computation of the term $m_{M\text{–PSK}}(\mathbf{H}_u)$ of Eq. (39) has to consider $(\frac{M}{4}+1)$ possible θ_n values. For each θ_n, the complexity of evaluating $\left|\mathcal{R}\{\mathbf{h}_u(i)^H\mathbf{h}_u(j)\}\cos\theta_n - \mathcal{I}\{\mathbf{h}_u(i)^H\mathbf{h}_u(j)\}\sin\theta_n\right|$ is 4 flops. Moreover, for a specific $m_{M\text{–PSK}}(\mathbf{H}_u)$ and a fixed combination (i, j), the computation of $\|\mathbf{h}_u(i)\|_F^2 + \|\mathbf{h}_u(j)\|_F^2 - 2m_{M\text{–PSK}}(\mathbf{H}_u)$ in Eq. (40) requires 3 flops. Hence, the overall complexity of the M-PSK modulated EVM-based ED-TAS is

$$\begin{aligned} C_{\text{EVM}} &= 2N_t^2N_r - N_t^2 + \binom{N_t}{2}\left\{4\left(\frac{M}{4}+1\right)+3\right\} \\ &= 2N_t^2N_r - N_t^2 + \frac{1}{2}N_t(N_t-1)(M+7). \end{aligned} \tag{48}$$

For the M-QAM scheme, this complexity depends on the parameter K. Specifically, the simplified versions of $d_{\min}^{\text{joint}}$ are different for different values of K. In general, for a given K, we first characterize all possible combinations of $|s_a|^2$ and $|s_b|^2$ by using the method of Section IV-B. Let us assume that the number of these combinations is G. For each combination, we can simplify Eq. (37) similar to the process of Eqs. (43)-(44), which corresponds to G simplified equations and each requires 15 flops, as shown in Eq. (37). Since $\binom{N_t}{2}$ legitimate TA combinations (i, j) should be considered in Eq. (37), we arrive at a complexity of $15G\binom{N_t}{2}$ for all possible combinations. Overall, the complexity of the EVM-based TAS for M-QAM modulated SM is

$$C_{\text{EVM}} = 2N_t^2N_r - N_t^2 + 15G\binom{N_t}{2}. \tag{49}$$

Note that the complexity of Eq. (49) is an approximate result, which can be further refined based on the specific simplified version of $d_{\min}^{\text{joint}}$. For example, based on Eqs. (41) and (43) derived for $K = 1$ and $K = 3$, similar to the complexity analysis of M-PSK, the computational complexity orders of the EVM-based TAS for $K = 1$ and $K = 3$ are

$$C_{\text{EVM}-\text{TAS}} = 2N_t^2N_r - N_t^2 + 6\binom{N_t}{2}, \tag{50}$$

and

$$C_{\text{EVM}-\text{TAS}} = 2N_t^2N_r - N_t^2 + 22\binom{N_t}{2}. \tag{51}$$

C. The Proposed PA & TAS

The exhaustive-search based TAS&PA algorithm has to calculate all legitimate PA matrix candidates. According to Section V, there are $N_U = \binom{N_t}{L}$ legitimate PA matrix candidates $\mathbf{P}_u(u = 1, \cdots, N_U)$, which can be obtained by using the method proposed in [29]. The complexity of computing each PA matrix is C_{PA} (Eq. (22) in [29]) flops. Hence, the associated complexity of the exhaustive-search based TAS&PA algorithm is $N_U C_{\text{PA}}$ flops. By contrast, the low-complexity TAS&PA algorithm first selects the optimal TA subset and then calculates the PA matrix for the selected set. Hence, the associated complexity order of the low-complexity TAS&PA algorithm is $C_{\text{TAS}} + C_{\text{PA}}$ flops, where C_{TAS} is the complexity of the TAS algorithm employed, i. e. C_{EVM} or C_{PQRD}.

References

[1] R. Y. Mesleh, H. Haas, S. Sinanovic, C. W. Ahn, and S. Yun, "Spatial modulation," *IEEE Trans. Veh. Technol.*, vol. 57, no. 4, pp. 2228–2241, Jul. 2008.

[2] M. Di Renzo, H. Haas, A. Ghrayeb, S. Sugiura, and L. Hanzo, "Spatial modulation for generalized MIMO: Challenges, opportunities and implementation," *Proc. IEEE*, vol. 102, no. 1, pp. 56–103, Jan. 2014.

[3] S. Sugiura, S. Chen, and L. Hanzo, "A universal space-time architecture for multiple-antenna aided systems," *IEEE Commun. Surveys Tuts.*, vol. 14, no. 2, pp. 401–420, May 2012.

[4] M. Di Renzo, H. Haas, and P. M. Grant, "Spatial modulation for multiple-antenna wireless systems: A survey," *IEEE Commun. Mag.*, vol. 49, no. 12, pp. 182–191, Dec. 2011.

[5] A. Stavridis, S. Sinanovic, M. Di Renzo, and H. Haas, "Energy evaluation of spatial modulation at a multi-antenna base station," in *Proc. IEEE Veh. Technol. Conf.*, Barcelona, Spain, Sep. 2013, pp. 1–5.

[6] M. Di Renzo and H. Haas, "Bit error probability of SM-MIMO over generalized fading channels," *IEEE Trans. Veh. Technol.*, vol. 61, no. 3, pp. 1124–1144, Mar. 2012.

[7] P. Yang, M. Di Renzo, Y. Xiao, S. Li, and L. Hanzo, "Design guidelines for spatial modulation," *IEEE Commun. Surveys Tuts.*, vol. 17, no. 1, pp. 6–26, Mar. 2015.

[8] S. Sugiura and L. Hanzo, "On the joint optimization of dispersion matrices and constellations for near-capacity irregular precoded space-time shift keying," *IEEE Wireless Commun.*, vol. 12, no. 1, pp. 380–387, Jan. 2013.

[9] P. Yang, Y. Xiao, Y. Yi, and S. Li, "Adaptive spatial modulation for wireless MIMO transmission systems," *IEEE Commun. Lett.*, vol. 15, no. 6, pp. 602–604, Jun. 2011.

[10] P. Yang, Y. Xiao, L. Li, Q. Tang, Y. Yu, and S. Li, "Link adaptation for spatial modulation with limited feedback," *IEEE Trans. Veh. Technol.*, vol. 61, no. 8, pp. 3808–3813, Oct. 2012.

[11] M. Di Renzo and H. Haas, "Improving the performance of space shift keying (SSK) modulation via opportunistic power allocation," *IEEE Commun. Lett.*, vol. 14, no. 6, pp. 500–502, Jun. 2010.

[12] S. Sanayei and A. Nosratinia, "Antenna selection in MIMO systems," *IEEE Commun. Mag.*, vol. 42, no. 10, pp. 68–73, Oct. 2004.

[13] W. H. Chung, C. Y. Hung, Q. Zhang, and M. Gao, "Multi-antenna selection using space shift keying in MIMO systems," in *Proc. IEEE Veh. Technol. Conf.*, May 2012, pp. 1–5.

[14] B. Kumbhani and R. S. Kshetrimayum, "Outage probability analysis of spatial modulation systems with antenna selection," *Electron. Lett.*, vol. 50, no. 2, pp. 125–126, 2014.

[15] S. Sugiura, S. Chen, and L. Hanzo, "Coherent and differential space-time shift keying: A dispersion matrix approach," *IEEE Trans. Commun.*, vol. 58, no. 11, pp. 3219–3230, Nov. 2010.

[16] J Wang *et al.*, "Closed-loop spatial modulation with antenna selection," in *Proc. IEEE 11th Int. Conf. Signal Process.*, Oct. 2012, pp. 1291–1294.

[17] Z. Zhou, N. Ge, and X. Lin, "Reduced-complexity antenna selection schemes in spatial modulation," *IEEE Commun. Lett.*, vol. 18, no. 1, pp. 14–17, Jun. 2014.

[18] M. Maleki, H. R. Bahrami, and A. Alizadeh, "Adaptive antenna subset selection and constellation breakdown for spatial modulation," *IEEE Commun. Lett.*, vol. 18, no. 9, pp. 1649–1652, Sep. 2014.

[19] X. Wu, M. D. Renzo, and H. Haas, "Direct transmit antenna selection for transmit optimized spatial modulation," in *Proc. IEEE Veh. Technol. Conf. (VTC'13-Fall)*, Las Vegas, NV, USA, Sep. 2013, pp. 1–5.

[20] X. Wu, M. Di Renzo, and M. Haas, "Adaptive selection of antennas for optimum transmission in spatial modulation," *IEEE Trans. Wireless Commun.*, vol. 14, no. 7, pp. 3630–3641, Jul. 2015.

[21] R. Rajashekar, K. V. S. Hari, and L. Hanzo, "Antenna selection in spatial modulation systems," *IEEE Commun. Lett.*, vol. 17, no. 3, pp. 521–524, Mar. 2013.
[22] N. Pillay and H. Xu, "Comments on "Antenna selection in spatial modulation systems"," *IEEE Commun. Lett.*, vol. 17, no. 9, pp. 1681–1683, Sep. 2013.
[23] K. Ntontin, M. Di Renzo, A. Perez-Neira, and C. Verikoukis, "A low-complexity method for antenna selection in spatial modulation systems," *IEEE Commun. Lett.*, vol. 17, no. 12, pp. 2312–2315, Aug. 2013.
[24] N. Wang, W. Liu, H. Men, M. Jin, and H. Xu. "Further complexity reduction using rotational symmetry for EDAS in spatial modulation," *IEEE Commun. Lett.*, vol. 18, no. 10, pp. 1835–1838, Oct. 2014.
[25] J. Zheng and J. Chen, "Further complexity reduction for antenna selection in spatial modulation systems," *IEEE Commun. Lett.*, vol. 19, no. 6, pp. 937–940, Jun. 2015.
[26] R. Rajashekar, K. V. S. Hari, and L. Hanzo, "Quantifying the transmit diversity order of Euclidean distance based antenna selection in spatial modulation," *IEEE Commun. Lett.*, vol. 22, no. 9, pp. 1434–1437, Sep. 2015.
[27] N. Pillay and X. Hongjun, "Low-complexity transmit antenna selection schemes for spatial modulation," *IET Commun.*, vol. 9, no. 2, pp. 239–248, Jan. 2015.
[28] P. Yang, Y. Xiao, B. Zhang, S. Li, M. El-Hajjar, and L. Hanzo, "Power allocation aided spatial modulation for limited-feedback MIMO systems," *IEEE Trans. Veh. Technol.*, vol. 64, no. 5, pp. 2198–2204, May 2015.
[29] P. Yang, Y. Xiao, S. Li, and L. Hanzo, "A low-complexity power allocation algorithm for multiple-input multiple-output spatial modulation systems," *IEEE Trans. Veh. Technol.*, vol. 65, no. 3, pp. 1819–1825, Mar. 2016.
[30] M. Di Renzo and H. Haas, "Improving the performance of space shift keying (SSK) modulation via opportunistic power allocation," *IEEE Commun. Lett.*, vol. 14, no. 6, pp. 500–502, Jun. 2010.
[31] Y. Xiao, Q. Tang, L. Gong, P. Yang, and Z. Yang, "Power scaling for spatial modulation with limited feedback," *Int. J. Antennas Propag.*, vol. 2013 5 p., 2013.
[32] Z. Shi and H. Leib, "Transmit antenna selection V-BLAST systems with power allocation," *IEEE Trans. Veh. Technol.*, vol. 57, no. 4, pp. 2293–2304, Jul. 2008.
[33] R. Rajashekar, K. V. S. Hari, and L. Hanzo, "Reduced-complexity ML detection and capacity-optimized training for spatial modulation," *IEEE Trans. Commun.*, vol. 62, no. 1, pp. 112–125, Jan. 2014.
[34] S. Sugiura, C. Xu, S. X. Ng, and L. Hanzo, "Reduced complexity coherent versus non-coherent QAM-aided space time shift keying," *IEEE Trans. Commun.*, vol. 59, no. 11, pp. 3090–3101, Nov. 2011.
[35] A. Younis, S. Sinanovic, M. Di Renzo, R. Y. Mesleh, and H. Haas, "Generalised sphere decoding for spatial modulation," *IEEE Trans. Commun.*, vol. 61, no. 7, pp. 2805–2815, Jul. 2013.
[36] A. Goldsmith, *Wireless Communications*. Cambridge, U.K.: Cambridge Univ. Press, 2005.
[37] G. Golub and C. F. van Loan, *Matrix Computations*, 3 rd ed. Baltimore, MD, USA: The Johns Hopkins Univ. Press, 1996.
[38] J. K. Zhang, A. Kavcic, and K. M. Wong, "Equal-diagonal QR decomposition and its application to precoder design for successive-cancellation detection," *IEEE Trans. Inf. Theory*, vol. 51, no. 1, pp. 154–172, Jan. 2005.
[39] J. Lee, S. Y. Jung, and D. Park, "Simplified maximum-likelihood precoder selection for spatial multiplexing systems," *IEEE Trans. Veh. Technol.*, vol. 59, no. 9, pp. 4628–4634, Nov. 2010.
[40] Z. Chen, J. Yuan, and B. Vucetic, "Analysis of transmit antenna selection/maximal-ratio combining in Rayleigh fading channels," *IEEE Trans. Veh. Techol.*, vol. 54, no. 4, pp. 1312–1321, Jul. 2005.
[41] V. Raghavan, J. J. Choi, and D. J. Love, "Design guidelines for limited feedback in the spatially correlated broadcast channel," *IEEE Trans. Commun*, vol. 63, no. 7, pp. 2524–2540, Jul. 2015.

Q3 **Ping Yang** (SM'xx) received the Ph.D. degree from the University of Electronic Science and Technology of China (UESTC), Chengdu, China, in 2013. From September 2012 to September 2013, he was a Visiting Student at the School of Electronics and Computer Science, University of Southampton, Southampton, U.K. Since May 2014, he has been a Research Fellow in EEE of NTU, Singapore. Also, he is an Assistant Professor with UESTC. His research interests include MIMO/OFDM, machine learning, life science, and communication signal processing.

Yue Xiao (M'xx) received the Ph.D. degree in communication and information systems from the University of Electronic Science and Technology of China, Chengdu, China, in 2007. He is now a Full Professor with the University of Electronic Science and Technology of China. He has authored more than 30 international journals and been involved in several projects in Chinese Beyond 3G Communication R&D Program. His research interests include wireless and mobile communications.

Yong Liang Guan (M'xx) received the Ph.D. degree from the Imperial College of Science, Technology, and Medicine, University of London, London, U.K., in 1997, and the B.Eng. degree (with first class Hons.) from the National University of Singapore, Singapore, in 1991. He is now an Associate Professor with the School of Electrical and Electronic Engineering, Nanyang Technological University, Singapore. His research interests include modulation, coding and signal processing for communication, information security and storage systems.

Shaoqian Li (F'16) received the B.S.E. degree in communication technology from Northwest Institute of Telecommunication (Xidian University), Xi'an, China, in 1982, and the M.S.E. degree in communication system from the University of Electronic Science and Technology of China (UESTC), Chengdu, China, in 1984. He is a Professor, Ph.D. Supervisor, and the Director of the National Key Laboratory of Communication, UESTC, and member of the National High Technology R&D Program (863 Program) Communications Group. His research interests includes wireless communication theory, anti-interference technology for wireless communications, spread-spectrum and frequency-hopping technology, and mobile and personal communications.

Lajos Hanzo (F'xx) received the degree in electronics, in 1976, the doctorate degree, in 1983, and the D.Sc. degree. During his 37-year career in telecommunications, he has held various research and academic posts in Hungary, Germany, and the U.K. Since 1986, he has been with the School of Electronics and Computer Science, University of Southampton, Southampton, U.K., where he holds the chair in telecommunications. He has successfully supervised over 80 Ph.D. students, coauthored 20 John Wiley/IEEE Press books on mobile radio communications totalling in excess of 10 000 pages, published 1400+ research entries at IEEE Xplore, acted both as TPC and the General Chair of the IEEE conferences, presented keynote lectures and has been awarded a number of distinctions. Currently, he is directing a 100-strong academic research team, working on a range of research projects in the field of wireless multimedia communications sponsored by industry, the Engineering and Physical Sciences Research Council (EPSRC) U.K., the European Research Council's Advanced Fellow Grant and the Royal Society's Wolfson Research Merit Award. He is an enthusiastic supporter of industrial and academic liaison and offers a range of industrial courses. He is also a Governor of the IEEE VTS. From 2008 to 2012, he was the Editor-in-Chief of the IEEE Press and a Chaired Professor also at Tsinghua University, Beijing, China. His research is funded by the European Research Council's Senior Research Fellow Grant. He has more than 19 000 citations. In 2009, he was received the honorary doctorate "Doctor Honoris Causa" by the Technical University of Budapest, Budapest, Hungary. He is the fellow of the REng, IET, and EURASIP.

QUERIES

Q1: Please be advised that per instructions from the Communications Society this proof was formatted in Times Roman font and therefore some of the fonts will appear different from the fonts in your originally submitted manuscript. For instance, the math calligraphy font may appear different due to usage of the usepackage[mathcal]euscript. We are no longer permitted to use Computer Modern fonts.

Q2: Note that if you require corrections/changes to tables or figures, you must supply the revised files, as these items are not edited for you.

Q3: Please provide IEEE membership details of authors "Ping Yang, Yue Xiao, Yong Liang Guan, and Lajos Hanzo."